Universitat de Girona

THEORETICAL STUDIES OF THE EXOHEDRAL REACTIVITY OF FULLERENE COMPOUNDS

Sílvia OSUNA OLIVERAS

ISBN: 978-84-693-3377-8
Dipòsit legal: GI-555-2010
http://www.tdx.cat/TDX-0421110-125909

Universitat de Girona

PhD thesis:

Theoretical studies of the exohedral reactivity of fullerene compounds

Sílvia Osuna Oliveras
2009

Doctorat Interuniversitari en Química Teòrica i Computacional

PhD supervisors:
Prof. Miquel Solà i Puig
Prof. Marcel Swart

Memòria presentada per a optar al títol de Doctora per la Universitat de Girona

Universitat de Girona

El professor Miquel Solà i Puig, catedràtic d'Universitat a l'Àrea de Química Física de la Universitat de Girona, i el professor Marcel Swart, investigador ICREA a l'Institut de Química Computacional de la Universitat de Girona,

CERTIFIQUEM:

Que aquest treball titulat "Theoretical studies of the exohedral reactivity of fullerene compounds", que presenta la Sílvia Osuna Oliveras per a l'obtenció del títol de Doctora, ha estat realitzat sota la nostra direcció i que compleix els requeriments per poder optar a Menció Europea.

Signatura

Prof. Miquel Solà Puig Prof. Marcel Swart

Girona, 4 de Desembre de 2009

a la mama, al papa

a l'àvia Maria i a l'avi Miguel,

a en Narcís.

Preface

Since the buckminster fullerene discovery in 1985, a huge interest for understanding the chemical reactivity as well as the chemical properties of fullerene compounds has been awakened. The exohedral functionalization of the archetypal compound C_{60} is nowadays considered to be quite well-established. Still, the research in this field is open as a wide variety of derivatives with intriguing potential applications have been synthesized. Among all future applications, some fullerene compounds might be potential agents to treat some neurodegenerative disorders or could be useful as magnetic resonance image (MRI) contrast agents. In this thesis, the chemical reactivity of metallofullerenes and free fullerenes is studied in detail.
The thesis is divided into fifteen chapters that contain seven related publications. The first two studies are based on the Diels-Alder reaction involving the Trimetallic Nitride Template (TNT) endohedral metallofullerenes $X_3N@C_{78}$, $X = Sc, Y$. This investigation project was basically motivated by the unclear evidence about the possible consequences of the X_3N encapsulation on the exohedral fullerene reactivity of $X_3N@C_{78}$, because two opposite effects counteract. First, the introduction of the metal cluster produces an increment of the pyramidalization of the carbon atoms, which leads to an increase of strain energy and, therefore, a higher reactivity of the cage. Second, the charge transfer from the metal cluster to the fullerene structure causes a reduction of the electron affinity, thus diminishing the reactivity of the endohedral compound. In addition, it is important to note that the effect of encapsulation for the different bond types can be different. In these two first studies, detailed theoretical calculations are given to determine the change in reactivity of the different bond types upon encapsulation, to finally obtain a detailed description of the $X_3N@C_{78}$ reactivity. Moreover, different isomers for the C_{78} cage are considered for the yttrium cluster encapsulation. In chapter 8, the same cycloaddition reaction was studied in detail involving single and noble gas dimers endohedral fullerenes. It was found that the encapsulation of large noble gas dimers inside the C_{60} cavity produced large deviations on the C-C bond distances of the cage, therefore the exohedral reactivity of these compounds is expected to be extremely different to that of free C_{60}. Moreover, a genuine chemical bond is formed between xenon atoms once they are forced into contact inside the cage due to the electronic charge transfer produced. This third study thoroughly describes the change on the exohedral functionalization upon noble gas encapsulation. The first part of this thesis involving endohedral metallofullerenes is of significant interest due to the potential application of these compounds in the field of (bio)medicine.

Treating fullerene compounds that present a large number of atoms with full *ab-initio* methodologies usually requires a high computational cost. In this context,

the use of QM/QM' approaches such as the ONIOM methodology is widely spread. The computational time is substantially decreased and results obtained are usually pretty accurate. In the fourth study included in this thesis, the performance of the ONIOM approach for studying cycloaddition reactions involving fullerene compounds is studied in detail. Results from the latter project are of interest for the following studies involving the 1,3-dipolar and the Diels-Alder cycloaddition reactions where the ONIOM strategy is employed. In collaboration with the experimental group led by Prof. N. Martín at the Universidad Autónoma de Madrid, the retro-cycloaddition reaction of azomethine ylide and C_{60} is assessed. In contrast with other cycloaddition products, pyrrolidinofullerenes were thought to be extremely stable. Therefore, the study of the reaction mechanism of this retro-process remains extremely relevant to fully understand how the retro-cycloaddition is experimentally achieved. The ONIOM approach has also been used to treat some compounds in the last study involving cycloaddition reactions included in this thesis. Although the mechanism of cycloaddition reactions is quite well understood, it was recently found that the activation barrier for the 1,3-dipolar and Diels-Alder reactions involving acetylene and ethylene can be basically attributed to the distortion energy required to deform initial reactants to the geometry they present at the transition state. The latter distortion/interaction model is investigated in detail involving a wide variety of large organic molecules including fullerene and nanotube compounds.

Finally, the last part of this thesis is based on the antioxidant properties of fullerene compounds. Experimentally, it was found that some fullerene derivatives were able to dismutate the prejudicial superoxide anion to hydrogen peroxide and molecular oxygen at a rate within the range of several inorganic superoxide dismutase (SOD) mimetic compounds. Although several biological/medical studies where a fullerene compound was administered in mice indicated very promising results, the mechanism of action is still unknown. In chapter 12, the mechanism of action for the superoxide removal involving fullerene compounds is unraveled. The understanding of the SOD removal mechanism could represent a big improvement to design new fullerene derivatives with higher antioxidant properties.

Des del descobriment del buckminster ful.lerè el 1985, s'ha despertat un interès enorme per entendre la reactivitat química així com les propietats d'aquests compostos. La funcionalització exoèdrica del ful.lerè més abundant, el C_{60}, està força ben establerta. Tanmateix, la investigació en aquest camp encara continua oberta ja que s'han sintetitzat una gran varietat de derivats molt prometedors donades les seves futures aplicacions. Alguns derivats podrien ser utilitzats per tractar malalties neurodegeneratives o fins i tot com agents de contrast a les tècniques de ressonància magnètica (MRI). En aquesta tesi, la reactivitat química de determinats metal.loful.lerens i ful.lerens lliures amb futures aplicacions en el camp de la (bio)medicina s'estudia en detall.

La tesi comprèn quinze capítols que contenen set publicacions relacionades. Els

primers dos estudis es basen en la reacció Diels-Alder sobre els anomenats metal.lofullerens endoèdrics TNT $X_3N@C_{78}$, $X = Sc, Y$. Aquest projecte de investigació està motivat pel desconeixament existent sobre les possibles conseqüències de l'encapsulació del grup X_3N a la reactivitat exoèdrica dels ful.lerens endoèdrics $X_3N@C_{78}$. D'una banda, la introducció del cluster metàl.lic produeix un augment de la piramidalització dels àtoms de carboni, cosa que implica un augment de la tensió de la caixa i, per tant, un increment de la reactivitat de la caixa. D'altra banda, la transferència electrònica des del clúster metàl.lic al ful.lerè produeix una reducció de l'afinitat electrònica, que per tant porta a una disminució de la reactivitat del compost endoèdric. A més, cal destacar que l'efecte d'encapsulació pot ser diferent per als diferents tipus d'enllaç considerats. En aquests dos primers estudis, la realització de càlculs teòrics permet determinar el canvi de reactivitat dels diferents tipus d'enllaços en produir-se l'encapsulació, i per tant, obtenir una descripció detallada de la reactivitat de $X_3N@C_{78}$. Cal també tenir en compte els diferents possibles isòmers per a l'encapsulació de clústers grans com el d'itri. Al capítol 8, s'estudia la mateixa reacció Diels-Alder però implicant ful.lerens endoèdrics amb gasos nobles (Ng) o dímers de Ng (Ng_2). L'encapsulació de dímers dels gasos nobles més grans (Ar_2-Xe_2) dins del C_{60} produeix grans desviacions en les distàncies d'enllaç de la caixa, i per tant es podria esperar que es produís un canvi en la reactivitat en comparació al C_{60} lliure. En el cas de Xe_2, es forma un enllaç químic entre els àtoms de xenó una vegada introduït dins del ful.lerè, a causa de la transferència de càrrega produïda del dímer al C_{60}. Aquest tercer estudi descriu minuciosament els canvis detectats en la funcionalització exoèdrica un cop s'ha produït l'encapsulació dels diferents gasos nobles. La primera part d'aquesta tesi inclou l'estudi de ful.lerens endoèdrics d'alt interès científic degut a les possibles aplicacions d'aquests compostos en el camp de la (bio)medicina.

El tractament dels ful.lerens i derivats mitjançant mètodes ab-initio normalment implica un alt cost computacional. En aquest context, l'ús d'estratègies del tipus QM/QM', com la metodologia desenvolupada per Morokuma i col.laboradors, anomenada ONIOM, està àmpliament estesa. El temps computacional disminueix substancialment i els resultats obtinguts són normalment força acurats. En aquesta tesi s'estudia en detall l'ús de l'aproximació ONIOM per a estudiar reaccions de cicloaddició en compostos de ful.lerens. Els resultats d'aquest projecte són d'alt interès per a la realització dels estudis que es detallaran a continuació. En col.laboració amb el grup experimental del prof. N. Martín de la Universidad Autónoma de Madrid, s'ha investigat la retro-cicloaddició entre l'ilur d'azometil i el C_{60}. A diferència d'altres productes de cicloaddició, els pirrolidinoful.lerens eren considerats extremadament estables. Per aquest motiu, l'estudi del mecanisme de la retro-cicloaddició és important per entendre com s'aconsegueix el retro-procés experimentalment. La metodologia ONIOM també s'utilitza en determinats composts de l'últim estudi on es tracten reaccions de cicloaddició. Encara que el mecanisme de les cicloadicions està ben establert, es va trobar que la barrera d'activació de les reaccions 1,3-dipolar i Diels-Alder produïdes sobre l'acetilè i l'etilè s'atribueix bàsicament a l'energia de distorsió,

la qual correspon a l'energia necessària per a deformar els reactius inicials a la geometria que presenten a l'estat de transició. El model anomenat de distorsió/interacció s'investiga en detall considerant una gran varietat de molècules orgàniques grans incloent compostos ful.lerènics i nanotubs de carboni.

Finalment, l'última part d'aquesta tesi es basa en les propietats antioxidants de determinats ful.lerens. Experimentalment, s'ha trobat que alguns derivats són capaços de convertir el perjudicial anió superòxid en aigua oxigenada i oxigen molecular en una proporció similar a la d'alguns compostos inorgànics mimètics de la superòxid dismutasa (SOD). S'han obtingut resultats molt prometedors en diferents estudis biològic/mèdics on un derivat ful.lerènic és administrat a ratolins. Tot i això, el mecanisme d'acció és encara desconegut. Així doncs, a l'últim treball inclòs en aquesta tesi s'estudia en detall el mecanisme de reacció per a la eliminació del ió superòxid involucrant ful.lerens.

Contents

Chapter 1

Free Fullerenes

1.1 Introduction

Fullerenes are carbon clusters constituted by an even number of carbon atoms in the form of a hollow sphere. The cage is formed by hexagonal and pentagonal rings that prevent the sheet from being planar, and they are generally represented by the formula C_n, where n denotes the number of carbon atoms present in the structure. Fullerenes are carbon allotrope forms together with diamond, graphite and carbon nanotubes or CNTs. Although diamond and graphite have been known since ancient times (in fact, the word diamond comes from the greek word *adamas*, which means untameable), the latter structures have been discovered within the last two decades. The specific hybridization of carbon, and its bonding to surrounding atoms will determine which allotrope carbon will assume. In the diamond, carbon atoms have an sp^3 hybridization and will form a tetrahedral lattice; an sp^2 hybridization is found either in graphite, fullerenes or carbon nanotubes, the formation of the different allotropes will be given by the conditions in which they are formed.

Fullerene cages are constituted by sp^2 carbons with high electron withdrawing character, thus easily reacting with nucleophiles. In fact, fullerenes and electron deficient conjugated hydrocarbons have similar reactivity.

The most abundant and studied fullerene is C_{60}, also called [60]-fullerene or buckminsterfullerene because of the similar shape of the molecule to the geodesic dome popularized by the noted architect Richard Buckminster Fuller. As the discovery of the fullerene family came after buckminsterfullerene, the name was shortened to illustrate that the latter is a type of the former. C_{60} was discovered by Kroto, Smalley, Curl and coworkers [1] in 1985, although its possible existence had been discussed by other chemists years earlier. Thanks to the buckminsterfullerene discovery, Kroto, Smalley and Curl were awarded the Nobel Prize of Chemistry in 1996.

1.2 Carbon Studies prior to the Discovery of C_{60} Stability

Buckminsterfullerene has a high degree of symmetry, this could probably be one of the main reasons for the huge interest engendered by this molecule. The possibility of making large hollow carbon cages was suggested by Jones[2] in 1966, and Osawa [3] in 1970 suggested the C_{60} molecule in an imaginative and prescient paper. A Hückel calculation on the hypothetical unsaturated purely carbon system C_{20} and the derivative B_2C_{18} was done by Bochvar and Gal'pern[4] in 1973, and Davidson [5] used graph theory to deduce an algebraic solution of the Hückel calculation for fullerene-[60]. Moreover, Haymet[6] published his studies on the Archimedean solids: footballene (C_{60}) and Archimedene (C_{120}), and although the former structure had not been synthesized yet, his studies on the molecule closely coincided with the structure found in 1985 when it was produced for the first time. In the previous paper, Haymet deduced that C_{60} and C_{120} would be stable if a synthetic route could be found.

In the experimental field, Smalley and co-workers developed a laser vaporization technique at Rice University[7] in 1981, where clusters were made by laser vaporization of refractory materials into a pulse of helium or argon in the throat of a supersonic nozzle. The vaporized material nucleated in the gas pulse which then expanded supersonically into a vacuum chamber where it was cooled and skimmed. The skimmed beam passed into a second chamber where the entrained clusters were ionized by a second laser pulse and the cluster ion mass distributions were determined by time of flight mass spectrometry (TOF-MS). Rohlfing et al.[8] used this method and found that for clusters composed of less than 30 atoms all cluster sizes were detected, however they observed for the first time clusters composed of greater than 30 carbon atoms with the novel characteristic that only even atom clusters were seen. Bloomfield et al.[9] used the same technique with some variations on the apparatus and they obtained either negatively or positively charged even-numbered ions.

1.3 The Discovery of C_{60}: Buckminsterfullerene

In 1985, Kroto, Smalley, Curl and co-workers tried to simulate the conditions under which carbon nucleates in the atmospheres of cool N-type red giant stars, and during the course of the experiments a striking discovery was made.[1] Under the conditions of the study, the 720 mass peak i.e. C_{60} appeared to be extremely strong, and in fact, the cluster distribution was clearly dependent on the vaporization conditions. Clusters of up to 190 carbon atoms were observed, and it was noted that for clusters of more than 40 atoms, only those containing an even number of atoms were detected.

They concluded that the C_{60} structure had to adopt a spheroidal structure in order to satisfy all sp^2 valences, and moreover the Buckminster Fuller's studies were consulted. It was noticed that as the diameter of the molecule was ~ 7 Å, it provided an inner cavity which appeared to be capable of holding a variety of atoms. Because of the stability when it was formed under very violent conditions, they guessed that it might be a major constituent of circumstellar shells with high carbon content. Moreover, the C_{70} was found to be the second more stable fullerene.

Since the buckminsterfullerene detection, many different studies about stability, properties, aromaticity of the compounds, as well as reactivity studies have been carried out.

1.4 The Isolation, Separation and Structural Characterization of C_{60}

After the revelation it still remained for unequivocal proof of the soccerball structure to be obtained, and although calculations of many physical properties had been made, including electron energies, the optical spectrum, vibrational modes, and the electric and magnetic properties, they could not be tested because it was not possible to obtain macroscopic quantities of the molecule.

Almost five years to the day that C_{60} was discovered, Krätschmer et al.[10] succeeded to obtain macroscopic quantities of buckminsterfullerene, and by using their new technique a person could produce of the order of 100 mg of the purified material in a day. The starting material was pure graphitic carbon soot, and it was produced by evaporating graphite electrodes in an atmosphere of ~ 100 torr of helium. The resulting black soot was gently scraped from the collecting surfaces inside the evaporation chamber and dispersed in benzene. The material giving rise to the spectral features attributed to C_{60} dissolved to produce a wine-red to brown liquid, depending on the concentration. The liquid was then separated from the soot and dried using gentle heat, leaving a residue of dark brown to black cristalline material.

They performed a mass spectrometry analysis, and obtained mass spectra that had a strong peak at 720 a.m.u. Moreover, electron and X-ray diffraction studies on the individual crystals were done, as well as absorption spectra of the graphitic soot which showed evidence for the presence of C_{60} in macroscopic quantities.

Independently, Taylor et al.[11] using a similarly arc-processed carbon, showed that C_{60} was present by FAB-sampled mass spectrometry and that a red soluble extract could be obtained by treating the carbon deposit directly with benzene. They first

reported the chromatographic separation of C_{60} and C_{70} using alumina/hexane, the resultant fractions were magenta and red respectively. $^{13}C - NMR$ measurements yielded a single line for C_{60}, providing the definitive proof that all carbons were equivalent, and supporting the proposed buckminsterfullerene structure.

These techniques for obtaining and separating fullerene structures are still being used.

1.5 The IPR rule

The bond structure of fullerenes corresponds to a polyhedron where atoms are situated in vertices, bonds in edges, and rings in faces. According to the Euler Theorem formulated in 1752, two hundred years before the fullerene discovery, the relationship between vertices (v), edges (e) and faces (f) is:

$$v + f = e + 2 \tag{1.1}$$

The restriction to three σ-bonds to each carbon site relates the number of vertices (v) and the number of edges (e) (equation 1.2).

$$2e = 3v \tag{1.2}$$

Let f_n denote the number of n-sided faces (or rings), the following relationship is accomplished.

$$2e = \sum_n n f_n \tag{1.3}$$

If we consider a fullerene C_k, the number of vertices (atoms) is equal to k, and by using the relation 1.2 the number of edges is obtained (equation 1.4).

$$e = 3k/2 \tag{1.4}$$

Thanks to the Euler theorem, the number of faces is given by equation 1.5.

$$f = k/2 + 2 \tag{1.5}$$

More conclusions can be derived, e.g. all C_k fullerenes must contain a certain number of hexagonal and pentagonal rings. As the number of faces can also be expressed as

$$f = \sum_n f_n \tag{1.6}$$

and making use of the expression 1.5, equation 1.7 holds.

$$\sum_n f_n = k/2 + 2 \tag{1.7}$$

If only fullerenes with hexagonal and pentagonal rings are considered, the sum can be developed as in equation 1.8.

$$f_5 + f_6 = k/2 + 2 \tag{1.8}$$

By considering 1.3, a linear system is obtained, whose solutions indicate that C_k fullerenes must have:

$$\begin{aligned} f_5 &= 12 \\ f_6 &= \tfrac{k}{2} - 10 \end{aligned} \tag{1.9}$$

12 pentagonal rings and $k/2 - 10$ hexagonal rings.[12]
By increasing the number of hexagonal and pentagonal rings distribution, a wide range of fullerenes can be generated, and moreover, different isomers are obtained. Based on this theorem, the smallest possible fullerene is C_{20} which has 0 hexagonal rings $(20/2 - 10)$. Fowler et al.[13] concluded that at least one isomer is possible for fullerenes C_k, where k is even and $k > 24$. In addition, the number of isomers for each fullerene increases exponentially.[14]

Schmalz et al.[12] proposed the following constraint criteria, in order to reduce the number of carbon clusters to study, and focus on the most stable ones: (i) cage homeomorphic to a sphere, (ii) higher symmetry, (iii) non abutting five-sided rings, and (iv) curvature spread uniformly over the cage.

A one-dimensional (sp-hybridized) chain bent to close into a two-dimensional ring should exhibit little resonance energy. An sp^3-hybridized array of carbons would be three-dimensional and either fill the space as diamond does, or have a surface with destabilizing dangling bonds. In the same way, an sp^2-hybridized planar fragment of the graphite lattice would have a reactive edge with dangling bonds, so in order to satisfy criterion (i), sp^2-hybridized networks bent around to close on themselves are proposed. The formation of the closed cages has associated a steric strain energy because of the structure curvature. In some cages, the strain energy is greater than the energy related to the formation of the cage.

Criterion (i) is based on the relationship between curvature and stability. The more stable the structure, the less the curvature. Basically, it is due to two reasons: first, the σ-skeleton to achieve as closely as possible the ideal sp^2 geometry, and second, in order for the overlap between adjacent π-like orbitals to be as large as possible. If we consider the 1s electrons localized, every carbon atom has 4 free electrons, and 4 valence orbitals to contribute to the fullerene bond. In order to form the σ bonds of the fullerene structure (they can be seen as the edges of a polyhedron) 3 electrons are used, the last one is situated in the π C-C bond system. The π electron is situated in

an hybrid orbital sp^m, which could be the pure 2p orbital if the molecule is planar.[15] Likewise, if the π-like orbitals on neighboring atoms do not align exactly parallel to one another, the π-interaction (as moderated by the resonance integral β in Hückel theories or exchange integrals in valence-bond theories) will be diminished. Davidson [5] applied the Hückel molecular orbital (HMO) to C_{60}, and found a resonance energy of $0.5527|\beta|$ per atom (the graphite value is $0.5761|\beta|$), and an energy HOMO-LUMO gap of $0.7566|\beta|$, compared to $2|\beta|$ for benzene.

As a general rule, π-electron stabilization is greatest for rings of six members, somewhat less for sizes 5 and 7, and dramatically less for sizes 4 and 8. Rings of size 3 are rather unstable because of σ-strain, while rings of size ≥ 9 lead to generally diminishing π-resonance stabilization. Furthermore, for each ring of size larger than 6 there must be "compensating" rings of size less than 6.

The energy stabilization seems to be dominated by more or less local features, so the repetition of more stable local structures should yield the more stable global structure, and thus the study of high symmetry cages is proposed.

Finally, the rationale for excluding fused five-membered rings is that when they abut there occurs an eight-cycle around the periphery of these two rings, and according to the Hückel 4n+2/4n rule it has a destabilizing effect over the π electronic structure. The latter criterion suggested by Schmalz[12] supported the Isolated Pentagon Rule (IPR) proposed by Kroto in 1987.[16]

The IPR states that most stable fullerenes are those where the 12 pentagonal rings are isolated. When two pentagons are abutted a severe steric tension is produced which impedes the fullerene formation, in addition to the destabilizing effect of the π electronic structure (4n Hückel rule). It is specially significant that the steric tension and π electronic structure support the isolated pentagon rule. Therefore, fullerene stability is given by a balance between these two aspects.

1.6 IPR fullerene isomers

The IPR substantially reduces the number of isomeric possibilities of the larger fullerenes, which range from 2 in the case of C_{76} to 24 in the case of C_{84}. In this section, the IPR fullerene isomer for the most studied cage (C_{60}) will be given, as well as the IPR isomers of the fullerene C_{78} subject at hand.

As mentioned before, the first characterized fullerene was $I_h - C_{60} : \mathbf{1}$ which is usually called C_{60}.[1] The latter C_{60} isomer is the only one obeying the IPR rule (among

the 1812 possible isomers for C_{60}) and, until very recently, it was the unique buckminsterfullerene isomer identified and isolated. However, in 2008 Tan and coworkers reported the synthesis of chlorinated species of the non-IPR C_{2v} and C_s-C_{60} symmetries.[17] C_{78} was first characterized in 1991,[18] and a mixture of three among the 5 possible isomers were obtained. The different isolated pentagon structures have symmetry $C_{2v'}$, D_3, C_{2v}, $D_{3h'}$ and D_{3h} which are candidates for its ground state (see Figure 1.1). The three isomers obtained were $D_3 - C_{78}$: **1**, $C_{2v} - C_{78}$: **2**, $C_{2v'} - C_{78}$: **3** (where boldface denotes the isomer number).[18–20] A trifluoromethylated adduct of the $D_{3h'} - C_{78}$: **5** can be obtained at high temperatures using the arc-generated carbon soot.[21,22] The existence of $D_{3h} - C_{78}$: **4** in carbon soot has not been reported yet.[23–25] The stabilities calculated at the HF level with 6-31G* basis set (with the relative electronic energies in $kcal.mol^{-1}$ represented in brackets) for the different IPR isomers are: $C_{2v'} - C_{78}$: **3**(0) > $D_3 - C_{78}$: **1**(3) > $C_{2v} - C_{78}$: **2**(4) > $D_{3h'} - C_{78}$: **5**(7) > $D_{3h} - C_{78}$: **4**(20).[26] In addition to these 5 IPR cages, there are 24105 more isomers that do not obey the IPR rule.

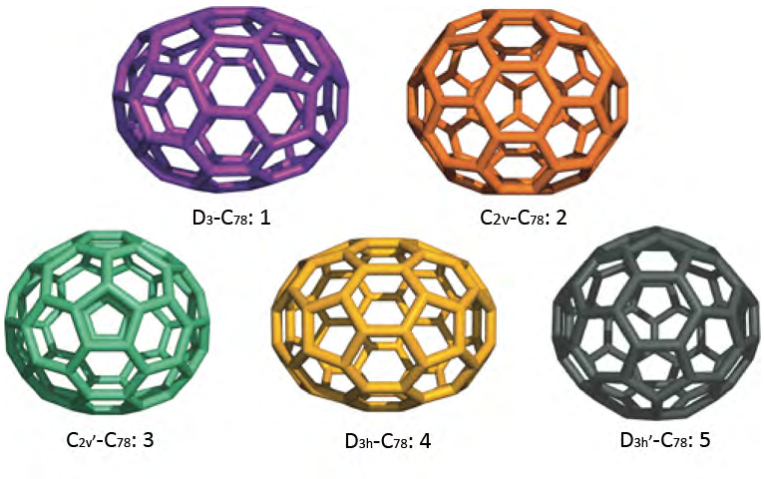

Figure 1.1: IPR isomers of C_{78}.[27]

1.7 Properties and Characterization

1.7.1 C-C bond types

As the fullerene cage is constituted by hexagonal and pentagonal rings, the structure has two different bond types, [6,6] bonds which are those situated between 2 hexagonal rings, and [5,6] between an hexagonal and a pentagonal ring (Figure 1.2). If the type of the rings that surround the C-C bond is taken into account, [6,6] bonds can be classified in 3 different subtypes: (a) Pyracylenic or type A, (b) Type B, (c) Pyrenic or type C. The former corresponds to a C-C bond situated between two

pentagonal rings, they are the shortest bonds, with highest pyramidalization angles and they have a stronger double bond character. Type B bond is the one situated between an hexagon and a pentagon, and finally pyrenic or type C is localized between two hexagonal rings, and it has the lowest pyramidalization angles which produces a more planar region of the fullerene structure (Figure 1.2).

Similarly, [5,6] bonds can also be classified in two different subtypes: (d) Corannulene or type D and (e) Type F. Finally, [5,5] bonds are (f) Pentalene or type E. As Type F and type E (Pentalene) bonds have two pentagons abutted, they cannot be found in C_{60} and free $D_{3h} - C_{78}$ structures which obey the IPR.

Bond type together with C-C distance and piramidalization angles are the parameters usually employed to justify the exohedral reactivity of the cage. However, fullerene strain energy as well as the deformation of the cage do also contribute.

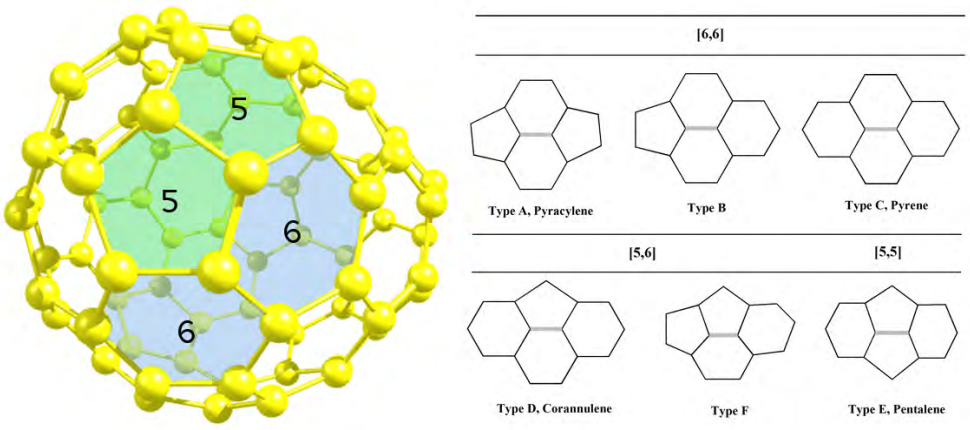

Figure 1.2: Picture of the the different bond types [5,5], [5,6], and [6,6] that might be present in any fullerene structure.

1.7.2 Electronic Structure

The HOMO orbitals of the C_{60} have bonding π interactions in the [6,6] C-C bonds, and antibonding π interactions in the [5,6]. Therefore, the occupation of the HOMO orbitals leads to cut down the [6,6] bond distance, and obviously to extend the [5,6] bond types. The LUMO and LUMO+1 represent an inverse situation, so the population of these orbitals causes an increase of the [6,6] bond distance, and a decrease of the [5,6], which favor the aromatic character because all different types for C-C bond have a similar bond distance. This is the main reason for the C-C

bond distance alternation and the proof of the non-homogeneous delocalization of the π electron over different bonds.

1.7.3 Aromaticity

Because of the presence of hexagonal rings in the C_{60} structure, it was originally considered as a possible superaromatic molecule. Whether or not fullerenes have to be considered aromatic has been debated since their discovery. This is partially due to the multidimensional character of this property.[28–30] Fullerenes cannot undergo substitution reactions, characteristic of the aromatic compounds, because of the lack of hydrogen bonds that could be substituted. Moreover, the high pyramidalization of C atoms, responsible for the strain, should be taken into account to discuss the fullerene aromaticity.

From the structural point of view, C_{60} has bond length alternation which is a clear difference from the prototypical aromatic molecule benzene. For spherical fullerenes, the $2(N+1)^2$ rule was proposed[31] which is an equivalent to the $4N+2$ Hückel rule for planar polycyclic aromatic compounds. According to this rule, charged C_{60} structures, such as C_{60}^{10+} are much more aromatic and their bond differences are reduced.

The aromaticity of C_{60} and C_{70} has been analyzed using the structure-based harmonic oscilator model of aromaticity (HOMA),[32] the magnetic-based nucleus independent chemical shift (NICS)[33] and the electronic-based paradelocalization (PDI) [34] indices. For the C_{60}, the values of the electron-delocalization-based fluctuation (FLU) index[35] have also been reported. These studies have shown that six-membered rings are partially aromatic, while five-membered rings are antiaromatic. Magnetic properties as well as electron delocalization studies[36] show a delocalized character of the π-system, similar to that of clearly aromatic systems such as benzene or naphthalene.

The fullerene chemical reactivity is more similar to the electron-deficient olefins, and is to great extent driven by the reduction of strain. As a consequence of the previous reasons, C_{60} and fullerenes in general are considered to show only modest forms of aromaticity.

Chapter 2

Endohedral Metallofullerenes

2.1 Introduction

Soon after the fullerene discovery, the possibility of the encapsulation of metals inside the fullerene cage was considered. In fact, the metal can be (1) incorporated into the fullerene carbon surface (heterohedral metallofullerenes) (2) located outside the cage (exohedral metallofullerenes) or (3) trapped inside the hollow fullerene cage (endohedral metallofullerenes) (Figure 2.1).

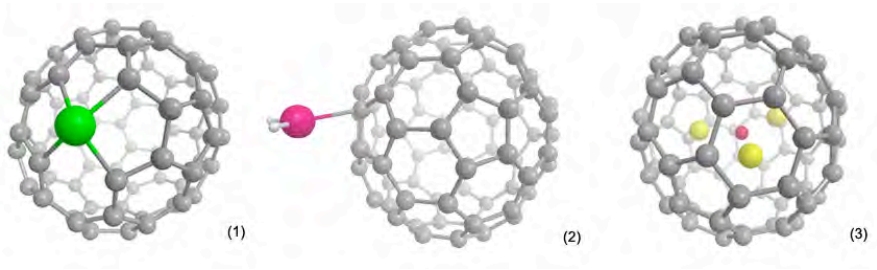

Figure 2.1: Different types of metallofullerenes (1) Heterohedral metallofullerene (2) Exohedral metallofullerene and (3) Endohedral metallofullerene.

Heterohedral metallofullerenes present carbon atoms replaced by non-carbon atoms, i.e nitrogen, boron, silicon, platinum or iridium. Azafullerenes were the first type of heterohedral fullerenes spectroscopically detected, and are the most studied as they can be obtained in macroscopic quantities.[37] On the other hand, fullerene derivatives with either boron, platinum or iridium have only been detected in mass spectroscopy.[38] In all cases, they exhibit reduced stability compared to their respective fullerene compounds with only carbon atoms.

When a metal reacts with the fullerene surface, an exohedral metallofullerene is formed. Hawkins et al.[39] completely characterized the first exohedral fullerene synthesized which was $1,2-C_{60}(OsO_4(4-t-BuC_5H_4N_2)_2)$. Complexes formed in these reactions where fullerene cages react with electron-rich metallic centers are pretty stable.

Endohedral fullerenes (from Greek: *endon* (within) and *hedra* (face of a geometrical form)) are formed when the metal atom is encapsulated inside the cage. The existence of this type of metallofullerenes was considered in the same year of the discovery of the C_{60}, when Heath et al.[40] presented evidence for the formation of a stable $C_{60}La$, with the La atom trapped inside the C_{60} cage.

Although the IUPAC nomenclature suggests $i-MC_k$ to describe endohedral metallofullerenes, the most commonly used nomenclature is $M@C_k$ where the symbol @ indicates that the metal M is trapped inside the cage C_k.

Endohedral metallofullerenes (EMFs) can be classified in four different subtypes: the so-called classical, metallic carbides, metallic tri-nitride template (TNT), and metallic oxide EMFs (see Figure 2.2). The classical metallofullerenes present the formula

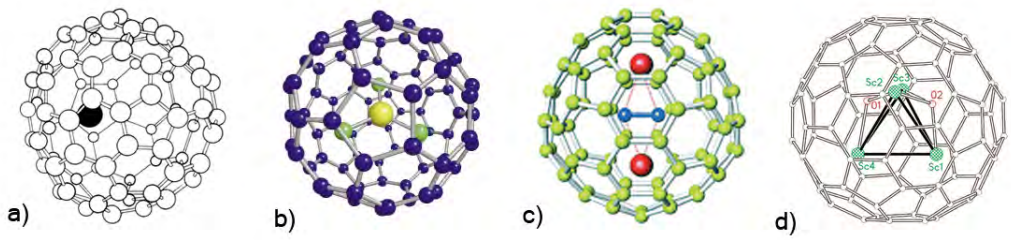

Figure 2.2: Classification of the endohedral metallofullerenes: a) classical ($La@C_{82}$), [41] b) metallic carbide ($Sc_2C_2@C_{80}$), [42] c) TNT ($Sc_3N@C_{80}$), [43] and d) metallic oxide ($Sc_4(\mu_3-O)_2@C_{80}$). [44]

$M_x@C_{2n}$, where x=1-2 and $68 \leq 2n \leq 92$. The most abundant classical EMF family corresponds to $M@C_{82}$, being $La@C_{82}$ the first example synthesized.[41,45] Other metal atoms were encapsulated inside the C_{82} cage, such as scandium, yttrium and lanthanide, among many others.[45–47]

Metallic carbide EMFs present an M_xC_2 cluster encapsulated inside the fullerene cage. In 2001, Shinohara and coworkers reported the first characterization of a metallic carbide endohedral compound.[42] The synthesized fullerene consisted on a

Sc_2C_2 unit encapsulated inside the D_{2d} isomer of the C_{84} cage. Other examples are $Y_2C_2@C_{82}$ (isomers C_s, C_{2v}, and C_{3v}), $Ti_2C_2@D_{3h}-C_{78}$, $Sc_2C_2@C_{2v}-C_{68}$, $Sc_2C_2@C_{3v}-C_{82}$, $Sc_3C_2@I_h-C_{80}$, and $Gd_2C_2@D_3-C_{92}$.[48] Recently, the metal carbide metallofullerene $Sc_4C_2@I_h-C_{80}$ (or more exactly $C_2@Sc_4@I_h-C_{80}$) has been synthesized where a C_2 unit is surrounded by a Sc_4 tetrahedron and then encaged inside the I_h-C_{80} cage.[49]

The most studied endohedral fullerenes are the metallic nitride (TNT) endohedral compounds because they can be produced in macroscopic quantities using the Krätschmer-Huffman arc method with presence of nitrogen (see next section).[43] Their formula is $A_{3-x}B_xN@C_y(x=0-3, A, B=metal, y=68, 78, 80)$ and the archetypal compound is $Sc_3N@C_{80}$,[43] which is the third most abundant fullerene, only exceeded by C_{60} and C_{70}. Other TNT members are $Sc_3N@C_{78}$ and the non-IPR $Sc_3N@C_{68}$.

Finally, in 2008 Stevenson and coworkers synthesized the first type of metallic oxide EMFs, which consists on a scandium-based oxide cluster ($Sc_4(\mu_3-O)_2$) encapsulated inside the I_h-C_{80} cage.[44]

Apart from the encapsulation of metal-based compounds inside fullerene structures (i.e the so-called metallofullerenes), diatomic molecules,[50] and noble gases[51] have been trapped inside fullerene cages as well.

The TNT endohedral metallofullerenes $X_3N@C_{78}$ (X=Sc, Y) and the noble gases endohedral complexes $Ng@C_{60}$ and $Ng_2@C_{60}$ are the main interest of this thesis, hence a more detailed description will be given in the next sections.

2.2 Trimetallic nitride template (TNT) endohedral metallofullerene: $X_3N@C_{78}$ (X=Sc,Y)

2.2.1 Synthesis of TNT endohedral fullerenes

Although several methods for the production of endohedral metallofullerene compounds exist,[46] the most extended procedure is the modified arc-discharged Krätschmer-Huffman method (also called *trimetallic nitride template (TNT)* method) with presence of a nitrogen source.[43] In the latter process, an arc-discharged reactor is used for the fullerene production (see Figure 2.3), where graphite rods packed with the desired metal oxide (i.e. Sc_2O_3 for scandium-based EMFs or different metal oxides if one wants to obtain mixed endohedral fullerenes) are employed. Packed rods are annealed over several hours before they are finally burned in an helium or argon atmosphere. It was found that the presence of N_2 resulted in significantly enhanced yields, and $Sc_3N@C_{80}$ was obtained in macroscopic quantities which exceeded those of, at that time, the third most-abundant fullerene cage C_{84}. This method presents

some drawbacks, most notable is that it produces a large amount of empty C_{60} and C_{70}. Dunsch and coworkers attempted to produce TNT endohedral fullerenes using calcium cyanamide ($CaNCN$) packed into the graphite rods during the arcing. Although they were able to produce $Sc_3N@C_{80}$ and $Sc_3N@C_{78}$ the yields obtained ranged between 3% and 42%.[52] A substantial improvement was achieved with the development of the *reactive gas atmosphere* method developed by Dorn and coworkers.[52] The graphite rods were packed using the same metal oxide as in the TNT method, but ammonia gas was introduced as the nitrogen source. Using the latter conditions, EMFs were produced as the major products with less than 5% of empty fullerenes.

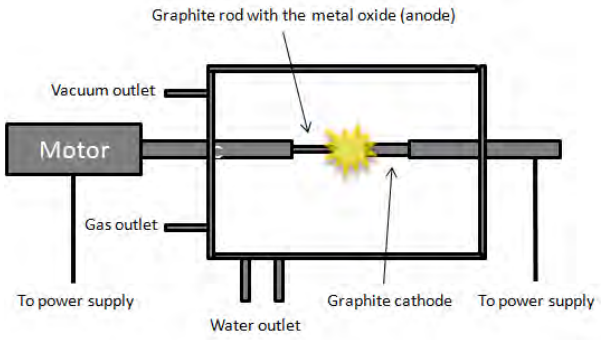

Figure 2.3: Arc-discharge reactor for the production of fullerene compounds (adapted from ref.[48]). The graphite rod can be packed with different metal oxides which determine the final endohedral metallofullerene generated. The presence of a nitrogen source in the gas atmosphere enhances the production of TNT metallofullerenes.

Stevenson and coworkers improved the TNT method by combining with what is called CAPTEAR (Chemically Adjusting Plasma Temperature, Energy, and Reactivity) approach.[53] The temperature and the energy of the plasma inside the reactor during the arcing process is modulated introducing a source of NO_x gas. Following this strategy, a 96% of the soot extract was shown to be $Sc_3N@C_{80}$, whereas the remaining 4% $Sc_3N@C_{78}$ and small amounts of empty cages. It should be emphasized that the original TNT method only produced 4 % of $Sc_3N@C_{80}$.[43]

Several TNT endohedral metallofullerenes have been synthesized using the abovementioned procedures. Figure 2.4 shows the synthesized TNT endohedral fullerenes ($X_3N@C_x$) up to date.[54]

2.2.2 Bond model

It is widely accepted that the charge distribution in $Sc_3N@C_k$ metallofullerenes may be formally described as $(Sc_3N)^{6+}@C_k^{6-}$, however the abovementioned charges are only formal because covalent interactions between the cluster and the cage are rather

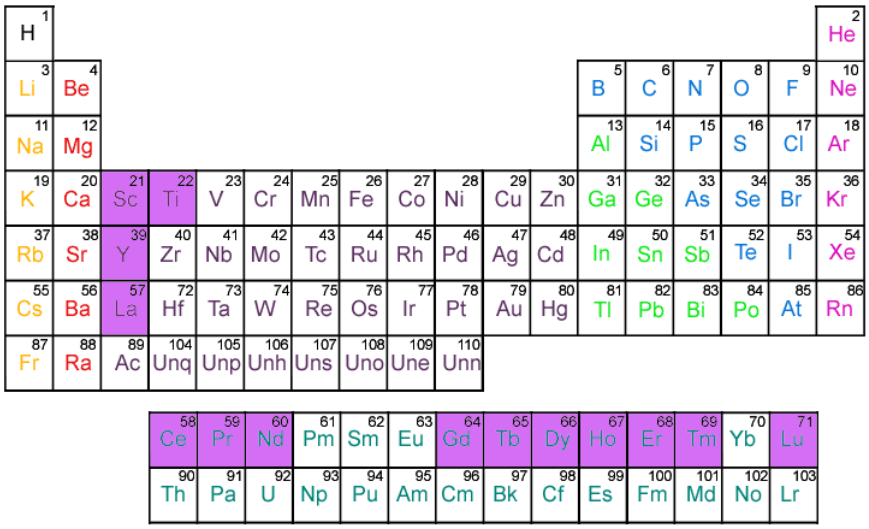

Figure 2.4: TNT endohedral metallofullerene that have been prepared up to date (marked in lilac).[54]

strong.[55]

The HOMOs of C_{78}, C_{78}^{6-}, and $Sc_3N@C_{78}$ have contributions mostly located at the equatorial belt, and C_{78} LUMOs are basically antibonding π orbitals centered in pyracylenic bonds, that will be occupied when the TNT unit is situated inside the cage. A more detailed description will be given in the results and discussion chapters.

The HOMO-LUMO gap for $Sc_3N@C_{78}$ is 1.24 eV, whereas C_{78} has a gap of 0.63 eV, which could explain the endohedral fullerene stability. By comparing the HOMO-LUMO gaps with other TNT metallofullerenes, one can notice that they have similar values, 1.27 and 1.18 eV for $Sc_3N@C_{68}$ and $Sc_3N@C_{80}$ respectively, so these electronic considerations could be an important factor when it comes to determining which fullerenes can exist in the endohedral form. Poblet *et al.* proposed the LUMO+3-LUMO+4 rule to predict the most favorable fullerene isomers for encapsulating cluster metals (see next sections).[56]

2.2.3 Structure and Isomers of $X_3N@C_{78}$ (X=Sc,Y)

Several endohedral fullerenes containing the C_{78} cage have been synthesized. Most of them involve the D_{3h} : **5** cage, which is the second most unstable isomer for

the free cage. The X-ray crystallography revealed that the flat Sc_3N cluster is oriented so that it lies near the horizontal plane of the C_{78} cage, and every Sc atom is situated over a [6,6] pyracylene-type carbon bond (see Figure 2.5).[57] Moreover, the N-Sc distances are 1.988 Å(Sc1), 1.983 Å (Sc2), and 2.125 Å (Sc3), and the shortest C-Sc have bond distances from 2.02 to 2.11 Å. It is important to remark that most of TNT endohedral fullerenes present a planar configuration of the encapsulated cluster metal, that is indeed the case of $Sc_3N@C_{78}$[57] but also of other TNT endohedral compounds such as $Sc_3N@C_{80}$,[43] $Sc_3N@C_{68}$,[58] $ErSc_2N@C_{80}$,[59] $Lu_3N@C_{68}$,[60] $Tb_3N@C_{68}$[61] among many others. However, it was found that the large Gd_3N cluster inside $I_h - C_{80}$ adopts a non-planar conformation.[62] X-ray crystallographic data indicated a pyramidal structure, where the nitrogen atom of the cluster is displaced 0.5 Å out of the Gd_3 plane. In contrast, a nearly planar structure (the nitrogen atom is displaced 0.07 Å) was found for the relatively large Dy_3N unit encapsulated inside C_{80}, even though the ionic radius of Dy^{3+} is similar to that of Gd^{3+} (0.91 and 0.94 Å, respectively).[63] An slight pyramidalization of the central nitrogen atom (only 0.13 Å) of the Y_3N unit in the pyrrolidine adduct of $Y_3N@C_{80}$ was also detected.[64]

Other endohedral fullerenes that employ the $D_{3h} - C_{78}$ are $La_2@D_{3h} - C_{78}$[65,66] and $Ce_2@D_{3h} - C_{78}$,[67] where the metal dimers lie on the C_3 axis close to the polar caps of the carbon cage. Finally, the endohedral fullerene originally described as $Ti_2@C_{80}$ was found both by theory and experiment to correspond to the titanium carbide $D_{3h} - C_{78}$ based endohedral fullerene (i.e. $Ti_2C_2@D_{3h} - C_{78}$).[68,69]

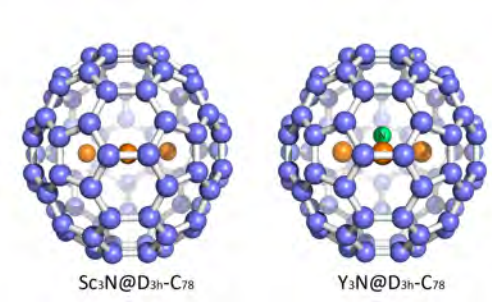

Figure 2.5: Position of the metal cluster inside the endohedral compounds $Sc_3N@D_{3h} - C_{78}$ and $Y_3N@D_{3h} - C_{78}$. The Sc_3N unit is situated in the horizontal symmetry plane of the endohedral compound, whereas in the case of Y_3N the nitrogen atom is slightly pyramidalized.

Popov et al.[70] reported that the stability order of the isomers of $D_{3h} - X_3N@C_{78}$ strongly depends on the cluster size. The TNT unit Sc_3N inside the $D_{3h} - C_{78}$ remains planar, whereas Y_3N and Lu_3N are forced to adopt a pyramidal structure which produces a high destabilization (see Figure 2.5). Therefore, when relatively large metal clusters are encapsulated inside $D_{3h} - C_{78}$, those isomers where the unit

can adopt a planar configuration are preferred (in the case of Y_3N, Lu_3N, Dy_3N, Tm_3N, and Gd_3N the most stable isomer is the non-IPR $C_2(22010)$, see Figure 2.6).

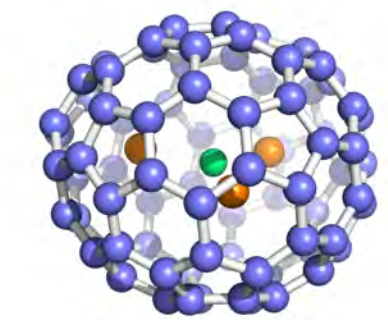

Figure 2.6: The most favorable cage $C_2(22010) - C_{78}$ for the encapsulation of large metal clusters such as Y_3N, Gd_3N, Dy_3N, or Tm_3N.

Some experimental spectroscopic studies of the TNT $Tm_3N@C_{78}$,[71] and the major isomer of $Dy_3N@C_{78}$[72] indicated that the C_2 cage rather than the D_{3h} was obtained. The ionic radii of the metal atoms thulium and dysprosium are 0.87 and 0.91 Å, respectively.[73] The spectroscopic properties of the yttrium based endohedral fullerene $Y_3N@C_{78}$ are expected to be similar to that of Dy and Tm, due to the high similarity of their ionic radii (the radius for Y is 0.90 Å).[73] Recently, the $Gd_3N@C_2(22010) - C_{78}$ has been synthesized and characterized by single crystal X-ray diffraction.[27] Two of the gadolinium atoms are directly faced to the [5,5] bonds, whereas the third gadolinium is at the center of an hexagonal face of fullerene. This study represents the first structural examination of large metal ions encapsulated inside the relatively small C_{78} cage.

The $C_2 - C_{78}$ isomer does not obey the IPR rule, therefore it presents pentagonal rings abutted with one of the metal atoms directly faced to them (see Figure 2.7). This characteristic is common in all non-IPR TNT isomers that have been synthesized up to date: $Gd_3N@C_s(39663) - C_{82}$,[74] $M_3N@C_s(51365) - C_{84}$ (M=Gd, Tb, Tm),[61,75] as well as $La@C_2 - C_{78}$.[76] In these non-IPR compounds from one up to three adjacent pentagonal rings can be located. For instance, $La@D_2(10611) - C_{72}$, [77–79] and $DySc_2N@C_s(17490) - C_{76}$[80] present two pairs of [5,5] bonds, whereas $Sc@C_{66}$,[81] $Sc_3N@C_{2v}(7854) - C_{70}$,[82] as well as the cyrstallographically determined structures $Sc_3N@D_3(6140) - C_{68}$,[83] and $Sc_2C_2@C_{2v}(6073) - C_{68}$[84] have three [5,5]

bonds. The pentalene unit (i.e. two pentagonal rings attached) produces an eight-cycle around the periphery which is anti-aromatic in character. Due to the electronic transfer from the inner cluster to the fullerene cage produced in endohedral fullerenes and the proximity of the metal atoms to pentalene units, the aromaticity of these rings is highly enhanced.[85] The coordination of several metal ions to isolated pentalene units has been studied by some organometallic chemists.[86,87]

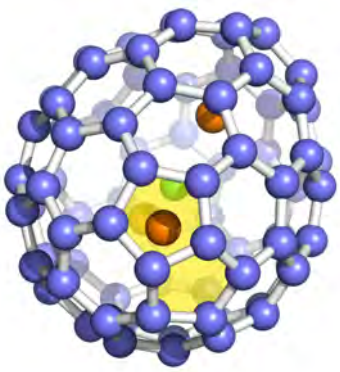

Figure 2.7: Position of the metal cluster inside the $C_2(22010) - C_{78}$ cage. One of the metal atoms is directly faced to the pentalene unit ([5,5] bond).

The metal cluster not only determines the stabilization for the different isomers, but also dictates the exohedral reactivity of the cage.[88] Apart from that, $Sc_3N@D_{3h}-C_{78}$ has a cage motif similar to the empty C_{60}, and is one of the few TNT endohedral metallofullerenes that have pyracylene-type sites (the D_{5h} isomer of C_{80} does also present type A bonds). Thus, the reactivity of the $Sc_3N@C_{78}$ is expected to be similar to C_{60}. The exohedral reactivity of these TNT endohedral compounds will be explained in detail in the Reactivity, and Results chapters.

2.2.4 Stability of the TNT endohedral metallofullerenes

As already mentioned, this new class of metallofullerenes exhibits a large stability. The IPR rule for predicting metallofullerene stability seems less of a rule and more a suggestion, as a growing number of endohedral compounds containing [5,5] bonds have been found. Therefore, other criterions are needed.

Aihara proposed in the context of HMO calculation the bond resonance energy (BRE),[89] which although departure from planarity could not be described, it has been applied satisfactorily not only to TNT endohedral compounds but also to classical endohedral metallofullerenes to study the kinetic stability of these molecules. The BRE gives the contribution of a certain π bond to the topological resonance energy of a molecule. If the minimum BRE has a negative value, the molecule will be kinetically unstable, so kinetically unstable fullerenes will tend to form kinetically stable metallofullerenes. The increase of the stability of the endohedral fullerene can be attributed to the stabilization of the π-electronic system of the cage due to the positively charged metal, and moreover, there exists an electrostatic interaction between the anionic cage and the cationic metal. The main inconvenience of this method is the inability of determining the capacity of fullerenes cages to encapsulate TNT units.

Campanera et al. proposed the LUMO+3-LUMO+4 gap method.[56] As in endohedral metallofullerenes a formal transfer of six electrons from the metal to the cage is produced, the final HOMO-LUMO gap of the TNT endohedral metallofullerene can be estimated from the LUMO+3 and LUMO+4 gap of the free cages. The calculated and estimated values were 1.27/1.17 eV for $Sc_3N@C_{68}$, 1.24/1.16 eV for $Sc_3N@C_{78}$, and 1.18/1.17 eV for $Sc_3N@C_{80}$. Therefore, only free isomers with a large (LUMO+3)-(LUMO+4) gap will be good candidates to encapsulate TNT units inside its cage. However, the latter criterion might significantly over- or underestimate the HOMO-LUMO gap when species other than Sc_3N are trapped inside, because of the different energy of the LUMO of the metal.[55] In addition, the LUMO+3-LUMO+4 gap rule does not account for the size of the encapsulated unit, which is very important to determine the most stable endohedral isomer.[70]

2.2.5 Potential applications

The discovery of the fullerene chemistry has given rise to several possible applications of these materials in the field of biology, nanotechnology, and medicine. Hereafter some examples are given.

In medical technology, gadolinium chelate compounds are used as magnetic resonance image (MRI) contrast agents, and they are being used to detect brain tumors and hepatic carcinoma.[90,91] The MRI techniques are not strongly sensitive, and sometimes more targeting probes have to be accumulated to enhance the image quality. Under these circumstances, new materials with stronger proton relaxivity and higher MR signal at lower concentration such as a gadolinium based fullerene could improve the process. A water-soluble polyhydroxylated gadolinium metallofullerene $Gd@C_{82}(OH)_n$ actually exhibits a more than 20-times higher water hydrogen MR imaging relaxivity than that of the commercial MRI contrast agents such as Gd-DTPA (Magnevist).[92] The proton relaxation mechanism of different lanthanoid

metallofullerenols, $M@C_{82}(OH)n$ (M=La, Ce, Gd, Dy, and Er) was studied in detail by Shinohara *et al.*[77] They found that the relaxivity values for the metallofullerenols is much higher than the respective free ions. As it can be seen in Figure 2.8, there is an strong signal enhancement for the case of gadolinium compounds, whereas for the rest only an slight increase on the signal was observed.

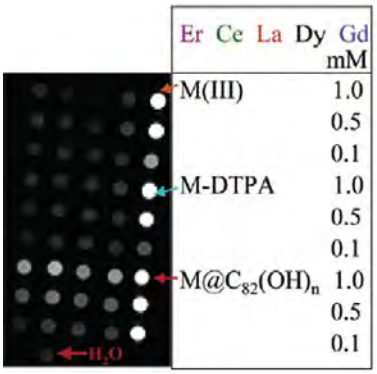

Figure 2.8: Phantom MR images of different lanthanoid ions (first three rows), lanthanoid-DTPA complexes (next three rows) and lanthanoid metallofullerenols(final rows).[77]

In TNT metallofullerenes, up to three metal atoms are encapsulated inside the cage. Therefore, a higher proton relaxivity might be expected taking into account that, at room temperature, the magnetic moments of the three magnetic ions fluctuate. [93] The difference in energy between the ferromagnetic (FM) and anti-ferromagnetic (AFM) couplings for $Gd_3N@C_{80}$ is only 0.1 $kcal.mol^{-1}$ at PBE+U/plane-waves level of theory.[94,95] The latter nearly degenerate situation, where the Gd_3N unit can either present a FM situation (21 unpaired electrons) or an AFM (7 unpaired electrons) is associated with enhanced proton relaxivity. *In vitro* and *in vivo* imaging studies on functionalized $Gd_3N@C_{80}$ indicated a higher proton relaxivity as compared to the commercial agent (e.g. gadodiamide).[96] Moreover, at concentrations of an order of magnitude lower an equivalent visualization to that of commercial compounds was observed. It was also detected that the functionalized $Lu_3N@C_{80}$ exhibited very low MR imaging relaxivity. Additionally, the encapsulation of the metal inside the cage would present the advantage of avoiding possible secondary reactions with biomolecules.

The encapsulation of a radioactive metal atom as holmium or lutetium could be useful as a tracer or as anticarcinogenic agent. In Figure 2.9, the different metals that can form endohedral fullerenes as well as those elements useful for nuclear medicine elements are marked.
The ^{165}Ho metallofullerenes were chemically functionalized to make them soluble in

Figure 2.9: Representation of the different elements capable of forming endohedral fullerenes (marked in lila), and those useful for nuclear medicine (marked in yellow). [97]

water, and were neutron activated to ^{166}Ho to investigate the biodistribution and metabolism properties.[97] The biodistribution of ^{166}Ho was studied during 48h on mice. Every 1, 4, 24 and 48 h mice that the holmium compound was administered were sacrificed to study the accumulation of the fullerene compound to several tissues: muscle (thigh), bone, skin, uterus/ovaries, large intestine, stomach (emptied), liver, kidneys, spleen, fat (abdominal), thymus, heart, lungs, brain, and blood. The metallofullerene was distributed throughout the body, except for brain and fat where the blood flow is limited. After 48h a significant percentage of the total injected compound was still retained, however all tissues decreased the ^{166}Ho concentration, except for the bone. In some other studies, water-soluble derivatives were basically accumulated in the liver ($>$ 90-95%), and an slow clearance was observed ($>$ 1 week). [98–100] The location of the holmium metallofullerenol in bone might suggest that it could be used as a chemotherapy agent for treating leukemia, bone cancer, or bone pain. There are other examples of polyhydroxylated compounds that exhibit a high affinity for bone.[97]

More applications as nanodevices in areas as diverse as spintronics are proposed. In addition, as endohedrals can stabilize reactive species inside the cage. They can be used as nondissociating salts in electrochemistry. Finally, due to their exciting electronic and magnetic properties they could be applied to quantum computing.

2.3 Noble gases endohedral fullerenes

2.3.1 Encapsulation of noble gases inside C_{60} and its stability

Six years after the fullerene discovery, the first endohedral compounds containing either helium, neon, or argon were synthesized.[101] The $Ng@C_{60}$ derivatives were obtained after collision of the noble gas cations and the neutral C_{60}. Another possibility for trapping He atoms into the C_{60} cage was employing the standard fullerene preparation procedure but in the presence of helium (approximately one $Ng@C_{60}$ molecule in a million free fullerenes was detected).[51] A wide range of studies involving the purification and enrichment of $Ng@C_{60}$ was also carried out.[102,103] The obtainment of $He@C_{60}$ and $Ne@C_{60}$ was additionally achieved heating C_{60} under several atmospheres of ^3He and Ne and in the presence of cyanide which clearly enhanced the reaction yield.[104] This synthesis procedure was satisfactorily applied to obtain all noble gases endohedral compounds.[51,104–106] The mechanism by which noble gases are encapsulated inside the cage is through the formation of an open "window" in the fullerene surface (see Figure 2.10).[107] This window is created by breaking some carbon bonds and should be large enough to permit the insertion of the noble gas moiety. The activation barrier for the release of the noble gas atoms from C_{60} was experimentally detected to be about 90 $kcal.mol^{-1}$.[108] Using classical statistical mechanics the equilibrium constants for the noble gas insertion were also estimated.[109] Scuseria and coworkers proposed a mechanism for the "window" formation that involved the rupture of a [5,6] bond at the triplet state, however the activation barrier found was approximately twice as large as the experimental prediction.[110]

Because of the hard-to-control method of production of fullerene compounds and the low selectivity of the process, it is quite appealing to obtain endohedral fullerenes from free fullerene compounds. In this context, Rubin proposed what he called the *molecular surgery*. This strategy consists of (1) *incision* of the fullerene cage to form an opening on the surface, (2) introduction of small molecule(s) or atom(s), and (3) *suture* of the opening.[111] For the past decade, the development of the *molecular surgery* has been a challenging task. Actually, the production of macroscopic quantities of noble gas endohedral fullerenes was not produced until Komatsu and co-workers applied the so-called *surgery of fullerenes*.[112] This process allowed the synthesis of $He@C_{60}$ and other endohedral fullerenes.[113–118]

The interaction between the C_{60} molecule and all noble gases was calculated theoretically using an atom-atom potential method, which indicate that the $Ar@C_{60}$ compound was the most stable complex among all possibilities.[119] In another study, classical molecular dynamics simulations performed on the endohedral complexes $Ng@C_{60}$ (Ng = He, Ne, Ar, Kr, Xe) showed a substantial stability relative to C_{60} + Ng, with the Ar complex being the most stable as well.[120] It was theoretically detected that the polarizability of $Ng@C_{60}$ increases from He-Kr, but is distinctly smaller than the sum of the Ng atoms and C_{60}.[121]

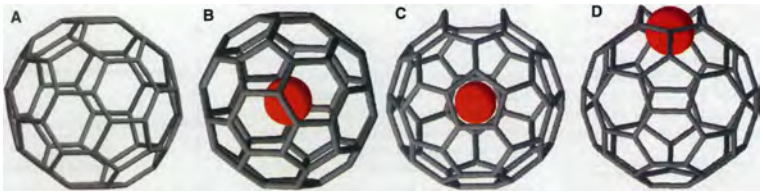

Figure 2.10: Representation of: (A) C_{60}, (B) $X@C_{60}$, (C) C_{60} with an open "window", a bond is broken and an atom X is inside, (D) $X@C_{60}$ with an open window where the atom X is being encapsulated.[97]

The possibility for obtaining noble gas dimer encapsulation inside fullerenes was considered in 1997 by Giblin and coworkers.[122] One year later, the first noble gas dimer endohedral compound was obtained corresponding to the addition of two helium and two neon atoms inside C_{70} (i.e. $He_2@C_{70}$, $Ne_2@C_{70}$).[123,124] However, the insertion of two helium atoms inside C_{60} was not produced until 2002 by Sternfeld and coworkers.[125] The ratio was very low as only one $He_2@C_{60}$ was obtained per each two hundred molecules of $He@C_{60}$ (i.e. 200:1), whereas in the case of C_{70} a relation of 20:1 was obtained. The $Ne_2@C_{60}$ and the mixed species $NeHe@C_{60}$ may have also been observed in experiment, although only $Ne_2@C_{70}$ and $NeHe@C_{70}$ could be identified using the heavier NMR active isotope ^{22}Ne.[124,126] The deformation energy of the noble gas endohedral complexes of C_{60}, i.e. $Ng@C_{60}$ (Ng = He, Ne, Ar, Kr, and Xe) and $Ng_n@C_{60}$ (Ng = He (n=2-4), and Ne (n=2)) was studied in detail by Scuseria *et al.*[127] In all cases, the distortion energy found at B3LYP/6-31G**//LDA/3-21G was very low (0.5 and 1 $kcal.mol^{-1}$ for the single and dimer noble gases compounds, respectively). They reported repulsive interaction energies for all systems (1 $kcal.mol^{-1}$ for $Ng@C_{60}$ Ng=He, Ne, 7 and 14 $kcal.mol^{-1}$ for Ng=Ar, Kr, and 7-30 $kcal.mol^{-1}$ for $He_2@C_{60}$ and $He_4@C_{60}$). However, the B3LYP method underestimated the interaction energy of the endohedral $H_2@C_{60}$ by approximately 5 $kcal.mol^{-1}$ as compared to the more appropriate M05-2X level.[128] The latter observation supports that Scuseria values for the interaction energies might be substantially underestimated.

The preparation of $He@C_{60}$ and $He_2@C_{60}$ using an explosion-based method has been recently published.[129] The explosion energy is converted to kinetic energy of the gas molecules which obtain sufficient energy to penetrate inside fullerenes. The procedure is simple, safe, and enables the preparation of endohedral non-metal fullerenes with a relatively high efficiency.

2.3.2 Bond model

In contrast with other endohedral compounds, the single noble gas encapsulation does not involve an electronic transfer. However, the situation is substantially changed

when two large noble gas atoms are encapsulated within the cage. Krapp and Frenking theoretically determined that the encapsulation of two xenon atoms inside C_{60} lead to an electronic transfer from 1 to 2 electrons from the Xe_2 moiety to the fullerene cage.[130] Therefore, a genuine chemical bond is formed between both xenon atoms, and the bond model for the endohedral compound can be represented as $Ng_2^{+2}@C_{60}^{-2}$. This charge transfer is also produced in $Ar_2@C_{60}$ and $Kr_2@C_{60}$ to a lesser extent.

2.3.3 Structure and Isomers of $Ng@C_{60}$ and $Ng_2@C_{60}$ (Ng=He, Ne, Ar, Kr, Xe)

Single noble gas endohedral complexes are considered to have icosahedral symmetry (see Figure 2.11).[127] Although helium and neon totally fit inside the C_{60} carbon cage, some overlap of the van der Waals radii occurs for the largest noble gases.

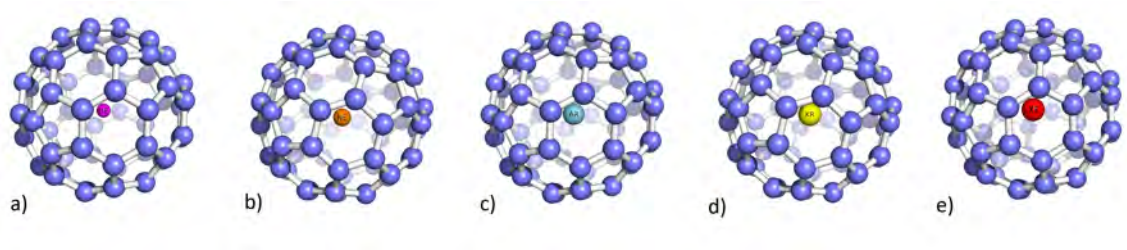

Figure 2.11: Single noble gas endohedral compounds a-e $Ng@C_{60}$ Ng= He-Xe.

Krapp and Frenking performed MP2/TZVPP//BP86/TZVPP calculations which indicated that the most favorable cage symmetry for the encapsulation of noble gas dimers was the D_{3d} with the exception of $Xe_2@C_{60}$ where the D_{5d} symmetry was preferred.[130] In the D_{5d} isomer, the noble gas dimer is facing two opposite pentagonal rings of the fullerene cage, whereas in the D_{3d} they are directly faced to the center of two hexagonal rings (see Figure 2.12). Another isomer with D_{2h} symmetry where the noble gas moiety is faced to two opposite pyracylene bonds could also be considered. Although the energy differences are very low (less than 2 $kcal.mol^{-1}$ in most of the cases, except for xenon) the D_{3d} isomer for He-Kr and the D_{5d} for Xe correspond to the most favorable situations.[130] Moreover, they observed that the noble gas dimer rotation is produced in the case of the lighter homologues.[130]

Free noble gas dimers are only observed at extremely low temperatures or for a very short period of time in collision, because of the small attractive force that exists between the two atoms (for instance, just 0.1 $kcal.mol^{-1}$ for Ne_2). The encapsulation of noble gas dimers inside fullerene cages involves the shortening of the Ng-Ng distance, and they are forced into contact by the cage and vibrate and rotate within it like diatomic molecules. High level ab-initio calculations predicted Ng-Ng bond distances for the free dimers: [He-He]=2.977 Å, [Ne-Ne]=3.099 Å, [Ar-Ar]=3.779

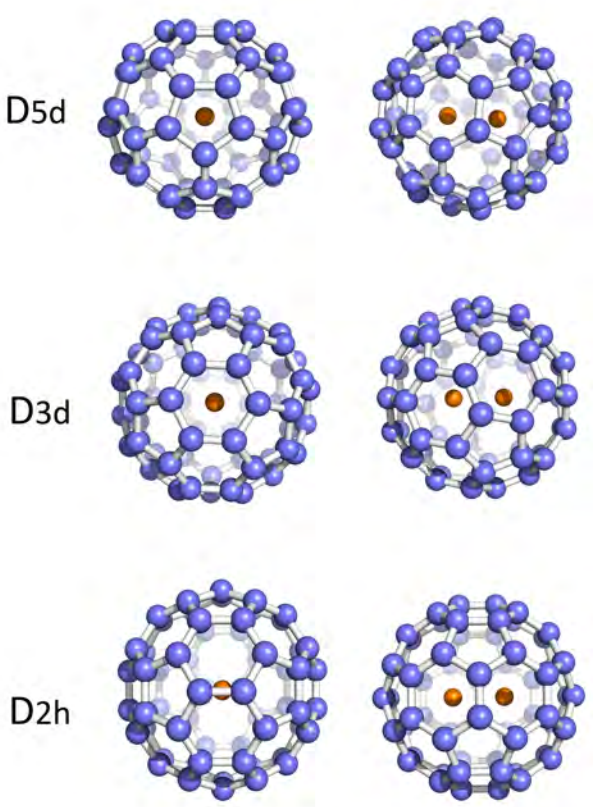

Figure 2.12: Noble gas dimer endohedral isomers $He_2@C_{60}$ presenting D_{5d}, D_{3d}, D_{2h} symmetry. The most favorable isomer for He-Kr is the D_{3d}, whereas for Xe is the D_{5d}.

Å, [Kr-Kr]=4.040 Å, and [Xe-Xe]=4.420 Å.[131,132] Calculated bond distances are in good agreement with the experimental values: 2.970, 3.091, 3.757 Å for He_2, Ne_2, and Ar_2, respectively.[133] The Ng-Ng distance is dramatically decreased after the insertion into the C_{60} cage: [He-He]=1.951 Å, [Ne-Ne]=2.104 Å, [Ar-Ar]=2.352 Å, [Kr-Kr]=2.447 Å, and [Xe-Xe]=2.503 Å (obtained at BP86/TZ2P, see chapter 8). The latter bond distances compared to free dimers are approximately decreased by 1 to 2 Å going from He to Xe. However, the bond distance for the xenon dimer in C_{60} should be better compared to that of the ion Xe_2^+ (3.087 Å, determined by X-ray analysis). Still, the Xe-Xe distance in Xe_2^+ is 0.6 Å larger than the one found for the encapsulated Xe_2 inside C_{60}.

The fullerene cage after the He_2 and Ne_2 introduction is not hardly affected, as the carbon bond distances and pyramidalization of the carbon atoms are not substantially changed.[130] However, this is not the case for the larger noble gas endohedral compounds $Ar_2@C_{60}$, $Kr_2@C_{60}$, and $Xe_2@C_{60}$. There is a clear elongation of the C-C bond distances of the cage, especially for the xenon case.[130]

2.3.4 Potential applications

Helium based endohedral fullerenes such as $^3He@C_{60}$ as a starting material can be used to follow the course of a certain reaction performing helium NMR spectrums of the reaction mixture.[42,51,134,135] The number of products formed and the relative amounts can be easily determined. Moreover, the separation of the different products might also be followed with helium NMR. Even the regioselectivity of a reaction might be detected evaluating the different helium shifts. Moreover, the release of He from inside the cage should be readily evaluated as the NMR signal for $^3He@C_{60}$ might be replaced by the characteristic signal of helium gas dissolved.

Noble gas derivatives could also be detected at extraordinarily low concentrations thanks to the high sensitivity of the mass spectrometer. For instance, if 1 mg of $^3He@C_{60}$ were dissolved in a 50 meter long swimming pool, the helium compound could be detected in 1ml of water. Because of the high sensitivity, these compounds might be useful as a tracers.[51]

Due to this highly sensitive detection of noble gas compounds, noble gas endohedral fullerenes of C_{60} and C_{70} could be detected in deposits associated to the impact of an asteroid or comet (bolide) with the Earth (i.e. Sudbury Impact Crater located in Ontario, Canada).[136] There are different scenarios for the fullerene presence in these diposits. Fullerene compounds might be formed during the impact of the asteroid or comet with the Earth, or might already be present in the bolide. Another possibility might be the formation of fullerene compounds during the wildfires triggered by the impact. However, the anomalous ratios of $^3He/^4He$ and $^{40}Ar/^{36}Ar$ found suggest that the fullerene compounds are extraterrestrial in origin.

Chapter 3

Exohedral reactivity

Fullerenes are generally involved in typical electron-deficient polyolefines reactions, as reductions, cycloadditions, nucleophilic additions, hydrogenations, radical additions, and halogenations. They can also form transition metal complexes and participate in hydrometalation reactions (see Figure 3.1). Moreover, fullerenes can be oxidized and give reactions with electrophiles. Hirsch et al.[137] have written several books about fullerenes reactions.

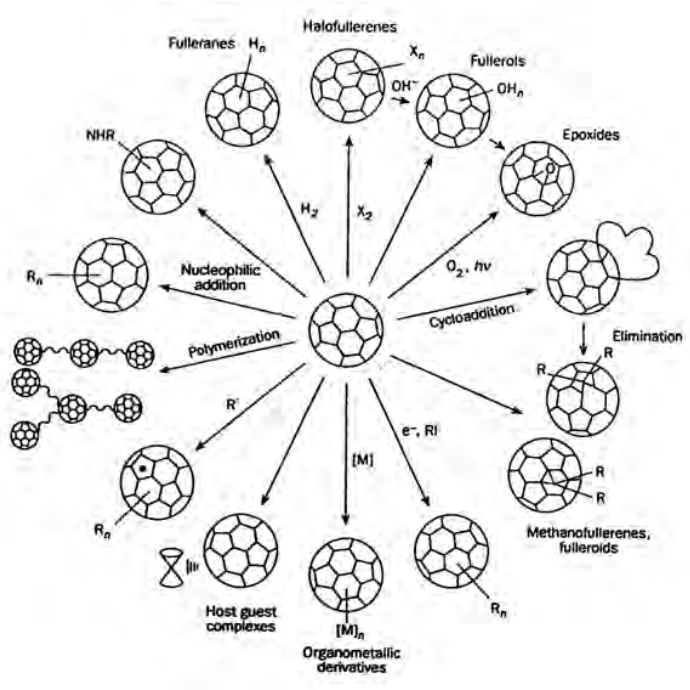

Figure 3.1: Scheme of the different reactivity of C_{60}.[138]

This thesis aims to study the exohedral reactivity of fullerene compounds. Hence, a

whole chapter concerning the main reactions studied will be presented. The project is basically based on two cycloadditions: Diels-Alder and 1,3-dipolar reactions between the 1,3-cis-butadiene and azomethine ylide (although in some studies other dipoles have also been considered) and either C_{60} or C_{78} fullerenes and their endohedral derivatives (see next chapter). Moreover, the antioxidant properties of some C_{60} derivatives, i.e. the capability of accepting electrons will be studied in detail. Hereafter, more general details about the reactions under study will be given.

3.1 Cycloaddition reactions

Most of the organic reactions involve polar or polarizable reactants, where one reactant can be identified as *electrophilic* and the other as *nucleophilic*. This work is based on a totally different reaction type, and it is one of the major classes of the so-called **pericyclic reactions**. They are usually rearrangement reactions wherein the transition state of the molecule has a cyclic geometry, and the reaction progresses in a concerted fashion. The most famous example is the **Diels-Alder reaction** which occurs between a conjugated diene and an olefin called the dienophile, usually also conjugated, to form a cyclohexene (see figure 3.2). It was formulated by Otto Diels and Kurt Alder in 1928,[139] and due to the big importance of this reaction in the organic synthetic chemistry, they were awarded the Nobel Prize in Chemistry in 1950. The Diels-Alder reaction goes in a single step, and its mechanism is often described as a rotation of the electrons round a six-membered ring (see figure 3.2). The reaction goes so well because of its transition state that has six delocalized π electrons, and thus is aromatic in character (see figure 3.2).[140] As a matter of fact, the electrons do not really rotate at all, but two π bonds disappear and two σ bonds take their place by the electrons moving smoothly out of the π orbitals into the σ orbitals. Such a reaction is called a **cycloaddition** (figure 3.3).

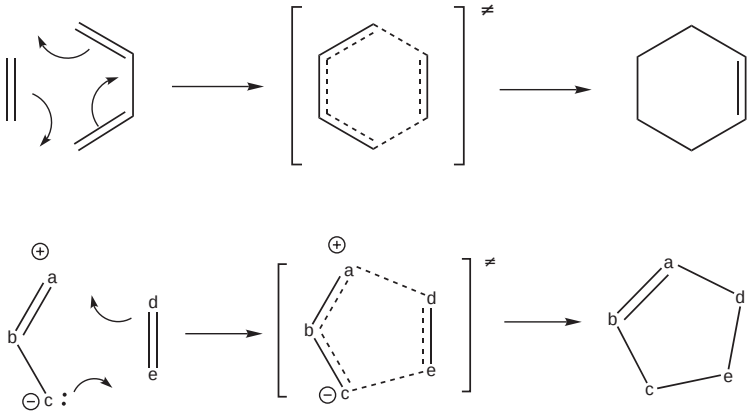

Figure 3.2: The Diels-Alder and 1,3-dipolar reaction mechanisms, where the transition states have six delocalized π electrons.

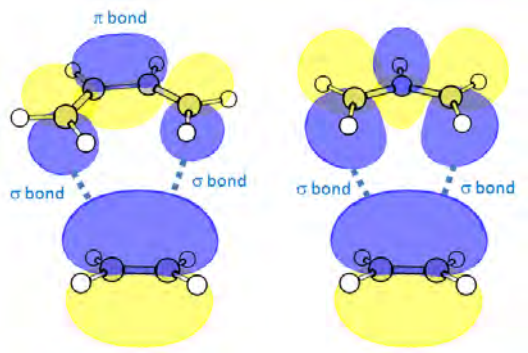

Figure 3.3: Representation of the new two σ bonds formed in the case of the Diels-Alder and 1,3-dipolar cycloadditions.

Another example of cycloaddition reaction is the so-called **1,3-dipolar reaction** (see Figure 3.2). The 1,3-addition of aliphatic diazo compounds, nitrones and structurally analogous molecules was reviewed in 1937 by Smith.[141] However, the generalization of this type of reaction was not produced until 1961,[142] when the knowledge of the reaction scheme led to the prediction and discovery of new 1,3-dipoles. The reaction is produced involving a 1,3-dipole species and a dipolarophile which can range from alkenes, alkynes to fullerenes and related compounds.

1,3-dipoles present four π electrons and at least one resonance structure that presents negative and positive charges in a 1,3 relationship. These compounds are ambiphilic as they can have either a nucleophilic or electrophilic character, although they can also react in the 1,3-position as a spin-coupled biradical. Most of 1,3-dipoles are isoelectronic with either 16 or 18 valence electrons.[143,144] Different types of dipoles exist, ranging from ozone (O_3) and nitrous oxide (N_2O) to azides (N_3R), imines (CR_2NR) or ylides ($CR_2N(R)CR_2$) (see Figure 3.4).

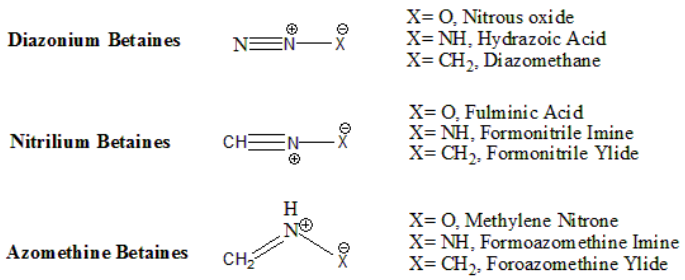

Figure 3.4: Representation of the different 1,3-dipoles

The Diels-Alder and 1,3-dipolar cycloaddition reactions are often described as a $[4\pi_s + 2\pi_s]$ cycloaddition thanks to the Woodward-Hoffmann description. Kenichi

Fukui and Ronald Hoffmann won the Nobel Prize in 1981 (Robert Burns Woodward died in 1979) for the application of orbital symmetry to pericyclic reactions.[145] In this notation, numbers followed by π denote the number of π electrons, therefore butadiene has 4π and dienophile 2π electrons. Most of 1,3-dipoles present a three-orbital system with 4π electrons, thus 1,3-dipolar cycloadditions are also included in the [4+2] cycloaddition group. The suffix $'s'$ stands for suprafacial. Antarafacial $'a'$ and suprafacial $'s'$ are two topological concepts that describe the relationship between two simultaneous chemical bond making and/or bond breaking processes in or around a reaction center. When both changes occur at the same face, the suprafacial interaction is produced.

The Diels-Alder reaction is stereospecific which means that it yields different stereoisomeric reaction products (whose atomic connectivity is the same but their atomic arrangement in space is different) from two stereoisomeric reactants depending on the reaction conditions. Thus, if there is stereochemistry in the dienophile, then it is faithfully reproduced in the final product. When unsymmetrical dienophiles are considered, there are two possible stereochemical orientations with respect to the diene, which are called *endo*, when the reference substituent on the dienophile is oriented toward the π orbitals of the diene in the transition state, and the *exo* approach which implies that the substituent is situated away from the π system. An analogous approach is produced for the 1,3-dipolar cycloaddition. Two possible stereoisomers can be formed by *syn* addition (both 1 and 3 additions are produced in the same face of the dipolarophile). 1,3-dipoles exhibit a characteristic regioselectivity upon reaction with certain dipolarophiles. The latter is easily explained in terms of the Frontier Molecular Orbital (FMO) theory (see next section). These considerations are well described in most of organic books, i.e. Advanced Organic Chemistry by Carey and Sundberg,[146] and Organic Chemistry by Clayden *et al.*, [147] but they will not be further discussed as most studies included in this thesis involve symmetric dienes, dipoles, dienophiles and dipolarophiles with no substituents.

Due to the versatility of these reactions, it is not surprising that during the last decades a lot of theoretical and experimental works have focused on the understanding of the mechanism of these cycloadditions.[143–145,148–159] Actually, there was a big controversy about the mechanism of this type of reactions. Huisgen proposed a concerted mechanism (sometimes asynchronous) on the basis of kinetic and stereochemical results, whereas Firestone suggested a two-step mechanism.[143,144,148,154–157] The majority of the actual theoretical papers studying cycloaddition reactions consider a concerted mechanism and it is widely accepted that a concerted $[4\pi_s + 2\pi_s]$ mechanism is followed in most of the cases, the two-step mechanism being higher in energy than the corresponding concerted one.[150,151,160–163]

3.1.1 Models for chemical reactivity

The prediction of reactivity and regioselectivity of cycloaddition reactions, and in general of all pericyclic reactions, is based on the Frontier Molecular Orbital (FMO) Theory developed by Fukui in 1967.[149,164–167] The regioselectivity of a certain cycloaddition reaction can be rationalized from the interaction of the highest occupied molecular orbital (HOMO) and the lowest unoccupied molecular orbital (LUMO) of reactant molecules (see Figure 3.5).

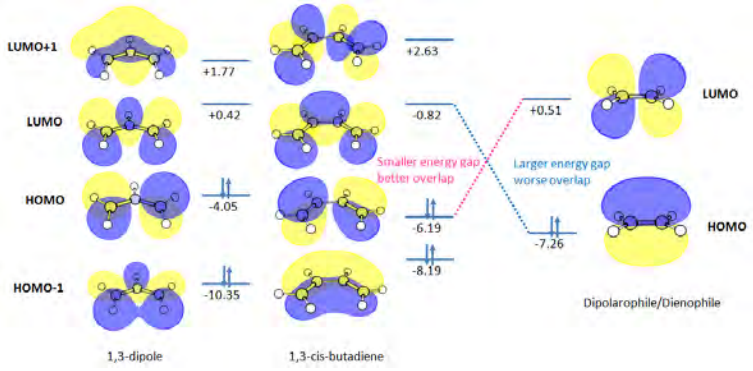

Figure 3.5: Representation of the frontier orbital description of cycloadditions. In this example, the strongest orbital interaction is produced between the HOMO of the diene/1,3-dipole and the LUMO of the dienophile/dipolarophile (ethylene). However, when substituted dienes or dienophiles react, the orbital interaction may be reversed.

According to this theory, 1,3-dipolar cycloaddition reactions can be classified in three different classes.[159,168] Class 1 reactions are those where the most significant orbital contribution is the one between the HOMO of the dipole and the LUMO of the dipolarophile. That is the case of diazomethane and ylides, which exhibit a nucleophilic character reacting with dipolarophiles with electron-withdrawing groups. Class 2 reactions present as the most important contribution the one between the LUMO of the dipole and the HOMO of the dipolarophile. Electrophilic dipoles such as ozone reacting with dipolarophiles that present electron-donating substituents are included in this group. Finally, the third class of reaction, usually referred as to ambiphilic, includes those 1,3-dipolar cycloadditions were both interactions are approximately equally favorable. The reactivity can be enhanced introducing either electron-withdrawing or electron-donating substituents which reduce one of the FMO gaps and, therefore, favor one of the two possible interactions. The FMO theory is also applied to the Diels-Alder reaction. The usual strongest orbital interaction is produced between the HOMO of the diene and the LUMO of the dienophile (figure 3.5). However, there exists a strong electronic substituent effect on the Diels-Alder addition, in the sense that, if an electron-poor diene and an electron-rich dienophile react, the strongest orbital interaction is the one between the HOMO of the dienophile and the LUMO of the diene, and an *inverse electron demand Diels-*

Alder reaction is produced.

The FMO theory has been widley used in organic chemistry, however it fails, for example, in predicting the reactivity of polyaromatic hydrocarbon (PAH) compounds. According to the FMO theory, the 1,4-addition to benzene is more favorable than to hexacene, which is exactly the opposite of what is observed and predicted with theoretical methods.[169]

Thermodynamic models such as Bell-Evans-Polanyi,[170] Brønsted,[171] and Marcus theory[172] have been used to describe chemical reactivity. The possibility of applying these thermodynamical models to cycloadditions was considered by Houk and coworkers.[173,174] A set of parabolic functions are used for the representation of reactant and product, whose intersection represents an approximation of the transition state of the reaction under consideration (see Figure 3.6). Using this assumption, Marcus had proposed for electron transfer reactions that the reaction energy (ΔG_{rxn}) can then be related to the activation barrier ($\Delta G^{\ddagger}$) of the reaction (see equation 3.1).

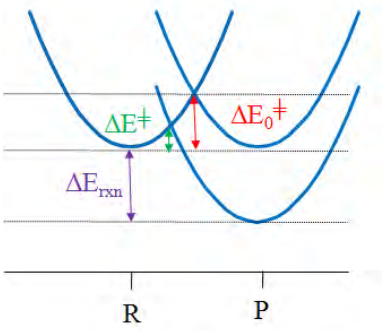

Figure 3.6: Representation of the Marcus curve crossing for a thermoneutral and exothermic reaction.

$$\Delta G^{\ddagger} = \Delta G_0^{\ddagger} + \frac{1}{2}\Delta G_{rxn} + \frac{\Delta G_{rxn}^2}{16\Delta G_0^{\ddagger}} \tag{3.1}$$

The term $\Delta G_0^{\ddagger}$ is defined by the intersection of the reactant and product parabola for a thermoneutral reaction (ΔG_{rxn}=0). This equation can be simplified neglecting the second-order term (this approximation will be valid as long as $\mid \Delta G_0^{\ddagger} \mid \gg \mid \Delta G_{rxn} \mid$). Moreover, the relationship remains correct considering either free Gibbs energies, enthalpies or electronic energies. If the previously mentioned simplification is included and electronic energies are used equation 3.2 is obtained.

$$\Delta E^{\ddagger} = \Delta E_0^{\ddagger} + \frac{1}{2}\Delta E_{rxn} \tag{3.2}$$

The latter relationship was also observed experimentally by Dimroth,[175] Brønsted,[171] and Bells-Evani-Polanyi.[170] Recently, Ess and Houk have shown that the energy to distort the 1,3-dipole and dipolarophile to the transition state geometry, rather than FMO interactions or reaction thermodynamics, controls reactivity for cycloadditions of 1,3-dipoles with alkenes or alkynes.[173,174] Although the reaction barrier is not a simple function of the reaction energy it is clearly correlated to the distortion energy. The distortion energy,[176–178] also called deformation energy[179] or activation strain,[180] is defined as the energy required to distort the dipole and dipolarophile into the geometry they present in the transition state, without allowing the interaction between the fragments. Thus, the activation energy of a reaction can be expressed as the deformation energy ($\Delta E_d^{\ddagger}$) and the interaction energy ($\Delta E_{iint}^{\ddagger}$) between addends involved in the transition state (see equation 3.3).

$$\Delta E^{\ddagger} = \Delta E_d^{\ddagger} + \Delta E_{int}^{\ddagger} \tag{3.3}$$

In a unimolecular reaction, the activation barrier is of course only related to the required energy to distort the molecule to the geometry of the TS. A good correlation has been found between activation barriers and distortion energies, showing that a higher reaction barrier implies a higher deformation of dipole and dipolarophile in the transition state.

This interaction/distorion model has been applied to the 1,3-dipolar cycloaddition between different dipoles and ethylene and acethylene,[173,174] and to the hydrogenation and the Diels-Alder reactions over planar arenes.[181] Moreover, the applicability of this model for the 1,3-dipolar and Diels-Alder reactions has also been tested in other more complex compounds, such as curved arenes, fullerene and single-walled carbon nanotubes (SWCNTs)(see chapter 11). This new distortion/interaction model provides a new way of understanding of reactivity trends for cycloadditions and should be applicable to bimolecular reactions in general.

Domingo and coworkers observed that the activation barrier of the Diels-Alder reaction is decreased in those systems presenting a larger charge transfer (CT) at the transition state.[182] According to this CT, the Diels-Alder reactions can be classified as non-polar (if the CT $<$0.1 e), polar (0.1e $<$ CT $<$ 0.4 e), and ionic (CT $>$ 0.4 e). The lowest activation barriers are found for the case of ionic Diels-Alder reactions (where one of the reactants is a cation or anion). The activation barrier of the reaction was found to be highly correlated to the CT, as well as to the electrophilicity indexes of reacting ethylenes.[182] Finally, in a recent study where molecular dynamics of 1,3-dipolar cycloadditions involving diazonium betaines and either acetylene or ethylene indicated that the bending vibrations are mainly responsible for facilitating the reaction.[183]

The Diels-Alder and 1,3-dipolar cycloaddition reactions have become one of the most important methods to obtain six and five- heterocyclic membered rings. These re-

actions have been succesfully produced involving alkenes, arenes but also fullerenes and related carbon nanostructures. This method is actually one of the most straightforward procedures for fullerene and nanotube functionalization.[184–188] The applicability of these cycloaddition reactions has been extended to a wide range of chemistry areas such as material chemistry,[189,190] chemical biology[191] and drug discovery.[192,193] Hereafter, the Diels-Alder and 1,3-dipolar cycloadditions succesfully produced on fullerene and related compounds will be discussed.

3.1.2 The Diels-Alder and 1,3-dipolar cycloaddition reactions on C_{60} and related compounds

C_{60}

The [4+2] Diels-Alder and 1,3-dipolar cycloaddition reactions are performed readily thanks to the electrodeficient nature of C_{60}. The latter feature makes C_{60} an ideal dienophile/dipolarophile for undergoing cycloaddition reactions. As said in chapter 1, different bond types are present in any fullerene structure. In the case of C_{60}, there are only two bond types: the [6,6] (between two hexagonal rings, also called pyracylene) and the [5,6] (between an hexagonal and a pentagonal ring, also called coranulenne) bonds. Cycloaddition reactions to C_{60} are mainly produced through addition to [6,6] bonds[194,195] which are shorter and present a larger π-density as compared to [5,6].

A wide range of dienes were shown to react with C_{60}, such as anthracene, tetracene, furan, or cyclopentadiene among many others.[196–207] A large number of mono-, di-, and up to six Diels-Alder additions can be produced on C_{60}.[208–213] However, some of the final cycloaddition adducts were shown to undergo the retro-Diels-Alder reaction (i.e. the initial fullerene and diene are recovered) upon heating.[42,196,198] The retro-reaction can be avoided involving dienes such as ortho-quinodimethane whose cycloaddition products gain aromaticity.[201,214,215] In contrast to the Diels-Alder and Bingel cycloaddition adducts, the retro-1,3-dipolar cycloaddition involving dipoles such as azomethine ylides, alkyl azides and nitrile oxides is only produced under very special conditions.[216–219] It was shown that the addition of another dipolarophile (maleic anhydride) in the reaction media favored the retro-reaction. After reversing the 1,3-dipolar reaction, the generated unstable 1,3-dipole is trapped by maleic anhydride which converts the process from highly endothermic to substantially exothermic. Although the reaction barriers that need to be surmounted are high, the retro-reaction can still be achieved at high temperatures.[216]

Most of 1,3-dipolar cycloadditions to C_{60} involve the addition of azomethine ylides. The reaction was initially produced by Prato and Maggini in 1993,[220] and has become one of the most straightforward procedures for fullerene functionalization. This 1,3-dipolar reaction, usually known as *Prato reaction*, is performed smoothly and in good yields. As it happens with the Diels-Alder reaction, the 1,3-dipolar cycload-

ddition is highly selective as the addition is produced only on [6,6] bonds. Different dipoles react with C_{60} such as nitrile oxides, nitrile imines,[221–225] sulinimides,[226] thiocarbonyl ylides,[227,228] carbonyl ylides,[229] nitrile ylides,[230,231] and isonitriles.[232] The 1,3-dipolar cycloadditions of diazomethane, nitrile oxide, and nitrone to C_{60} were theoretically studied at the B3LYP/6-31G(d)//AM1 level. A concerted mechanism was followed, where the closed [6,6] adducts were predicted as the most stable cycloaddition products.[233] The 1,3-dipolar cycloadditions to C_{60} were also theoretically studied for alkyl azides and azomethine ylides.[234–236]

Endohedral fullerenes

TNT endohedral metallofullerenes

The obtaining of endohedral compounds such as $Sc_3N@C_{80}$, $Sc_3N@C_{78}$ or $Sc_3N@C_{68}$ in high yields using the so-called trimetallic nitride template (TNT) process, led to the organic functionalization of these new molecules.
In 2002, the Diels-Alder reaction was succesfully produced for the first time on the I_h isomer of $Sc_3N@C_{80}$.[237] The crystallographic characterization of the first Diels-Alder adduct performed on an endohedral metallofullerene indicated that a symmetric adduct was obtained after reaction with 6,7-dimethoxyisochroman-3-one.[238] The addition was shown to occur on the corannulene-type [5,6] bonds. Campanera *et al.* [239] performed theoretical calculations that correctly describe the reactive exohedral sites of $Sc_3N@C_{80}$ for the Diels-Alder reaction. Based on these studies, the most reactive sites were those with high Mayer Bond Order (MBO)[240] and high pyramidalization angles.[241,242] The geometry of the DA adduct was similar to that found for the reaction on C_{60}, where the usual reactive bonds are the pyracylene-type [6,6] bonds. It should be mentioned here, that the I_h isomer of $Sc_3N@C_{80}$ does not possess the reactive pyracylene-type bonds. In 2005, the 1,3-dipolar cycloaddition of N-ethylazomethine ylide and $Sc_3N@C_{80}$ was reported[243] where the same addition pattern, i.e. over the [5,6] bonds, was produced. Interestingly, the 1,3-dipolar cycloaddition to the parent $Y_3N@C_{80}$ lead to the [6,6] addition.[88] The same regioselectivity was observed in the cyclopropenation reaction of diethyl bromomalonate and $Y_3N@C_{80}$.[88] X-ray structure indicated that the C-C bond attacked is open rather than closed and that one of the yttrium atoms is positioned near the site of the cleaved bond. It should be noted here that the carbene addition to $Y@C_{82}$ was shown to yield an open fulleroid [6,6] regioisomer whose attacked bond was situated close to one of the yttrium atoms.[244] Moreover, the 1,3-dipolar cycloaddition performed on the $M_2@I_h{-}C_{80}$ (M= La, Ce) yielded two regioisomeric adducts corresponding to the [6,6] and [5,6] addition.[245] Interestingly, the M_2 cluster is facing the attacked bond in the case of the [5,6] product. The isomerization from the [6,6] to the [5,6] regioisomer was observed in the case of $Y_3N@(N-Ethylpyrrolidino-C_{80})$.[64,246] This was also the case for the N-ethylazomethine ylide addition to $Er_3N@C_{80}$.[246] Theoretical calculations at BP86/TZ2P for the $Y_3N@(N-Ethylpyrrolidino-C_{80})$ indicated that the isomerization process takes place through a pirouette-kind of mechanism instead of involving the retro-cycloaddition reaction from the [6,6] adduct.[247] The

1,3-dipolar cycloaddition was also produced to the encapsulated mixed-metal clusters $Sc_2YN@C_{80}$ and $ScY_2N@C_{80}$.[248] As said previoulsy, the reaction on $Sc_3N@C_{80}$ and $Y_3N@C_{80}$ was shown to give [5,6] and [6,6] cycloaddition adducts, respectively. Interestingly, the major adduct obtained in the case of the metal mixed Sc_2YN endohedral compound corresponded to the [5,6] addition as it happens with its parent $Sc_3N@C_{80}$. A change on the regioselectivity is produced with the encapsulation of two or more yttrium atoms (i.e. ScY_2N and Y_3N) inside the cage. The [6,6] product is the minor adduct in the case of $ScY_2N@C_{80}$, whereas in $Y_3N@C_{80}$ only the [6,6] regioisomer is obtained. These findings suggest that the nature of the metal cluster encapsulated inside dictates the exohedral functionalization of the endohedral metallofullerenes.

The Diels-Alder on D_{5h} isomer of $Sc_3N@C_{80}$ and $Lu_3N@C_{80}$, and 1,3-dipolar cycloadditions to the D_{5h} isomer of $Sc_3N@C_{80}$ indicated a higher reactivity of the D_{5h} isomer as compared to the I_h.[249] The latter increase on the reactivity was explained in terms of the HOMO-LUMO energy gaps for both isomers.[249] The LUMO orbitals of the D_{5h} isomers of $Sc_3N@C_{80}$ and $Lu_3N@C_{80}$ are comparable to those of I_h, whereas a destabilization of the HOMOs for the D_{5h} isomer is produced. The D_{5h} isomer was shown to be 21.1 $kcal.mol^{-1}$ less stable at PBE/TZ2P than the corresponding I_h.[70] Interestingly, the D_{5h} isomer presents the reactive pyracylene-type [6,6] bonds (the most reactive bond in the case of C_{60}). The Diels-Alder with cyclopentadiene and either $D_{5h} - Lu_3N@C_{80}$ or $D_{5h} - Sc_3N@C_{80}$ was succesfully performed on the highly reactive pyracylene-type bond. In contrast, the 1,3-dipolar cycloaddition involving N-tritylazomethine ylide and $D_{5h} - Sc_3N@C_{80}$ led to two different monoadducts. The thermodynamic control product was shown by both NMR and X-ray crystallography to correspond to the [5,6] addition, however the [6,6] adduct was the kinetic control addition product.[250]

The Diels-Alder reaction with ortho-quinodimethane and the gadolinium based metallofullerene $Gd_3N@C_{80}$ was achieved in 2005.[251] The latter compound is of significant interest because of its potential applications as MRI contrast agent (see chapter 2). It was shown that two o-quinodimethane molecules were attached to the $Gd_3N@C_{80}$ surface (i.e. the formation of a bisadduct). The yield of the reaction was modest as only 0.5 to 1 mg of bisadduct was obtained from 5 mg of $Gd_3N@C_{80}$ (10-20%). For comparison, the yield of the 1,3-dipolar reaction on $Sc_3N@C_{80}$ is 30-40%.[252] A combined theoretical and experimental investigation of the change on the regioselectivity of the 1,3-dipolar cycloaddition and a series of gadolinium and scandium mixed endohedral metalofullerenes ($Sc_xGd_{(3-x)}N@C_{80}$) was performed in 2007.[253] The regioselectivity of the reaction was changed upon introduction of gadolinium atoms. The [5,6] product was the major adduct in $Sc_3N@C_{80}$, $Sc_2GdN@C_{80}$, $ScGd_2N@C_{80}$, however the [6,6] adduct was also obtained in $Sc_2GdN@C_{80}$ and $ScGd_2N@C_{80}$. The [6,6] regioisomer was the major cycloaddition product in the case of $Gd_3N@C_{80}$. Interestingly, the thermal treatment of the final products led to the partial or total isomerization of the [6,6] adducts formed

in the case of $Sc_2GdN@C_{80}$ and $ScGd_2N@C_{80}$ to the [5,6] regioisomers, respectively. Experimental and theoretical findings showed that the difference in stability between [6,6] and [5,6] products in the case of $ScGd_2N@C_{80}$ is very small (the [5,6] adduct is at PBE/DNP just 2.3 $kcal.mol^{-1}$ more stable than [6,6]). This energy difference ranges from 11.7 to -0.4 $kcal.mol^{-1}$ along the series $Sc_3N@C_{80} > Sc_2GdN@C_{80} > ScGd_2N@C_{80} > Gd_3N@C_{80}$. The reactivity of the gadolinium based endohedral compounds $Gd_3N@C_{80}$, $Gd_3N@C_{84}$, and $Gd_3N@C_{88}$ was investigated to study the effect of the cage size on the exohedral reactivity.[254] They observed that among all considered compounds $Gd_3N@C_{80}$ was the most reactive cage through reaction with bromomalonate. The fattened shape of C_{84} and C_{88} cages makes them less pyramidalized and thus less reactive upon the Bingel reaction.

The synthesis and characterization of the first N-tritylpyrrolidino derivative of $Sc_3N@C_{78}$ utilizing the Prato reaction was succesfully produced in 2007.[255] On the basis of NMR spectra and DFT calculations, Cai and coworkers concluded that the two monoadducts obtained corresponded to the addition to two different type B [6,6] bonds (called c-f and b-d). The X-ray diffraction of one of the obtained compounds (c-f addition) confirmed that the 1,3-dipole was attached to a [6,6] bond.[255] It is interesting to remark here that the cyclopropenation reaction of $Sc_3N@C_{78}$ and diethyl bromomalonate yielded one monoadduct and one dominant symmetric bisadduct, which corresponded to the same type B [6,6] addition.[256] The photochemical addition reaction of adamantyldene to $La@C_{78}$ was produced on both a [6,6] and a [5,6] bond.[66]

Noble gas endohedral fullerenes

The Diels-Alder reaction of 9,10-dimethylanthracene (DMA) and either $^{129}Xe@C_{60}$ or $^{3}He@C_{60}$ was investigated by Saunders and coworkers.[257] In the case of the helium compound, they obtained 85% of bisadducts, whereas for xenon some unreacted C_{60} and lots of monoadduct were detected. At low temperatures, the thermodynamics of the Diels-Alder reaction was favored for helium, however at high temperatures the equilibrium constant of the reaction was larger for xenon. The decreased reactivity at low temperatures for Xe (the effect of substituting He by Xe in C_{60} is small with energy differences of ca. 0.1 $kcal.mol^{-1}$) was attributed to the fact that the electron cloud of the cage is pushed outward by the xenon atom encapsulated inside. This justification was also employed to explain the reduction of reactivity of $(H_2)_2@C_{70}$ compared to $(H_2)@C_{70}$ by Komatsu and coworkers.[118] Finally, the Diels-Alder reaction and its retro-reaction was produced on $H_2@C_{60}$, where the reported equilibrium constant was similar to that obtained for $^{3}He@C_{60}$.[258]

Other related derivatives

The 1,3-dipolar cycloaddition involving azomethine ylide has been experimentally produced to other carbon nanostructures, such as carbon nanotubes (CNT),[259–263]

nanofibers,[264] nanohorns,[265] nanoonions,[266,267] and nanorods.[268] The reaction has also been reported involving other 1,3-dipoles such as nitrile imines and ozone.[95,259,269,270] The Diels-Alder reaction has also been satisfactorily produced on the sidewalls of CNT using ortho-quinodimethane (generated in situ from 4,5-benzo-1,2-oxathiin-2-oxide) and microwave irradiation.[271] The latter reaction was theoretically studied by Lu and co-workers within the ONIOM approach.[272] Finally, the retro-cycloaddition reaction involving CNTs was succesfully produced through microwave-assisted synthesis.[273]

3.2 Radical reactions

Radical reactions are chemical processes where molecules having unpaired electrons are involved. The majority of radical reactions contain radicals as intermediates, although radical species could also be the starting compound or a product of the reaction. The generation of a radical is often due to the homolytic bond cleavage.

The lifetime of a radical is usually very short, however the stability might be enhanced with certain structural features. Radical species present one orbital with one unpaired electron which is called the Single Occupied Molecular Orbital (SOMO). Of course, any interaction or structural feature that stabilizes the energy of the molecular orbitals, gives extra-stability to the radical molecule (i.e. it is less reactive). For example, the presence of the electron-withdrawing groups $C = O$ and $C \equiv N$ (they have low-lying empty π^* orbitals) produces the formation of two new MOs where the new SOMO is lower in energy (see Figure 3.7). The introduction of electron-rich groups (such as -OR) which present relatively high-energy filled n orbitals (their lone pairs) produces the formation of two new orbitals. Although the new SOMO is higher in energy than the old one, the energy of the lone pairs is reduced thus an overall stabilization is also observed (see Figure 3.7). Those radicals that do not present extra stability usually dimerize or disproportionate. Moreover, they can also react with oxygen and abstract hydrogen atoms from many different solvents. A few free radicals are indefinitely stable, and usually permit extensive delocalization of the unpaired electron into aromatic rings. Radical molecules can be classified in two different groups: electrophilic radicals that present a low energy SOMO and are more willing to accept an electron, and nucleophilic ones that prefer to donate its unpaired electron due to its high energy SOMO orbital (see Figure 3.8).
The reaction mechanism involving radical intermediates consists of a cycle of repetitive steps which form many product molecules for each initiation event. Figure 3.9 shows an hypothetical chain reaction mechanism.
The first step of the reaction consists of an *initiation step*. In case of figure 3.9, it involves the generation of the radical species $A^{\cdot}$. The latter molecule reacts with other compounds creating more radicals. These steps correspond to the *propagation phase*. The term chain length refers to the number of propagation steps that take place per initiation step, and is employed to characterize chain reactions. Finally, the process

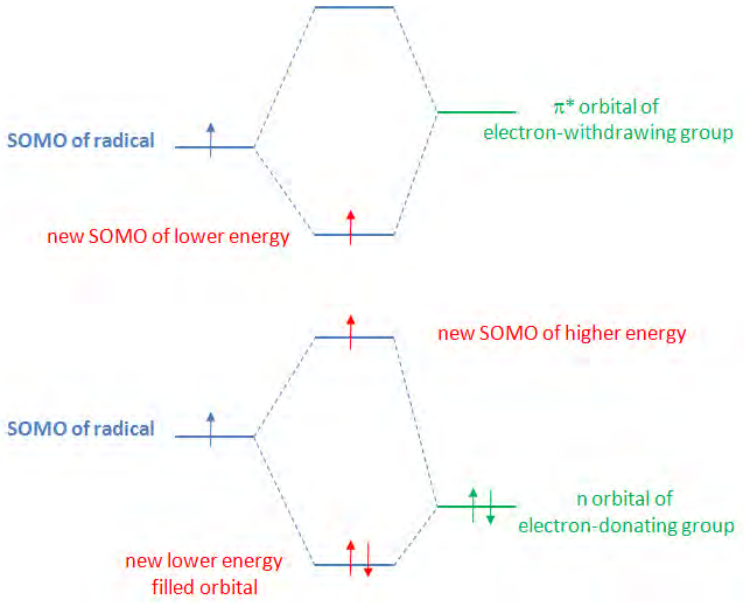

Figure 3.7: Representation of the best orbital interactions between electrophilic and nucleophilic SOMOs and electron-poor and rich alkenes.

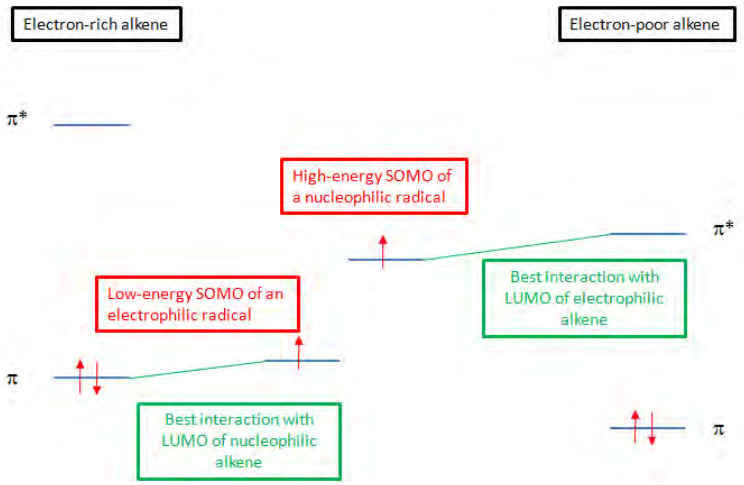

Figure 3.8: Representation of the SOMO stabilization of a radical species by the presence of electro-withdrawing (at the top) and electro-donating groups.

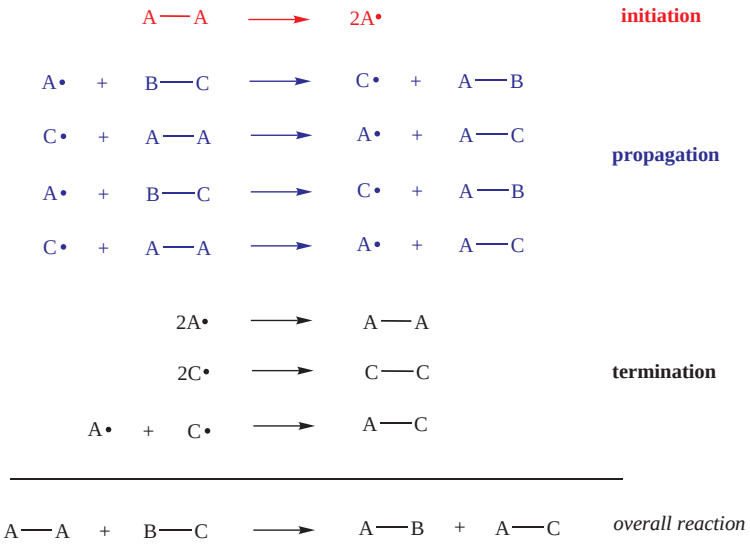

Figure 3.9: Representation of the three different phases of a radical chain reaction: the initiation, the propagation and the termination steps.

ends with the so-called *termination steps* that include all reactions that destroy one of the radical species needed for the propagation of the reaction. The regioselectivity of the radical additions relies on the strength of the bonds being formed and broken. Although the radical addition might be produced on several positions, the preferred addition site is always consistent with the one presenting the lowest activation and reaction energy. The latter is related to the formation of the most stable radical.

Many radical reactions of interest directly depend on the presence of an initiator, which creates initial free radicals necessary for the starting of the chain reaction. Peroxides or azo compounds are useful classes of *initiators*. However, another usual procedure is the initiation of the chain reaction by irradiation. Conversely, there exist some molecules sufficiently reactive toward a radical involved in the reaction or capable of retarding the initiation of the chain process. The latter compounds are called *inhibitors*. Those inhibitors that retard or terminate free-radical chain oxidations which rapidly deteriorate many organic molecules are usually named *antioxidants*. The chain mechanism for an oxidation chain reaction is depicted in figure 3.10. Antioxidant molecules react with peroxy radicals generated during the propagation phase, and therefore prevent the chain process. Another mechanism of action of antioxidants is through reaction with the initiator of the chain process. The presence of oxygen in a free-radical reaction can modify the course of the reaction, as oxygen molecule is highly reactive to radicals. The generated oxygen-related radicals during the chain oxidation are usually called reactive oxygen species (ROS). In living beings, when there exists an unbalanced situation between those biological processes respon-

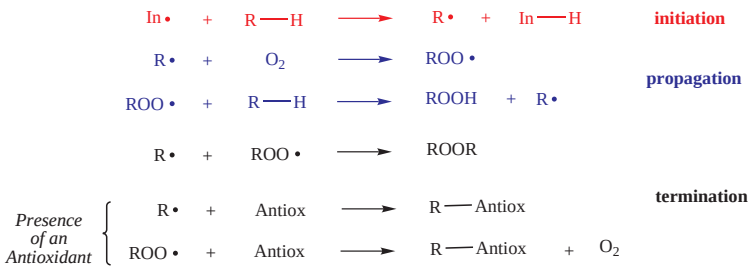

Figure 3.10: Representation of an hypothetical radical chain oxidation. The termination of the reaction might be produced due to the presence of an antioxidant molecule which reacts with the radicals generated during the course of the reaction.

sible for the production of ROS and those for their removal the so-called oxidative stress is produced. Actually, all cellullar biomacromolecules including sugars, DNA, lipids, and proteins are highly vulnerable to high concentrations of ROS. The brain is extremely sensitive to high levels of ROS because of three different factors. First, the highest concentration of oxygen is found in the central nervous system. Second, there is a high content of polyunsaturated lipids, and finally it contains the lowest levels of antioxidant molecules. The antioxidant molecules that organisms present to control the levels of ROS include superoxide dismutase enzymes (SOD1, SOD2, and SOD3 in humans), glutathione peroxidase and catalase, and non-enzymatic mechanisms such as vitamin E, ascorbic acid, and glutathione. It is widely believed that oxidative stress has a major role in the aging process and there is irrefutable evidence that oxidative stress for some components is produced in several neurodegenerative diseases, such as Alzheimer's, Parkinson's, Huntington's, and amyotrophic lateral sclerosis (ALS) disorders.[274,275] One of the most important ROS is the superoxide radical ($O_2^{\bullet -}$) which is produced because of errors in the oxidative phosphorylation in mitochondria.

Fullerene compounds present a high affinity for radicals, and are usually called *radical sponges*. A large variety of radicals react with C_{60}, such as benzyl,[276] tert-buthyl,[277,278] monoalkyl,[277,279–284] halogenated alkyl groups,[285,286] alkylthio and alkoxy radicals,[278,287–289] among many others. Moreover, the prolonged irradiation of C_{60} with an excess of radicals leads to multiple additions.[276,278,290] This high reactivity towards radicals has been used for the synthesis of new materials such as polymers and perfluoroalkylated fullerenes, but also for the use of fullerenes as radical scavengers. This characteristic makes C_{60} and its related compounds perfect antioxidant agents and potential novel therapeutic targets. Hereafter, an insight will be given into the medical and biological studies performed where the antioxidant properties of fullerene molecules have been tested.

3.2.1 Biological and medical studies of interest involving the antioxidant properties of C_{60} and its related derivatives

The study of the antioxidant properties of fullerene compounds including *in vivo* assays in some mammals was limited by the low solubility of C_{60} in water and most polar solvents, making them incompatible with biological systems. Fortunately, fullerene compounds exhibit a rich synthetic organic chemistry, which allows the preparation of water-soluble derivatives. The antioxidant properties of several hydroxyl and carboxyl fullerene derivatives were investigated in detail.

Among them, the most widely studied fullerene compound is the tris-malonyl-C_{60} compound (also called C_3). Three malonyl groups are attached to the fullerene surface through reaction of diethyl bromomalonate and C_{60} (i.e. Bingel reaction),[137,291] and is exclusively produced over [6,6] bonds (see Figure 3.11).

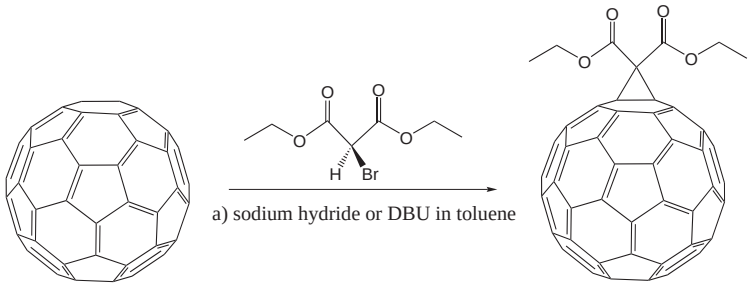

Figure 3.11: Scheme of the Bingel reaction between C_{60} and malonate.

The addition of the carboxyl groups can yield different regioisomers presenting C_3 or D_3 symmetry.[137] However, the antioxidant activity of the C_3 compound was found to be higher than for the D_3 compound.[292] The rate for efficiently removing superoxide radical of C_3 compound was found to be lower than for SOD1 (restricted to cytoplasma) or SOD2 (present in mitochondria), but within the range of several metal-containing SOD mimetics.[293] Monoadducts were also shown to exhibit antioxidant properties, and in some cases the capability of removing ROS was even higher than that found for trisadducts.[294] The latter observations suggest that the number of carboxyl groups as well as their position in the fullerene surface clearly modify the antioxidant properties of fullerene compounds.[294] In some structure-function studies, it was observed that the antioxidant properties were also dependent on redox behavior, charge, size and hydrophobicity.[295] Moreover, the capability of fullerenes for removing superoxide radicals is susceptible to the molecular structure of fullerene and its reduction potential.[294] The lower the reduction potential, the higher the antioxidant capability. Yin and co-workers perform an extensive comparison of the activity of the carboxyfullerene $C_{60}(C(COOH)_2)_2$, the hydroxyfullerene $C_{60}(OH)_{22}$, and the endohedral gadolinium-based hydroxyfullerene $Gd@C_{82}(OH)_{22}$ compounds.[296] Interestingly, the activity of the studied compounds was found to decrease along

the series $Gd@C_{82}(OH)_{22} > C_{60}(OH)_{22} > C_{60}(C(COOH)_2)_2$.

The *in vivo* evaluation of the antioxidant properties of fullerene compounds is extremely relevant for the future application of these compounds in medical and biological applications. Consequently, a wide range of studies of medical interest have been performed during the last years. Interestingly, administering the C_3 compound to mice that lack mitochondrial manganese superoxide (MnSOD) increased the lifespan (amount of time between birth and death) by 300%.[293] This finding supports that C_3 is a biological effective SOD mimetic and that it localizes in mitochondria.[297] Age-associated oxidative stress was reduced in middle age mice and, as observed in other studies, the lifespan was also increased.[298] The most relevant data show that those mice treated with C_3 improved memory and learning tasks. Lipid peroxidation in the brain region called *substantia nigra* was induced in mice by administrating an iron(II) compound.[299] Apart from the peroxidation processes, the content of dopamina in the stratium area in brain was decreased. Actually, one of the characteristics of Parkinson's patients is the high level of peroxidated lipids found in some brain areas.[300–302] The infusion of a carboxyfullerene to those Parkinson's induced mice supressed both lipid peroxidation and decrease of dopamine content in a dose-dependent manner. These studies suggest that carboxyl/hydroxyl fullerenes might be novel candidates to treat some neurodegenerative diseases such as Parkinson's disorder.
In addition, some biological studies concerning the applicability of these compounds to treat other neurodegenerative illnesses was studied in detail. The infusion of C_3 to mice model of familial amyotrophic lateral sclerosis (ALS) surprisingly retarded motor deterioration and death.[292]
Finally, the applicability of endohedral hydroxyfullerenes to treat tumors was also thoroughly investigated. It was found that the gadolinium based compound $[Gd@C_{82}(OH)_{22}]_n$ efficiently restored damaged liver and kidney of tumor-bearing mice.[303] Carboxyfullerenes were also shown to be protective against oxidative-stress induced apoptosis (cellular death) in human peripherial blood mononuclear cells and in rat cerebral granule cells.[304,305]

All previously mentioned studies indicate that carboxyl and hydroxyl fullerenes are prominent candidates to treat a wide variety of disorders related to oxidative stress. Any medical, biological and chemical study about the reactivity as well as the mechanism of action of these molecules represent a stringent test for the development of future therapies involving these fascinating compounds.

Chapter 4

Computational Chemistry

The fast evolution of computers gave rise to a new way of doing science besides experimental and theoretical, and the computational sciences emerged. Computational chemistry performs extremely complex calculations and is able to obtain very valuable information about, for example, geometrical structures or physical and chemical molecular properties.

In computational chemistry there are three different methodologies. First, the so called *ab initio* methods which are based on solving the Schrödinger equation. Second, the semi-empirical methods which are based on the Hartree-Fock formalism, where many approximations are made and some empirical parameters are included. And finally, the molecular mechanics methods which are based on the classical physics to predict the behavior of molecules and atoms.

In this chapter, the *ab initio* Hartree-Fock method will be explained not only because it is the most simple theory, but also because it is used as starting point for the so called post Hartree-Fock methods. Because of their elevated computational cost, these can not be routinely applied to fullerenes and will not be explained explicitly in this chapter. A good reference for them is in references 306-308. Instead, the Density Functional Theory will be described, as it is one of the most commonly used methods to study large molecules because with a low computational cost, it includes electron correlation and gives very accurate results.

4.1 The Hartree-Fock approximation

In this section the Hartree-Fock (HF) approximation will be described based on the book Modern Quantum Chemistry by Szabo and Ostlund.[306] Solving the Schrödinger equation is the main objective of quantum mechanics, either using *ab initio* methods, or semiempirical ones. The HF approximation has given an important tool to

find approximate solutions to the electronic structure of molecules, but it also has an important role as a starting point for more accurate approximations that include electron correlation. It assumes that the motion of each electron can be described by a simple function called orbital which is not explicitly dependent of the motion of other electrons.

The simplest approximation to the ground state of the N-electron system described by an electronic Hamiltonian $\hat{H}$, can be done using a single Slater determinant formed from a set of spin orbitals χ_a (equation 4.1).

$$|\Psi_0 >= |\chi_1\chi_2 \cdots \chi_a\chi_b \cdots \chi_N > \tag{4.1}$$

The variational principle specifies that the "best" set of spin orbitals are those which minimize the electronic energy E_0.

$$\begin{aligned} E_0 =< \Psi_0|\hat{H}|\Psi_0 >= \sum_a < a|h|a > +1/2 \sum_{ab} < ab||ab > \\ = \sum_a < a|h|a > +1/2 \sum_{ab} [aa|bb] - [ab|ba] \end{aligned} \tag{4.2}$$

The spin orbitals χ_a are for convenience and computational efficiency made orthonormal,

$$< \chi_a|\chi_b >= \delta_{ab} \tag{4.3}$$

and are systematically varied until the energy is a minimum. The equation for the best spin orbitals (the ones that make the energy a minimum) is the Hartree-Fock equation,

$$f_i\chi_i = \varepsilon_i\chi_i \tag{4.4}$$

where f_i is the Fock operator

$$\hat{f}(k) = \hat{h}(k) + \sum_b (\hat{J}_b(k) - \hat{K}_b(k)) \tag{4.5}$$

The first part of the Fock operator $\hat{h}(k)$ includes the kinetic energy and the attractive electron - nucleus potential, $\hat{J}$ is the Coulomb operator and $\hat{K}$ the Exchange term.

In an exact theory, the Coulomb operator includes the two-electron potential operator r_{ij}^{-1}, but in the HF approximation the latter operator is replaced by a *one-electron potential*, obtained by averaging the interaction r_{12}^{-1} of electron 1 and electron 2 over all space and spin coordinates x_2 of electron 2, weighted by the probability $dx_2|\chi_b(2)|^2$ that electron 2 occupies the volume element $d\mathbf{x}_2$ at $\mathbf{x}_2$. By summing over all $b \neq a$, one obtains the total averaged potential acting on the electron in χ_a,

arising from the N−1 electrons in the other spin orbitals.[306] The Coulomb operator associated with this interpretation is represented in the following equation.

$$\hat{J}_b(1) = \int d\mathbf{x}_2 \; \chi_b^*(2)\frac{1}{r_{12}}\chi_b(2) \tag{4.6}$$

The exchange term does not have a classical physical interpretation, and is due to the antisymmetric nature of the Slater determinant.

$$\hat{K}_b(1)\chi_a(1) = [\int d\mathbf{x}_2 \frac{\chi_b^*(2)\chi_a(2)}{r_{12}}]\chi_b(1) \tag{4.7}$$

Roothaan and Hall proposed the introduction of the linear combination of atomic orbitals (LCAO) approximation, which expands the spin orbitals in terms of atomic orbitals that are the eigenfunctions of the hydrogen-atom-like energy calculation,

$$\chi_i(1) = \sum_{\nu=1}^{k} C_{\nu i}\phi_\nu(1) \tag{4.8}$$

where k is the number of atomic orbitals. If a complete set ϕ_ν could be used, equation 4.8 would be an exact expansion. The calculation of the HF orbitals is now reduced to the calculation of the expansion coefficients $C_{\nu i}$. Introducing the LCAO approximation in the HF equation, the following expression is established.

$$\hat{f}(1)\sum_{\nu}^{k} C_{\nu i}\phi_\nu(1) = \varepsilon_i \sum_{\nu}^{k} C_{\nu i}\phi_\nu(1) \tag{4.9}$$

A matrix equation can be obtained when 4.9 is multiplied by $\phi_\mu^*(1)$ and integrated,

$$\sum_{\nu}^{k} C_{\nu i}\int d\mathbf{r}\phi_\mu^*(1)\hat{f}(1)\phi_\nu(1) = \varepsilon_i \sum_{\nu}^{k} C_{\nu i}\int d\mathbf{r}\phi_\mu^*(1)\phi_\nu(1) \tag{4.10}$$

where the *overlap matrix* **S** is defined as

$$S_{\mu\nu} = \int d\mathbf{r}\phi_\mu^*(1)\phi_\nu(1) \tag{4.11}$$

The overlap matrix is Hermitian whose magnitude is $0 \leq |S_{\mu\nu}| \leq 1$, because of the normalization and the non orthogonality of the atomic basis functions ϕ_μ. The *Fock matrix* **F** is also defined,

$$F_{\mu\nu} = \int d\mathbf{r}\phi_\mu^*(1)\hat{f}(1)\phi_\nu(1) \tag{4.12}$$

which is also Hermitian, and represents the Fock operator applied to ϕ_μ in a matrix form. In this way, the equation 4.9 can be written as,

$$\sum_{\nu}^{k} F_{\mu\nu}C_{\nu i} = \varepsilon_i \sum_{\nu}^{k} S_{\mu\nu}C_{\nu i} \quad i = 1, 2..., k \tag{4.13}$$

These are the *Roothaan-Hall equations*. An equivalent matrix equation is

$$\mathbf{FC} = \mathbf{SC}\varepsilon \tag{4.14}$$

where the matrix $\mathbf{C}$ contains the expansion coefficients $C_{\mu i}$, and the diagonal matrix ε the orbital energies ε_i. An iterative method to solve the Roothaan equations is needed as they are not linear.

The HF method is sometimes called the Self-Consistent Field method (SCF) because of the iterative procedure used to solve the Roothaan equations. An initial set of spinorbitals is needed to start the process of solving the Fock equations, which step by step will generate a new set until finally we will obtain the coefficients that lead to the minimum of the energy.

The SCF method does not give an accurate description of most of the chemical systems. It has a physical limitation because of the average potential considered, which does not describe the correlation of the motion of the electrons. This electronic correlation has to be included to improve the results and consequently, the post-HF methods were introduced. The correlation energy is described as the difference between the exact non-relativistic Born-Oppenheimer energy for a determined basis set (Full CI, see references 306-308) and the HF (equation 4.15).

$$E_{corr} = E_{exact} - E_{HF} \tag{4.15}$$

4.2 The Density Functional Theory

In this part, the Density Functional Theory (DFT) method will be described based on the books Química Teórica y Computacional[307] and Introduction to Computational Chemistry.[308] The DFT gives a different approach for solving the Schrödinger equation, and it is based on the Hohenberg and Kohn (HK) theorems. The first HK theorem states that the electronic density can fully determine the energy of a non-degenerate electronic ground state.[309] In fact, there exists a one-to-one relationship between the electronic density and the Hamiltonian, therefore not only the energy but also other observable properties of the system can be determined.

The second Hohenberg and Kohn (HK) theorem provides the variational principle for the energy, and establishes that the energy of the system $E[\rho]$ is a minimum (E_0) when the exact electronic density of the system ρ_0 is considered.

$$E_0[\rho_0] \leq E[\rho] \tag{4.16}$$

Consequently the variational equation is obtained,

$$\frac{\delta E[\rho]}{\delta \rho(\mathbf{r})} - \mu = 0 \tag{4.17}$$

where μ is the Lagrange multiplier that ensures the normalization of the electronic density.

$$\int d\mathbf{r}\rho(\mathbf{r}) = N \tag{4.18}$$

The Kohn-Sham formulation

Kohn and Sham (KS) introduced the orbital concept within the DFT framework,[310] and proposed an auto-consistent method similar to the SCF for the HF theory. So, a set of orthogonal orbitals which minimizes the energy is obtained. The KS orbitals may be expanded in a set of basis functions, analogous to the HF method.

$$\phi_i = \sum_{\mu}^{M} c_{\mu i}\chi_\mu \quad i = 1, 2..M \tag{4.19}$$

One of the basic assumptions was to divide the kinetic energy in an exact part with a correction term. A non interacting electron system is considered as it can be exactly solved, and if it is assumed that the Hamiltonian has the following expression,

$$H_\lambda = T + V_{ext}(\lambda) + \lambda V_{ee} \quad 0 \leq \lambda \leq 1 \tag{4.20}$$

where T is the kinetic energy, V_{ee} the Coulomb repulsion and λ a coupling parameter that varies from 0 (non-interacting system) to 1 (interacting system), then the external potential $V_{ext}(\lambda)$ has to be introduced. The latter is equal to the electron-nuclear attraction V_{ne} when $\lambda = 1$ (therefore an electron interacting system is considered) and $|\phi^\lambda>$ is the interacting ground state wavefunction that leads to the electron density ρ of the real system. However, when λ equals 0, $|\phi^\lambda>$ is the single determinant wavefunction built with the Kohn-Sham orbitals ϕ_i, and $V_{ext}(\lambda)$ is the so-called Kohn-Sham effective potential ($\upsilon(\mathbf{r})$). The kinetic energy functional of the fictitious system of non-interacting N particles follows equation 4.21.

$$T_s = \sum_{i=1}^{N} <\phi_i| -\frac{1}{2}\nabla_i^2|\phi_i> \tag{4.21}$$

It seems clear that the functional of the energy has to include the kinetic energy ($T[\rho]$), the nucleus-electron attraction potential ($E_{ne}[\rho]$) and finally the electron-electron repulsion potential ($E_{ee}[\rho]$). The repulsion potential between nuclei is not taken into account because the Born-Oppenheimer approximation is considered and is independent of the charge density. As it happened in the HF approximation, the electronic correlation can be divided into a Coulomb and an Exchange part, so equation 4.22 is obtained.

$$E[\rho] = T[\rho] + E_{ne}[\rho] + J[\rho] + K[\rho] \tag{4.22}$$

Consequently, the energy functional can also be written in the following form.

$$E[\rho] = T_s[\rho] + \int d\mathbf{r}\rho(\mathbf{r})\upsilon(\mathbf{r}) + \frac{1}{2}\int d(\mathbf{r})d(\mathbf{r'})\frac{\rho(\mathbf{r})\rho(\mathbf{r'})}{|\mathbf{r}-\mathbf{r'}|} + E_{xc}[\rho] \tag{4.23}$$

The first term of the equation is the above mentioned kinetic energy functional for the non-interacting electron system, and the second term gives the electron-nucleus interaction. The classical $J[\rho]$ Coulomb repulsion of the electron cloud, plus its self-interaction energy is represented in the third term of the equation. Finally the last term is the exchange-interaction energy functional $E_{xc}[\rho]$ which includes non-classical effects of the electron correlation, as well as the difference $T[\rho] - T_s[\rho]$.

If the previous equation is rearranged the following equation is obtained,

$$\upsilon_{eff}(\mathbf{r}) + \frac{\delta T_s[\rho]}{\delta\rho(\mathbf{r})} = \mu \qquad \upsilon_{eff}(\mathbf{r}) = \upsilon(\mathbf{r}) + \frac{\delta J[\rho]}{\delta\rho(\mathbf{r})} + \frac{\delta E_{xc}[\rho]}{\delta\rho(\mathbf{r})} \tag{4.24}$$

where the effective potential Kohn-Sham υ_{eff} and the chemical potential μ have been introduced. The effective Kohn-Sham potential together with the kinetic energy operator form the Hamiltonian for the noninteracting system.

$$\hat{H}_s = \sum_{i=1}^{N}[-\frac{1}{2}\nabla_i^2 + \upsilon_{eff}(\mathbf{r})] \qquad [-\frac{1}{2}\nabla_i^2 + \upsilon_{eff}(\mathbf{r})]\phi_i = \epsilon_i\phi_i \tag{4.25}$$

The solution of $\hat{H}_s$ forms the set of the orbitals ϕ_i whose associated electron density is equal to the exact one.

Therefore, the KS operational procedure, which is similar to the SCF for the HF theory, consists in constructing an exchange correlation potential, making a guess for the orbitals ϕ_i, building the electron effective potential, and solving the iterative equation 4.25 until self-consistency to finally obtain the DFT energy from equation 4.23.

The use of the electronic density has an advantage in relation to the wavefunction, because whereas the former only depends on three coordinates, the latter on the 3N coordinates, where N is the number of the electrons. However, the DFT method has the main problem that the exact functional that connects the electronic density

and the energy is not known. If the form of the exchange-correlation functional were known, DFT theory would be exact, therefore great efforts have been done (in fact, are being done) to find more accurate expressions.

The route to the expression for the exchange-correlation functional

Before the HK theorems and the KS formulation were introduced, the first attempt was to consider a *non-interacting uniform electron gas*. The classical formulation of $E_{ne}[\rho]$ and $J[\rho]$ were used, and the following kinetic $T[\rho]$ and exchange $K[\rho]$ expressions were proposed.

$$\begin{aligned} T_{TF}[\rho] &= C_F \int d\mathbf{r}\rho^{\frac{5}{3}}(\mathbf{r}) \\ K_D[\rho] &= -C_x \int d\mathbf{r}\rho^{\frac{4}{3}}(\mathbf{r}) \\ C_F &= \tfrac{3}{10}(3\pi^2)^{\frac{2}{3}} \\ C_x &= \tfrac{3}{4}(\tfrac{3}{\pi})^{\frac{1}{3}} \end{aligned} \tag{4.26}$$

By taking into account the above mentioned equations the *Thomas-Fermi-Dirac (TFD)* model is obtained.[311] Unfortunately, this model does not give a proper description of the chemical bond. Thus, the functionals $T[\rho]$ and $K[\rho]$ have to be improved by including not only the electronic density, but also its derivatives.

Kohn and Sham proposed the following expression for the exchange-correlation energy,

$$E_{xc}[\rho] = \int d\mathbf{r}\rho(\mathbf{r})\epsilon_{xc}[\rho(\mathbf{r})] + O(|\overrightarrow{\nabla}\rho(\mathbf{r})|^2) \tag{4.27}$$

where $\epsilon_{xc}[\rho(\mathbf{r})]$ is the exchange-correlation energy density of a non-interacting electron system, but the uniform electronic density has been replaced by the electronic density of the heterogeneous system $\rho(\mathbf{r})$.

If only the first term of the equation 4.27 is considered the local density approximation (LDA) (or the uniform electron gas) is reached. Slater implemented the first method of LDA, the X_α method,[312] and divided the exchange-correlation term in two parts: the exchange part which was treated following the equation 4.28,

$$\epsilon_x^{LDA}[\rho(\mathbf{r})] = -\frac{9}{4}\alpha\left(\frac{3}{4\pi}\right)^{\frac{1}{3}}\rho(\mathbf{r})^{\frac{1}{3}} \tag{4.28}$$

and the correlation part which was not taken into account. For spin polarized systems, both the spin-up and spin-down electrons are considered separately, and the local spin density approximation (LSD) is obtained.

$$\epsilon_x^{LSD}[\rho(\mathbf{r})] = -\frac{9}{4}\alpha\left(\frac{3}{4\pi}\right)^{\frac{1}{3}}[\rho_\alpha(\mathbf{r})^{\frac{1}{3}} + \rho_\beta(\mathbf{r})^{\frac{1}{3}}] \tag{4.29}$$

Vosko, Wilk and Nusair proposed an expression[313] for the correlation part, and the final exchange-correlation energy functional follows the equation 4.30.

$$\epsilon_x^{LSD}[\rho(\mathbf{r})] = \int d\mathbf{r}\rho(\mathbf{r})[\epsilon_x^{LSD}[\rho(\mathbf{r})] + \epsilon_c^{LSD}[\rho(\mathbf{r})]] \tag{4.30}$$

By using equation 4.30 the iterative process mentioned before can be started.

The LDA approach works moderately well for all kinds of systems, however some improvements might be introduced considering a non-uniform electron gas. LDA method can also be seen as the zeroth-order term in a Taylor expansion of the electron density, where higher-order terms might also be included. Thus the gradient expansion approximation (GEA) was introduced.

$$E_x^{GEA}[\rho(\mathbf{r})] = E_x^{LSD}[\rho(\mathbf{r})] + C_x \sum_\sigma \int \frac{|\overrightarrow{\nabla}\rho_\sigma(\mathbf{r})|^2}{\rho_\sigma^{\frac{4}{3}}(\mathbf{r})} d\mathbf{r} \tag{4.31}$$

Equation 4.31 is the exchange-correlation functional proposed by Becke,[314] where C_x is an estimated constant. This low order gradient expansion does not improve LSD results, but even gives worse descriptions. Therefore, the Generalized Gradient Approximation GGA was considered by Perdew and Wang,[315] where not only the local density was considered, but also their local gradients.

$$E_{xc}^{GGA}[\rho] = \int d\mathbf{r} f^{GGA}(\rho_\sigma, \overrightarrow{\nabla}\rho_\sigma); \quad \sigma = \alpha, \beta \tag{4.32}$$

There have been two different strategies to design suitable approximations for the function f^{GGA}. First of all, Becke proposed a widely-used *semi-empirical* exchange density functional (B or B88)[316] where a parameter is included which is chosen on the basis of a least-squares fit to the exact HF exchange energy of the noble gases. This exchange functional is usually used with either the correlation functional proposed by Lee, Yang and Parr[317] (and the BLYP functional is achieved) or the gradient correction proposed by Perdew[318] in 1986, which is known by the acronym P86 (which together with the Becke exchange functional constitutes the BP86).

On the other hand, Perdew and Wang suggested a non-empirical approach for the exchange density functional giving rise to the PW86,[315] and the widely used PW91.[319,320] This non-empirical functional was later on simplified (PBE), and contains only physical constants as parameters.

The meta Generalized Gradient Approximation functionals were proposed to improve upon GGA approaches, and they follow the general form

$$E_{xc}^{mGGA}[\rho] = \int d\mathbf{r} f^{mGGA}(\rho_\sigma, \overrightarrow{\nabla}\rho_\sigma, \nabla^2\rho_\sigma, \tau_\sigma); \quad \sigma = \alpha, \beta \tag{4.33}$$

where τ_σ is the KS orbital kinetic energy density for an electron of spin σ.

$$\tau_\sigma(\mathbf{r}) = \sum_{i=1}^{M} |\overrightarrow{\nabla}\psi_i(\mathbf{r})|^2; \sigma = \alpha, \beta \tag{4.34}$$

As meta-GGA functionals are explicitly orbital-dependent, solving the self-consistent KS equations is not straightforward, therefore mGGA functionals are usually used to calculate the energy using KS orbitals that have been obtained with a GGA functional.

Probably, the most used DFT functional is B3LYP, an adaptation of the hybrid approach as proposed by Becke (see equation 4.35). The parameters a, b, and c are equal to 0.20, 0.72, and 0.81, respectively.

$$E_{XC}^{B3LYP} = (1-a)E_X^{LSD} + aE_X^{HF} + b\Delta E_X^{B88} + cE_C^{LYP} + (1-c)E_C^{LSD} \tag{4.35}$$

DFT method gives surprisingly accurate results and it has become the best choice to study large molecules, as with a moderate computational cost it gives a good prediction for the molecular geometries. In this thesis, DFT has been the method used to study the large fullerene compounds.

4.2.1 Basis Functions

In quantum chemistry, all properties of interest are calculated using the wavefunction (or the electron density) which is generally unknown. The wavefunction is usually expanded in a set of known functions. Equation 4.36 gives the expression for a one-electron atomic orbital, where $\{\varphi_j\}$ forms a complete set of functions. One of the approximations introduced is the finite sum of a finite number of functions, as it is impossible to consider an infinite number of terms.

$$\phi_i = \sum_{j=1}^{\infty} C_{ij}\varphi_j \tag{4.36}$$

The expansion of the atomic orbitals can be developed in terms of the *Slater type orbitals* STOs or in *Gaussian type orbitals* GTOs. The expression for the STOs is given by

$$\phi_{nlm_l} = N_\xi r^{n-1} e^{-\xi r} Y_{lm_l} \tag{4.37}$$

where N_ξ is the normalization constant, Y_{lm_l} the spherical harmonics and ξ is a variational parameter which is related to the radial function and indicates the orbital compression. They reproduce a quite accurate electronic behavior round the nucleus, but the main disadvantage is that the analytical form of the two-electron integrals

is either computationally expensive or unknown,[308,321] so a numerical procedure is required. The *Gaussian type orbital* GTOs,

$$\phi_{nlm_l}^{GTO} = N_\xi r^{n-1} e^{-\xi r^2} Y_{lm_l} \tag{4.38}$$

have the only difference with respect to STOs that there is a quadratic dependence on r in the exponential part. This fact makes the analytical form of the two-electron integrals quite easy. However, a linear combination (contraction) of GTOs is needed to construct an atomic orbital in order to obtain an accurate representation of the electronic behavior close to the nucleus, and in the tail. This is because the GTOs do not have a cusp at the nucleus and fail off to zero too rapidly.

The so-called *minimal basis sets* present the form STO-nG, where n represents the number of GTOs combined to have an approximation of the STO. Every occupied atomic orbital is represented using a single basis function, which corresponds to the smallest set that one could consider. The *extended basis sets* give a more accurate description of the orbitals and account for the shape and size of the molecular size distributions. The latter basis sets can be divided in different categories: e.g. double-, triple-, quadruple-zeta, and split valence. A better representation can be obtained combining two GTOs in a different proportion to represent every atomic orbital (that is indeed the case of a double extended basis set). The value of ζ is included to represent how diffuse the orbital is. Equation 4.39 gives an example of linear combination of two GTOs ($\phi_{2s}^{GTO}(r,\zeta_1)$ and $\phi_{2s}^{GTO}(r,\zeta_2)$) to represent the *2s* orbital.

$$\phi_{2s}(r) = \phi_{2s}^{GTO}(r,\zeta_1) + d\phi_{2s}^{GTO}(r,\zeta_2) \tag{4.39}$$

If instead of using two GTOs a third and a fourth Gaussian orbital is included, a triple- and a quadruple-zeta basis sets are introduced, respectively. Of course, the more GTOs used to describe a single atomic orbital, the better the accuracy but the higher the computational cost. It is usually a high consuming task to use a double-, triple- or quadruple-zeta for every orbital. Calculations are usually simplified applying a double-zeta only for the valence-orbitals, and a single GTO is used to represent the inner-shell orbitals. This approximation is called *split valence*, and good examples of common-split valence basis sets are the Pople 3-21G or 6-31G.

Polarization is usually produced once two or more atoms are brought together. The charge distribution is not uniform as more electronegative atoms might be more negatively charged, whereas others might be more positive. The latter has an effect on the shape of the atomic orbitals. Basis sets can be improved including polarization functions, i.e. adding d-type functions to the first row atoms Li-F and p-type functions to H and He. The introduction of polarization functions leads to hybridized orbitals. For instance, in the case of the HCN molecule, the H-C bond is mainly described by the hydrogen s-orbitals and the carbon s- and p_z orbitals. Of course, the H atom is affected by the presence of the neighboring carbon atom and thus the

electronic cloud of H is deformed. The latter effect cannot be described only considering s-functions on H. However, if a set of p-orbitals is added to hydrogen, the p_z component can be used to improve the description of the C-H bond. Therefore, p-orbitals induce polarization to s-orbitals. Similarly, d-orbitals can be used to polarize p-orbitals. The introduction of polarization functions is denoted in Pople basis sets (such as the 6-31G) using an asterisk (*) if it has been taken into account only for the heavy atoms, or two asterisks (**) if it has also been included for hydrogen atoms. Finally, diffuse functions can also be added to increase the flexibility of the basis set which is especially needed for anionic species, and are usually represented in Pople basis sets using the (+) sign if an extra set of s- and p-type functions for the atoms of the first row is included. The (++) sign denotes that diffuse functions are included for both heavy and hydrogen atoms.

4.2.2 Treating core electrons

The computational time can be highly reduced if core electrons are not explicitly taken into account. There exist different strategies either introducing a model potential to mimic the inner-shell electrons (i.e. effective core potential ECP) or through the so-called frozen core approximation within the computational package ADF. ECPs are usually constructed on a grid using all-electron numerical wavefunctions, where the total pseudopotential is fitted to the analytical form,

$$U^{ECP} = \sum_{p=1}^{N'_{nuc}} \sum_{i=1}^{N_{val}} (U^p_{l_{max}+1}(r_{ip}) + \sum_{l=0}^{l_{max}} \sum_{m=-l}^{l} |Y_{lm}(\Omega_{ip}) > U^p_l(r_{ip}) < Y_{lm}(\Omega_{ip})|) \quad (4.40)$$

where the sum over p corresponds to those atoms having a pseudopotential. The r_{ip} and the Ω_{ip} represent the distance and the angle between electron i measured from the atom p, whereas l_{max} is the maximum orbital angular momentum among the core orbitals. U^p_l is the pseudopotential for an atom p and determines the form of the ECP.

In the frozen core approximation, deep-core atomic orbitals are kept frozen in the molecule calculation as they practically do not change upon bond formation. They are obtained from very accurate single-atom calculations using large STOs basis sets.[322] However, the deep-core orbitals are explicitly orthogonalized against valence orbitals and the frozen core density is included in the calculation, and it is therefore preferred over pseudopotentials (ECPs).[322] The orthogonality between valence basis sets and frozen core is achieved introducing one *core function* per frozen core orbital. Valence orbitals are therefore replaced by a linear combination as represented in equation 4.41.

$$\chi^{valence}_v \Rightarrow \chi^{valence}_v + \sum_{\mu} C_{\mu\nu} \chi^{core}_{\mu} \quad (4.41)$$

All coefficients $C_{\mu\nu}$ are obtained imposing the orthogonalization condition. In a frozen-core calculation, one obtains the total charge density and potential in the

valence and in the core region ignoring the small change in the deep-core orbitals upon bond formation.

4.3 Computational chemistry applied to fullerenes

4.3.1 General overview of the Geometry optimization scheme

In computational chemistry, the geometry of the molecules of interest is obtained after applying a series of iterations which modify the geometry until the energy of the system has reached a minimum. For the study of a certain reaction mechanism, one has to locate different stationary points that correspond to reactants, transition states and products. Reactants and products are minima on the potential energy surface (PES), whereas transition states are first-order saddle-points (see figure 4.1).

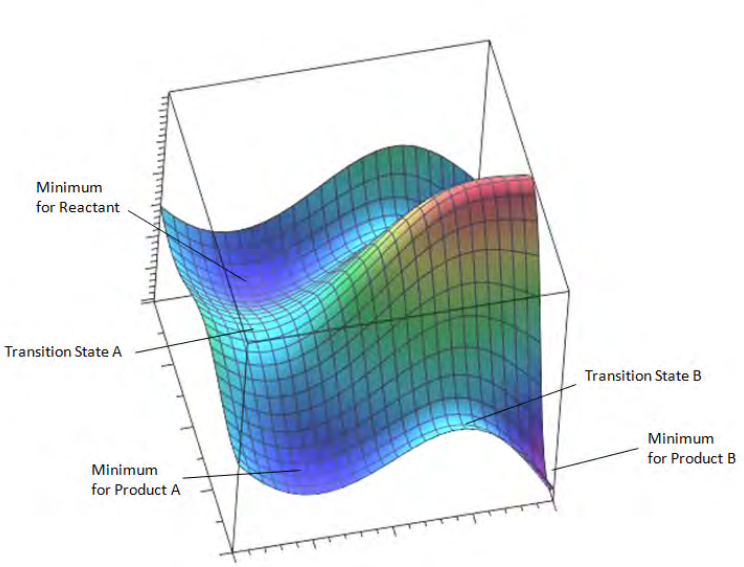

Figure 4.1: Representation of a Potential Energy Surface (PES) where minima and maxima (TS) are represented.

The geometry optimization of reactants and products is pursued calculating the derivatives of the PES with respect to the nuclear positions. An analytic (although very complicated) expression of the energy of the system can be obtained applying the equation 4.42, using the wavefunction and the Hamiltonian.

$$V =< \Psi|\hat{H}|\Psi >= \int d\mathbf{r}_1 d\mathbf{r}_2 ... d\mathbf{r}_N \Psi(r_1 r_2 .. r_N)\hat{H}\Psi(r_1 r_2 .. r_N) \qquad (4.42)$$

The first derivatives of the energy respect to the Cartesian coordinates of all the nuclei correspond to the so-called *gradient*. The gradient of a multi-dimensional

function can be considered to be equivalent to the slope for the two-dimensional function of height as a function of map coordinate. Following the slope downhill, a point where the slope will be equal to zero will be found. The latter corresponds to a minimum of the PES. This procedure is the main principle behind the geometry optimization of computational methods: one starts with an initial geometry, computes the potential energy and the gradient, and afterwards the geometry of the molecule is changed by moving downhill. Once a new geometry is obtained, the cycle starts again until the change on the geometry as well as on the energy of the system is below a certain threshold value.

The localization of transition states is slightly different as they correspond to a maximum along the reaction coordinate, but minima in the other directions. Although the gradient is used to locate transition state geometries, the second derivatives (or Hessian) of the energy are also required. The construction of the Hessian is computationally expensive, and there are different strategies for avoiding the latter problem. When working with large compounds, the best approach consists on either computing the Hessian at the first point of the geometry optimization and updating it following a certain scheme such as the Bofill updating method[323] or constructing a model Hessian with the correct number of eigenvalues corresponding to the approach of reacting molecules.[324]

The geometry optimization scheme is represented in figure 4.2.

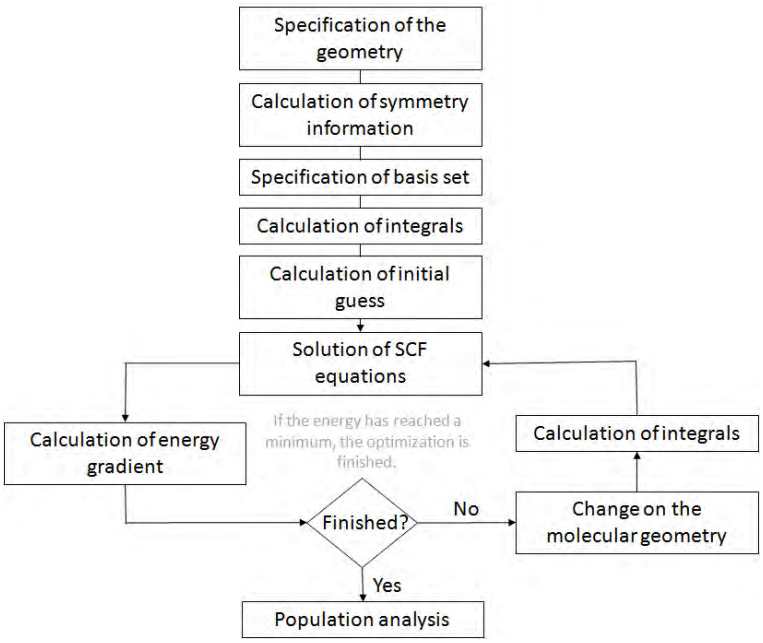

Figure 4.2: Scheme of the geometry optimization procedure

4.3.2 Computing the Energies: Reaction, Activation, Deformation and Interaction Energies

Once the geometry optimization procedure has finished, a final electronic energy is obtained for every optimized structure. Sometimes single point energy calculations (SP) are performed using higher basis sets or different methods. This strategy is usually performed for large systems such as fullerenes where the use of highly accurate methods or large basis sets for the optimization procedure is computationally expensive. Moreover, the assumption is made that the geometry is much less dependent on the size of the basis set than the energy. The latter is usually valid.

The thermodynamics and kinetics of a certain reaction can be extracted from the energies obtained for either reactants, products or transition states (see equations 4.43, 4.44 and figure 4.3).

$$\Delta E_{rx} = E_{products} - E_{reactants} \tag{4.43}$$

$$\Delta E^{\ddagger} = E_{transition\ state} - E_{reactants} \tag{4.44}$$

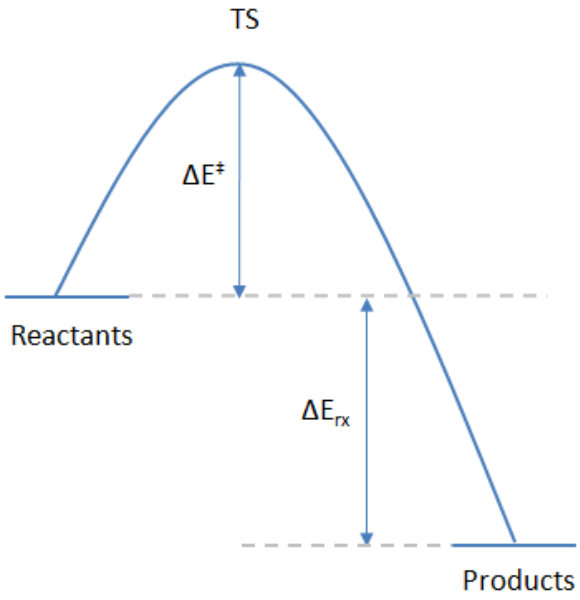

Figure 4.3: Schematic reaction profile where reactant, TS, and products are marked as well as the activation energy ($E^{\ddagger}$) and reaction energy (ΔE_{rx}).

These equations give the reaction and activation energies of the process and are valid either for electronic energies, enthalpies or Gibbs free energies. Of course, the more negative (i.e. the more exothermic) the reaction energy, and the lower the activation barrier obtained, the better the reaction performs. In some cases, activation and

reaction energies are better represented in terms of enthalpies or Gibbs free Energies. The latter is of significant interest when the number of reacting molecules changes along the reaction coordinate (which implies a reduction or an increase of the entropy of the system). The obtaining of enthalpies or Gibbs free energies requires a frequency calculation (second derivatives of the energy). Enthalpies and Gibbs free energy differences at 298.15K and 1 atm are usually computed from electronic energies (ΔE) according to equations 4.45 and 4.46 and assuming an ideal gas behavior.[325]

$$\Delta G_{298} = \Delta H_{298} - T\Delta S_{298} \tag{4.45}$$

$$\Delta H_{298} = \Delta E + \Delta E^0_{vib} + \Delta E^{298}_{trans} + \Delta E^{298}_{rot} + \Delta(\Delta^0_{vib})_{298} + \Delta(pV) \tag{4.46}$$

The terms ΔE^0_{vib}, ΔE^{298}_{trans}, ΔE^{298}_{rot} correspond to the energy differences between products (or transition state) and reactants in zero-point vibrational, translational, and rotational energy, respectively. The change in the vibrational energy difference going from 0 to 298.15K is given by $\Delta(\Delta^0_{vib})_{298}$. The molar work term $\Delta(pV)$ is equal to ΔnRT in the ideal gas approximation, where Δn is the change on the number of molecules $\Delta n = n_{final} - n_{initial}$. For instance, if two molecules react to form one unique compound the variation of molecules is $\Delta n = 1 - 2 = -1$.

The total electronic bond energy can be split up into two terms, the deformation (or preparation, e.g. valence excitation can also be included) and the interaction energies (E_{def} and E_{int}, respectively see equation 4.47).

$$\Delta E_{total} = \Delta E_{def} + \Delta E_{int} \tag{4.47}$$

As already defined in the previous chapter, the deformation energy is the energy required to deform the molecule to the geometry of the transition state or product. The interaction energy is the energy released when both reactant fragments are brought together to the position they will finally have at the final structure. As it can be seen in figure 4.4, the distortion energy along the reaction coordinate is always positive as one has to give energy to the system to distort the geometry. However, the interaction energy can either change from repulsive to stabilizing exactly when the transition state point is reached (see figure 4.4),[181] or in those reactions where negatively charged species are involved it can be stabilizing.[326] At the initial stages of the reaction, reactants might be distorted (which implies a positive interaction and deformation energy) to a certain point of the reaction coordinate (i.e. the transition state) where the overlap between the orbitals of reacting fragments becomes stabilizing.

The interaction energy can also be written as a sum of different terms (see equation 4.48). ΔE_{elstat} is the classical electrostatic interaction between the unperturbed charge distributions of the fragments, the Pauli repulsion ΔE_{Pauli} responsible for the steric repulsion, and the orbital interaction (ΔE_{oi}) which comprises the interactions between the occupied and unoccupied orbitals of both reacting fragments and the polarization.

$$\Delta E_{int} = \Delta E_{elstat} + \Delta E_{Pauli} + \Delta E_{oi} \tag{4.48}$$

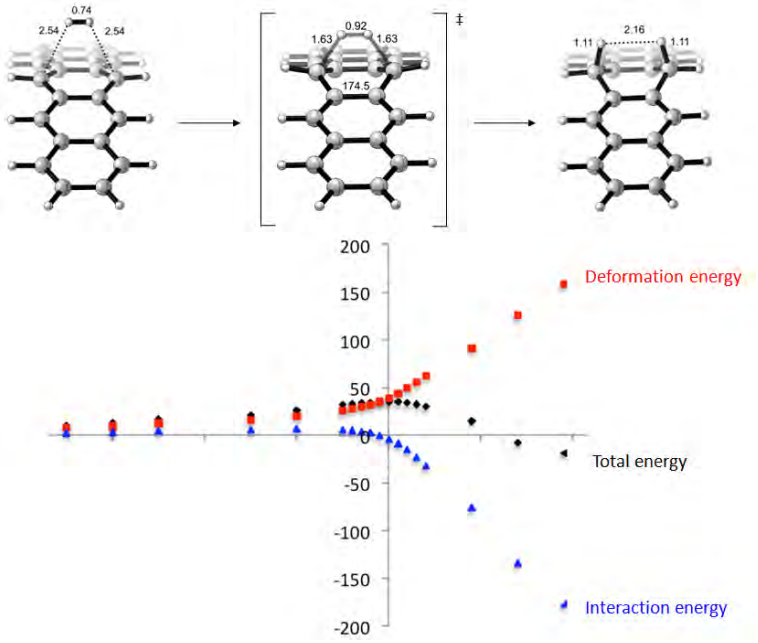

Figure 4.4: Transition state total energy (in black), deformation energy (in red), interaction energy (in blue) along the reaction coordinate for the reaction of pentacene with H_2. The transition state is at x=0.[181]

Deformation energy is actually an effective tool to understand the chemistry of fullerene compounds. The enhanced reactivity found for some bonds of the fullerene surface is usually well-understood if deformation energies of either the cage or the encapsulated cluster are concerned (see chapters 6-8, 10). In addition to that, the insertion of large compounds inside the fullerene cavity has associated with it a deformation energy that can range from small to substantially high. An extremely high deformation energy found theoretically for the encapsulation of large moieties inside fullerenes, will be experimentally translated into a lack of formation of the endohedral fullerene.

4.3.3 Solvation models

Most of chemical reactions are experimentally performed in solvent, hence the effect of the environment is usually an important aspect to evaluate computationally. For a realistic reproduction of the experimental conditions, a large number of solvent molecules might in principle be included. The application of quantum methodologies in the latter scenario is therefore limited, and statistic averages for accounting for all possible configurations of the degrees of freedom of the system might be also included. Different computational solvation models can be considered: those that explicitly account for solvent molecules and those that employ a continuous medium to treat the solvent. Of course, combinations of the two strategies are also possible.

Continuum Solvation models

In this approach, the solute **M** is placed in a suitable shaped hole in the solvent which is considered as a uniform polarizable medium characterized with a dielectric constant ε (see Figure 4.5).[327,328]

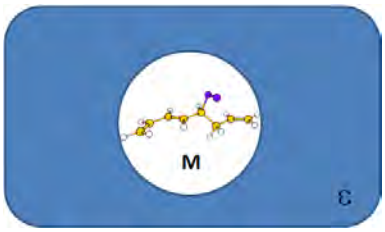

Figure 4.5: Representation of the Continuum Solvation Model, the solute molecule **M** is situated in a cavity inside the solvent medium characterized by a dielectric constant ε. Adapted from ref.[308]

Although the formation of the solute cavity produces a destabilization (it costs energy), the dispersion interactions between solute and solvent usually add stabilization (although a repulsive term might also be present). The solvation (free) energy may be written as in equation 4.49.

$$\Delta G_{solvation} = \Delta G_{cavity} + \Delta G_{dispersion} + \Delta G_{elec} \tag{4.49}$$

The continuum solvation models differ in (1) the definition of the shape and size of the solute hole, (2) the calculation of the cavity/dispersion contribution, (3) the representation of the charge distribution and the description of **M** (either using a force-field, or *ab initio* methodologies), and finally (4) the description of the dielectric medium. The latter is usually described using a dielectric constant ε which in most cases presents a constant value, and corresponds with the radius solvent to the only parameters characteristic of the solvent.

The shape of the solute hole can be considered as a sphere or an ellipsoid with the advantage that the electrostatic interaction between **M** and the dielectric medium can be calculated analytically. More realistic models define the van der Waals surface, which is defined as the atomic radius of every atom multiplied by an scale factor (typically 1.2, see Figure 4.6). However, this surface might present some small areas where no solvent molecules can enter.

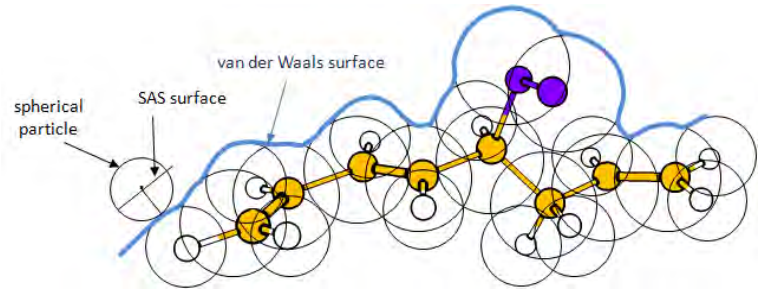

Figure 4.6: Representation of van der Waals surface resulting from the overlap of van der Waals spheres. The *Solvent Accessible Surface* (SAS) considers a spherical particle rolling on the van der Waals surface. Adapted from ref.[308]

The *Solvent Accessible Surface* (SAS) descriptor avoids the latter problem considering a spherical particle of a certain radius being displaced on the van der Waals surface (see Figure 4.6). The cavity can also be obtained from the wavefunction considering, for instance, a surface corresponding to an electron density of 0.001.[329] It has been generally observed that the shape of the cavity plays an important role in obtaining good agreement with experimental values. Main disadvantages of these models come from the incapability of accounting for short-range solvation effects (such as hydrogen bonds, van der Waals interactions, solvent shell structure, charge transfer and hydrophobic effects).

The formation of the solute cavity involves a destabilization because of entropy factors and loss of solvent-solvent interactions, and a stabilization (which could present some small repulsive component) due to the van der Waals interactions between solvent and solute. The energy required to create the cavity can be either calculated to be proportional to the SAS area (see equation 4.50) or parameterized with a constant

ξ (fitted to experimental data) specific for every atom type (see equation 4.51).

$$G_{cavity} + \Delta G_{dispersion} = \gamma SAS + \beta \tag{4.50}$$

$$G_{cavity} + \Delta G_{dispersion} = \sum_{i}^{atoms} \xi_i S_i \tag{4.51}$$

The electrostatic contribution included in equation 4.49 is produced due to the electric field created by the charge distribution of the solute that polarizes the continuum medium, which in turn creates an electrostatic potential inside the cavity. The interaction of the charge distribution of the solute and the latter potential is the main origin of this contribution. Different treatments have been proposed to characterize the electrostatic contribution such as the Poisson-Boltzmann and Born-Onsager-Kirkwood models.[308]

The description of the solute **M** in figure 4.5 can be performed either using a classical approach (a force-field with partial atomic charges) or involving the calculation of the electronic wavefunction (with a semi-empirical or *ab initio* method). In the case of using a quantum description of **M**, an iterative procedure is needed to calculate the interaction with the solvent model. Therefore the so-called *Self-Consistent Reaction Field* (SCRF) models are introduced. The iterative fashion for computing the interaction energy comes from the fact that the calculated electric moments induce charges in the dielectric medium, which consecutively affects the solute molecule thus changing the wavefunction and the electric moments. In SCRF models, the initial dipole moment polarizes the solvent medium which modifies the dipole moment and leads to a different polarization.

For molecular shaped surfaces of the solute cavity (such as SAS), the potential ϕ_σ which accounts for the surface charge of the cavity ($\sigma(\mathbf{r}_s)$) is included in the Hamiltonian operator (see equation 4.52). The potential ϕ_σ is determined by the molecular charge distribution, however as it is included in the Hamiltonian it also modifies the wavefunction. This procedure is thus iterative.

$$\hat{H} = \hat{H}_0 + \phi_\sigma; \qquad \phi_\sigma(\mathbf{r}) = \int d\mathbf{r}_s \frac{\sigma(\mathbf{r}_s)}{\mathbf{r} - \mathbf{r}_s} \tag{4.52}$$

Instead, if an spherical cavity of the solute is considered, the potential ϕ_σ is defined as in equation 4.53, where $\mathbf{r}$ is the dipole moment operator, and $\mathbf{R}$ is proportional to the molecular dipole moment.

$$\phi_\sigma = -\mathbf{r}\mathbf{R} \tag{4.53}$$

The SCRF term does not refer to a specific model, it is usually employed to denote those models where the cavity is defined as shperical or ellipsoidal, the charge

distribution is calculated using a multipole expansion, and the cavity/dispersion interactions are neglected. Although the SCRF solvation treatment is quite simplified, relative values can be reasonably accurate if the considered molecules are polar and similar enough in size and shape. Of course, the assumption that the molecules are spherical or ellipsoidal is only generally true for small compact molecules.

In the so-called *Polarizable Continuum Model* (PCM) a van der Waals cavity formed by overlapping atomic van der Waals radii scaled by an empirical factor is used. Moreover, it employs a detailed description of the electrostatic potential as well as parameterized contributions of the cavity/dispersion based on the surface area.[330] Molecular shaped cavities are also employed in the *COnductor-like Screening MOdel* (COSMO), and the electrostatic potential is defined by partial atomic charges. Although COSMO was originally implemented for semiempirical methods, it has been also used in conjunction with *ab initio* methods.[331,332]

The solute-solvent cavity/dispersion terms are implicitly included in those "mixed" models where the first solvation shell is represented using a certain number of discrete solvent molecules. However, the solute-solvent cavity/dispersion between the solvent molecules and the continuum medium is usually neglected. This strategy presents some limitations, as the number of possible configurations of solvent molecules increases and the parameterization of the continuum model might be performed explicitly taking into account the first solvation shell. In most cases, the first solvation shell is the most important and the obtained results are usually substantially better than those of pure continuum models. However, the application of "mixed" solvation models requires a higher computational cost.

4.3.4 QM/QM' approach: ONIOM

DFT approaches allowed the study of large systems at a reasonable accuracy with a reduced computational cost. However, the study of large molecules such as fullerenes is still in some cases prohibitive. In this context, the use of hybrid techniques employing a more accurate method and basis set for the most relevant parts of the molecules under study, and a cheaper strategy for computing the rest of the atoms (i.e. QM/QM') was proposed. Morokuma and coworkers implemented the n-layered integrated molecular orbital and molecular mechanics usually called ONIOM approach. In a two layer ONIOM calculation, the system is partitioned into two different parts which are treated using different methodologies (see figure 4.7). This process leads to the introduction of dangling bonds, as the partitioning of the molecule implies that covalent bonds have to be cut to generate the inner model. These dangling bonds at the border of the central model are saturated using *link atoms*, which are usually hydrogens.
The total energy of the system is calculated in the following fashion:

$$E^{ONIOM2} = E_{real,low} - E_{model,low} + E_{model,high} \tag{4.54}$$

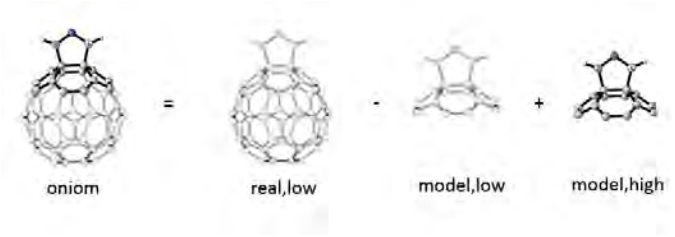

Figure 4.7: ONIOM scheme: the fullerene compound is partitioned into two different layers, the high layer is treated using a high accurate method, whereas the low level is using a less time demanding method (represented using transparency).

where $E_{real,low}$ corresponds to the energy of the real system calculated at the low level of theory, $E_{model,low}$ and $E_{model,high}$ are the energies of the model computed at the low and high-level methods, respectively.[333,334] The ONIOM gradient is obtained from equation 4.55.

$$\frac{\delta E^{ONIOM2}}{\delta q} = \frac{\delta E_{model,high}}{\delta q}.\mathbf{J} + \frac{\delta E_{real,low}}{\delta q} - \frac{\delta E_{model,low}}{\delta q}.\mathbf{J} \tag{4.55}$$

The Jacobian **J** is needed to convert the coordinate system of the model to that of the real one.[333,334] However, in so doing, an arbitrary parameter is introduced, upon which the gradient depends. This is in fact not needed as shown by the AddRemove link-atom model.[335] Similarly, the Hessian and other properties can be expressed. An efficient geometry optimization scheme is obtained when with the least expenditure of computational effort it reaches the optimized geometry. In the ONIOM approach an heuristic strategy to reduce the number of expensive energy and gradient calculations performed at the high level of theory is employed, even if the latter implies a larger number of calculations at the low level of theory. Still, the overall computational cost is usually lower. This is achieved using a microiteration scheme for optimizing the low level region. The ONIOM energy becomes a function of the $E_{real,low}$, if the coordinates of the atoms that determine the energies of the model system are frozen ($E_{model,low}$ and $E_{model,high}$ are constant). Then, it is possible to minimize the energy with respect to the coordinates in the low region using only real system low calculations. Afterwards, one geometry optimization step involving the coordinates of the model system and using the forces obtained with eq. 4.55 is performed. The process of minimizing the energy for the low level by microiteration and the geometry optimization step for the model system is repeated until the ONIOM energy is converged to a minimum with respect to all coordinates.

4.3.5 Tools to predict and understand fullerene reactivity

Bond distances

Carbon-carbon bond distances are frequently used to describe and predict the regioselectivity of a cycloaddition reaction on a fullerene compound. [6,6] bonds present the shortest bond distances as a result of the higher π electronic density and the π bonding orbital interactions on the highest occupied molecular orbital (HOMO). On the other hand, [5,6] bonds are usually larger as a consequence of the antibonding π orbitals also present in the HOMO. These different orbital interactions found in the HOMO of fullerenes are mainly responsible for the C-C bond alternation. Shorter C-C bond distances are in principle associated with enhanced reactivity, as they exhibit more double bond character that facilitates the interaction with dienes/dipoles. This is indeed the case for C_{60} whose exohedral functionalization is mainly produced on the shorter [6,6] bonds.[194,195] Although the bond distance criteria is widely used and in most of the cases the relation is fulfilled, there are some cases described where the most favorable addition site corresponds to the largest C-C bond (see chapter 7).

Pyramidalization angles

Haddon characterized the relationship between structure and chemical reactivity [241,242] with the carbon pyramidalization angle. The carbon pyramidalization angle (θ_p) is a simple measure of the local curvature of carbon containing systems, and it is represented as follows,

$$\theta_p = \theta_{\sigma\pi} - 90^o \tag{4.56}$$

where $\theta_{\sigma\pi}$ is defined as the vector that equalizes the three angles between this vector (centered in the atom in consideration) and the three attached C-C bonds (figure 4.8). The pyramidalization angle for sp^2 centers is 0^o and 19.47^o for sp^3 systems. In principle, those bonds with higher pyramidalization angles exhibit a higher reactivity. The more pyramidalized the carbon atoms are, the closer to the final sp^3 situation and the lower the deformation of the system during the transit from reactants to products. Although pyramidalization angles usually give a good prediction of the most reactive sites of fullerenes, there are some cases (for instance endohedral metallofullerenes) where the latter measure does not correctly describe the reactivities found (see next chapters). All pyramidalization angle measures included in this thesis were performed using the π-orbital axis vector approach (POAV1)[15] as implemented in the POAV3 program.[336]

Frontier orbitals

As pointed out in the previous chapter, cycloaddition reactions are usually described using the FMO theory. Hence, the interaction might be described either between the HOMO of fullerene and the LUMO of diene/dipole or vice-versa. In most cases the most prominent contribution consists of the HOMO of the diene/dipole and the

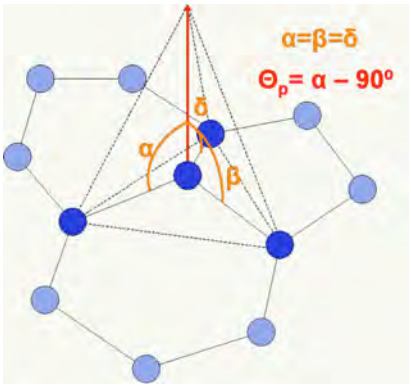

Figure 4.8: Representation of the pyramidalization angle. A vector (red coloured in the figure) that equalizes the α, β and δ angles is defined in order to compute the final pyramidalization angle value ($\theta_p = \alpha - 90^o$). It is 0^o and 19.47^o for sp^2 and sp^3 centers respectively.

LUMO of the fullerene, due to the highly stabilized LUMO orbitals of fullerene compounds. Therefore, the theoretical analysis of the shape of the LUMO orbitals of fullerene compounds might give a prediction of the most reactive C-C bonds. Only those bonds presenting a suitable shape (i.e. antibonding π interactions) to interact with the HOMO of the diene/dipole will be reactive. Although the predictions from the LUMOs are qualitatively correct, fullerene orbitals are highly delocalized. Therefore, a large number of C-C bonds with suitable orbitals for interacting with diene/dipole are usually found.

Apart from using orbitals to predict fullerene reactivity, the stability of the compounds can be compared and estimated from the HOMO-LUMO gap. The difference in energy between the HOMO and the LUMO orbitals gives an idea of how reactive the species is. Highly reactive compounds usually exhibit small HOMO-LUMO gaps. For instance, the encapsulation of metal clusters inside fullerene cages normally produces an increase in the HOMO-LUMO energy difference (the gap is 0.61 eV for C_{78}, whereas 1.27 eV for $Sc_3N@C_{78}$ at BP86/TZ2P) which usually leads to a reduction of the exohedral reactivity (see chapters 6-8).

The electron affinity can also be theoretically predicted using the *Koopmans' theorem*. According to this theory, the electron affinity of a certain compound might be calculated as the negative of the LUMO orbital. For example, the formation of endohedral metallofullerene frequently leads to a decrease of the approximated electron affinity (from 5.98 to 4.89 eV in the case of C_{78} and $Sc_3N@C_{78}$, respectively). A reduction of the electron affinity is usually associated with a decrease of the exohedral reactivity of the compound.

Chapter 5

Objectives

A huge interest for understanding the properties and reactivity of fullerene compounds was sparked since the C_{60} discovery in 1985. Although the reactivity of free fullerene compounds is quite well-established, there are some open issues that make the fullerene research field still highly appealing. In this thesis, the chemical reactivity of endohedral and free fullerene compounds that present prominent applications in chemistry and (bio)medicine is thoroughly investigated.

The reactivity of the so-called TNT endohedral metallofullerenes is still unclear as there are two opposite effects that counteract. First, the introduction of the metal cluster produces an increment of the pyramidalization of the carbon atoms, which leads to an increase of strain energy and, therefore, a higher reactivity of the cage. Second, the charge transfer from the metal cluster to the fullerene structure causes a reduction of the electron affinity, thus diminishing the reactivity of the endohedral compound. In addition, it is important to note that the effect of encapsulation for the different bond types can be different. *The first objective of this thesis is to investigate the effect of the encapsulation of different metals and compounds on the exohedral reactivity of fullerene compounds.* Therefore, the Diels-Alder [4+2] cycloaddition reaction on the TNT endohedral metallofullerenes $X_3N@C_{78}$, $X = Sc, Y$, and on the noble gas endohedral compounds $Ng@C_{60}$, and $Ng_2@C_{60}$, Ng= He-Xe has been investigated in detail. The exohedral reactivity of the endohedral metallofullerene compounds is an important key aspect to determine before any medical application is assessed.

Treating fullerene compounds that present a large number of atoms with full *ab-initio* methodologies is computationally expensive. The computational time needed to study the fullerene properties and reactivity can be highly decreased using QM/QM' approaches such as the so-called ONIOM. *The second objective of this thesis is to assess the performance of the ONIOM strategy for studying the exohedral reactivity of fullerene compounds.*

As said previously, the reactivity of C_{60} has been intensively studied and is considered to be quite well-understood. Still, there are some interesting aspects to determine. In contrast with other cycloaddition products, pyrrolidinofullerenes were thought to be extremely stable. However, the retro-reaction of pyrrolidinofullerenes to revert to initial reactants was experimentally achieved. *The third goal of this thesis is to investigate the reaction mechanism of the retro-cycloaddition to fully understand how it is experimentally achieved.*

A wide variety of reactions have been produced over fullerene compounds. Among them, cycloaddition reactions correspond to the most commonly used procedure for fullerene functionalization. The mechanism of cycloaddition reactions has been intensively debated and different models to understand the mechanism of these interesting reactions have been proposed. *The fourth objective is to apply those chemistry models proposed for describing cycloaddition reactions to fullerene and related compounds.* The successful application of these models might represent an important tool for understanding the regioselectivity of cycloaddition reactions on fullerene compounds.

The great interest for studying fullerene compounds has been basically awakened for the potential applications of these compounds in a wide variety of fields. Interestingly, fullerene compounds might be potential antioxidant agents to treat some neurodegenerative diseases (such as Parkinson's, Alzhemier's, Huntington's) due to their high affinity for accepting electrons. *The fifth objective is to unravel the antioxidant properties of some fullerene derivatives by studying the mechanism of action for the removal of the prejudicial superoxide radical.*

Chapter 6

Chemical reactivity of D_{3h} C_{78} (metallo)fullerene: Regioselectivity changes induced by Sc_3N encapsulation

S. Osuna, M. Swart, J.M. Campanera, J.M. Poblet, M. Solà. "Chemical Reactivity of D_{3h} C_{78} (Metallo)Fullerene: Regioselectivity Changes Induced by Sc_3N Encapsulation". *Journal of the American Chemical Society*. Vol. 130, nº 19 (May 2008) : p. 6206-6214.

http://dx.doi.org/10.1021/ja711167v

Departament de Química, Universitat de Girona, 17071, Girona, Spain
Institut de Química Computacional, Universitat de Girona, 17071, Girona, Spain

Received 17 Dec. 2007; Published on Web 16 Apr. 2008

Abstract

We report here for the first time a full comparison of the exohedral reactivity of a given fullerene and its parent trinitride template endohedral metallofullerene. In particular, we study the thermodynamics and kinetics for the Diels−Alder [4 + 2] cycloaddition between 1,3-butadiene and free $D_{3h'}$-C_{78} fullerene and between butadiene and the corresponding endohedral D_{3h}-$Sc_3N@C_{78}$ derivative. The reaction is studied for all nonequivalent bonds, in both the free and the endohedral fullerenes, at the BP86/TZP//BP86/DZP level. The change in exohedral reactivity and regioselectivity when a metal cluster is encapsulated inside the cage is profound. Consequently, the Diels−Alder reaction over the free fullerene and the endohedral derivative leads to totally different cycloadducts. This is caused by the metal nitride situated inside the fullerene cage that reduces the reactivity of the free fullerene and favors the reaction over different bonds.

Chapter 7

The Diels-Alder reaction on Endohedral $Y_3N@C_{78}$: The importance of the fullerene strain energy

S. Osuna, M. Swart, M. Solà. “The Diels−Alder Reaction on Endohedral $Y_3N@C_{78}$: The Importance of the Fullerene Strain Energy”. *Journal of the American Chemical Society*. Vol. 131, nº 1 (Jan. 2009) : p. 129-139

http://dx.doi.org/10.1021/ja8048783

Departament de Química, Universitat de Girona, 17071, Girona, Spain
Institut de Química Computacional, Universitat de Girona, 17071, Girona, Spain

Received 25 Jun. 2008; Published on Web 04 Dec. 2008

Abstract

We have studied the Diels−Alder reaction of 1,3-butadiene with all nonequivalent bonds of $Y_3N@D_{3h}$-C_{78} at the BP86/TZP//BP86/DZP level of theory. The results obtained are compared with those extracted from a previous study on the free and Sc_3N-endohedral C_{78} fullerene (*J. Am. Chem. Soc.***2008**, *130*, 6206−6214). Our study shows that the most stable regioisomer for the Y_3N compound is obtained for the reaction over a corannulene-type [5,6] bond (**d**), which exhibits the longest bond distance (1.47 Å) and a large pyramidalization angle. As far as we know, this is the first case of a cycloaddition reaction where the most stable addition is obtained over one of the longest C−C bonds in the cage. In contrast to $Sc_3N@D_{3h}$-C_{78}, where bonds close to the scandium atoms were destabilized, this bond **d** has one of the yttrium atoms in close contact. This preference for reacting with those bonds situated close to the yttrium atoms is due to two different factors: first, the D_{3h} cage is extremely deformed, especially in the areas situated close to the yttrium atoms (which contain the most reactive bond **d**), so the attack reduces the strain energy of the cage; second, in the final adduct, the Y_3N cluster gets additional space to adopt a more planar configuration. Since it has been shown (*J. Phys. Chem. B***2007**, *111*, 3363−3369) that the D_{3h} isomer is not the most favorable isomer for endohedral $Y_3N@C_{78}$ (at variance with $Sc_3N@C_{78}$), we also studied the more favorable C_2 isomer. The latter contains [5,5] bonds, which are shown to be the most reactive bonds for cycloaddition, in contrast to previous theoretical predictions (*J. Org. Chem.***2006**, *71*, 46−54). This preference for [5,5] bonds is observed for the C_2 isomers of both endohedral (Sc_3N, Y_3N) and free C_{78} fullerene and is dictated by the fullerene strain energy. We therefore expect that the Diels−Alder reaction on other endohedral metallofullerenes that have already been synthesized (e.g., $Tm_3N@C_2$-C_{78}, $Dy_3N@C_2$-C_{78}) might lead to the same [5,5] adduct.

SUPPORTING INFORMATION

The Diels-Alder reaction on the endohedral $Y_3N@C_{78}$: The importance of the fullerene strain energy

Sílvia Osuna[a], Marcel Swart[a,b*] and Miquel Solà[a*]

a) Institut de Química Computacional and Departament de Química, Universitat de Girona, Campus Montilivi, 17071 Girona, Catalonia, Spain
b) Institució Catalana de Recerca i Estudis Avançats (ICREA), Pg. Lluís Companys 23, 08010 Barcelona, Catalonia, Spain

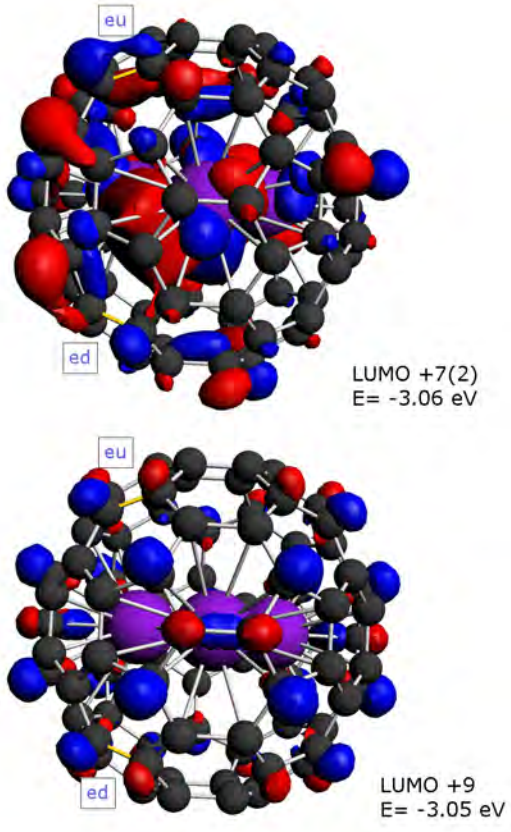

Figure 7.1: Representation of the LUMO+7 (2) and LUMO+9 orbitals of $Y_3N@D_{3h} - C_{78}$. In LUMO+7 (2) only bond e^d presents suitable orbitals to interact with the HOMO of the diene, whereas in LUMO+9 both bonds e^u and e^d can equally interact (isosurface value 0.02 a.u).

product	*bond-type*		$Y_3N@D_{3h}-C_{78}$ up h	$Y_3N@D_{3h}-C_{78}$ down h
1	*A*	*[6,6]*	**0.554**	
2	*C*	*[6,6]*	0.731	0.692
3	*B*	*[6,6]*	**0.547**	**0.625**
4	*B*	*[6,6]*	0.716	0.687
5	*B*	*[6,6]*	0.695	0.726
6	*B*	*[6,6]*	0.704	0.714
7	*A*	*[6,6]*	0.704	0.686
a	*D*	*[5,6]*	0.688	0.698
b	*D*	*[5,6]*	0.709	0.699
c	*D*	*[5,6]*	0.709	
d	*D*	*[5,6]*	**0.601**	**0.631**
e	*D*	*[5,6]*	0.713	0.721
f	*D*	*[5,6]*	0.701	0.711

Table 7.1: Pyramidalization of the nitrogen atom (h in Å) in the final adducts. As a reference, in the initial $Y_3N@D_{3h}-C_{78}$ the pyramidalization of the nitrogen atom is 0.693 Å. The highest reduction of this pyramidalization is obtained when the Diels-Alder reaction occurs over bonds 1, 3, and d which are situated close to one of the yttrium atoms.

product	*bond-type*		ΔE_R	R_{full}
1	*A*	*[6,6]*	-97.6	2.218
3	*B*	*[6,6]*	-97.7	2.318
6	*B*	*[6,6]*	-80.5	1.581
d	*D*	*[5,6]*	-95.7	2.200

Table 7.2: Reaction Energies (ΔE_R in $kcal.mol^{-1}$) of the methylene addition to $Y_3N@D_{3h}-C_{78}$ over four selected bonds and the final C C bond distance of the attacked carbon atoms (R_{full} in Å) are reported. The most favorable reaction energy is obtained for bond 3 which exhibits the largest final C C bond length.

product	*Deformation Energies*			
	Total	$D_{3h}-C_{78}$	diene	Y_3N
1	95.17	74.72	20.11	0.33
2^u	102.78	76.82	25.68	0.27
2^d	110.91	85.04	25.61	0.27
3^u	109.82	83.18	26.12	0.52
3^d	134.19	110.77	23.08	0.35
4^u	82.28	67.03	**14.98**	0.27
4^d	83.38	68.61	**14.46**	0.31
5^u	108.88	81.42	27.06	0.40
5^d	100.7	74.31	26.04	0.35
6^u	81.41	66.48	**14.60**	0.34
6^d	87.26	74	**12.90**	0.36
7^u	79.48	62.58	16.62	0.29
7^d**d**	80.58	63.98	16.30	0.31
a^u	94.20	75.12	18.70	0.38
a^d	95.09	76.06	18.68	0.36
b^u	97.97	73.80	23.88	0.29
b^d	94.96	76.19	18.46	0.31
c	81.83	65.78	15.63	0.42
d^u	84.35	69.99	**14.00**	0.36
d^d	90.24	76.29	**13.62**	0.33
e^u	102.02	79.02	22.66	0.34
e^d	84.08	73.36	**10.35**	0.37
f^u	87.30	68.70	18.26	0.33
f^d	86.51	69.21	16.98	0.32

Table 7.3: Deformation energies of the different fragments (in $kcal.mol^{-1}$) as compared to the initial reactants at the different TS of the Diels-Alder reactions of 1,3-butadiene to $Y_3N@D_{3h}-C_{78}$.

Chapter 8

Reactivity and regioselectivity of noble gas endohedral fullerenes $Ng@C_{60}$ and $Ng_2@C_{60}$ (Ng=He-Xe)

S. Osuna, M. Swart, M. Solà. “Reactivity and Regioselectivity of Noble Gas Endohedral Fullerenes Ng@C_{60} and Ng_2@C_{60} (Ng=He-Xe)”. Chemistry : a European journal. Vol. 15, issue 47 (Dec. 2009) : p. 13111-131123.

http://dx.doi.org/10.1002/chem.200901224

Departament de Química, Universitat de Girona, 17071, Girona, Spain
Institut de Química Computacional, Universitat de Girona, 17071, Girona, Spain

Received: 8 May 2009; Published Online: 26 Oct 2009

Abstract

Recently, it was shown that genuine Ng—Ng chemical bonds are present in the endohedral fullerenes Ng_2@C_{60} in the case of Ng=Xe, while it is more debatable whether a chemical bond exist for Ng=Ar and Kr. The lighter homologues with helium and neon are weakly bonded van der Waals complexes. The presence of a noble gas dimer inside the cage is expected to modify the exohedral reactivity of the C_{60} cage with respect to that of free C_{60}. To investigate the impact of encapsulated diatomic noble gas molecules on the chemical reactivity of C_{60}, we analyzed the thermodynamics and the kinetics of [4+2] Diels-Alder cycloaddition of 1,3-*cis*-butadiene at all nonequivalent bonds in free C_{60}, Ng@C_{60}, and Ng_2@C_{60} (Ng=He, Ne, Ar, Kr, and Xe). Our BP86/TZP calculations reveal that introduction of single noble gas atoms in Ng@C_{60} and noble gas dimers He_2 and Ne_2 in Ng_2@C_{60} has almost no effect on the exohedral reactivity compared to free C_{60}, in agreement with experimental results. In all these cases cycloaddition is clearly favored at the [6,6] bonds in the fullerene cage. For the endohedral compounds He_2@C_{60} and Ne_2@C_{60} a slight preference (by less than 2 kcal mol^{-1}) for bonds closer to the C_5 symmetry axis is found. This picture changes dramatically for the endohedral compounds with heavier noble gas dimers. Encapsulation of these noble gas dimers clearly enhances the reaction, both under thermodynamic and kinetic control. Moreover, in the case of Xe_2@C_{60}, addition to [6,6] and [5,6] bonds becomes equally viable. These reactivity changes in endohedral fullerenes are attributed to stabilization of the LUMO, increased fullerene strain energy, and greater compression of the encapsulated Ng_2 unit along the He to Xe series.

Keywords: cycloaddition • density functional calculations • fullerenes • noble gases • reaction mechanisms

SUPPORTING INFORMATION

Reactivity and regioselectivity of noble gas endohedral fullerenes $Ng@C_{60}$ and $Ng_2@C_{60}$ (Ng=He-Xe)

Sílvia Osuna[a], Marcel Swart[a,b*] and Miquel Solà[a*]

a) Institut de Química Computacional and Departament de Química, Universitat de Girona, Campus Montilivi, 17071 Girona, Catalonia, Spain
b) Institució Catalana de Recerca i Estudis Avançats (ICREA), Pg. Lluís Companys 23, 08010 Barcelona, Catalonia, Spain

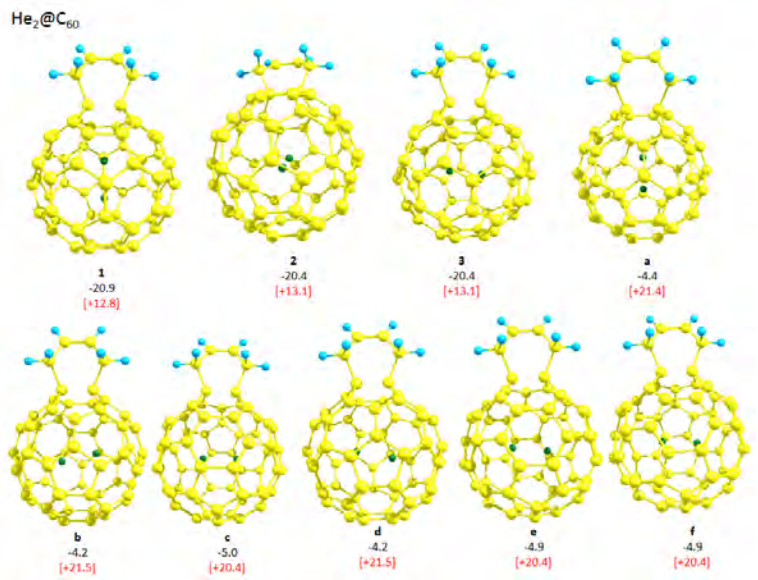

Figure 8.1: Optimized structures at BP86/TZP for the final adducts corresponding to the Diels-Alder reaction to all nonequivalent bonds of the endohedral compound $He_2@C_{60}$. The reaction energies (in black), activation barriers (in red, between brackets) have also been represented. The most favorable addition sites have been marked in boldface.

$Ng_2@C_{60}$	E_{def}
He	0.1
Ne	0.8
Ar	11.2
Kr	22.5
Xe	34.0

Table 8.1: Deformation energies of the noble gases endohedral fullerenes considered calculated as the difference in energy between the distorted, the free cage. All energies have been expressed in $kcal.mol^{-1}$.

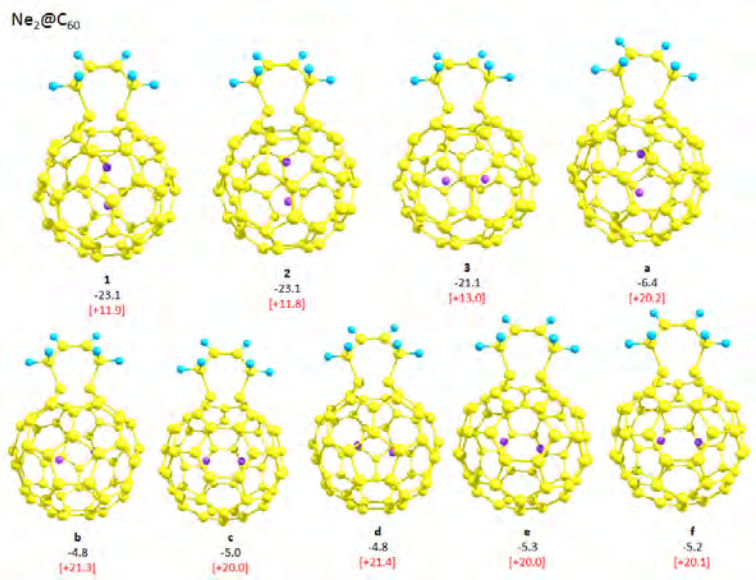

Figure 8.2: Optimized structures at BP86/TZP for the final adducts corresponding to the Diels-Alder reaction to all nonequivalent bonds of the endohedral compound $Ne_2@C_{60}$. The reaction energies (in black), activation barriers (in red, between brackets) have also been represented. The most favorable addition sites have been marked in boldface.

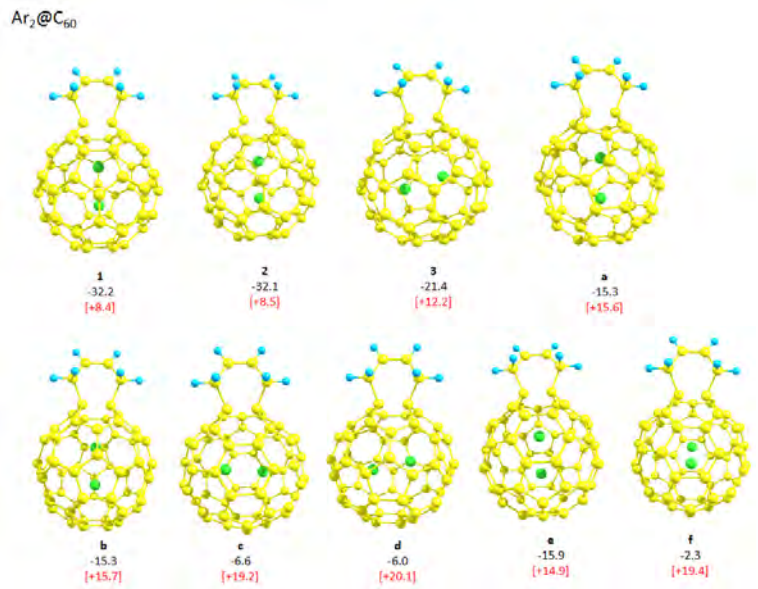

Figure 8.3: Optimized structures at BP86/TZP for the final adducts corresponding to the Diels-Alder reaction to all nonequivalent bonds of the endohedral compound $Ar_2@C_{60}$. The reaction energies (in black), activation barriers (in red, between brackets) have also been represented. The most favorable addition sites have been marked in boldface.

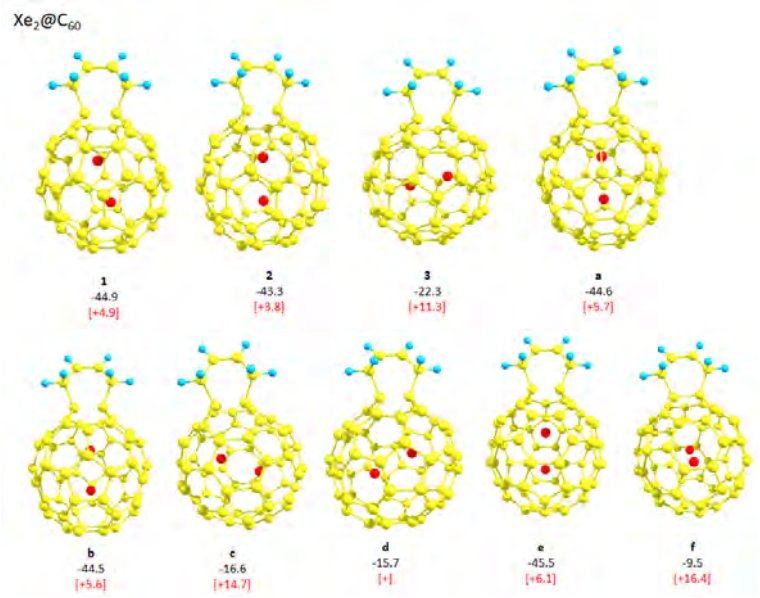

Figure 8.4: Optimized structures at BP86/TZP for the final adducts corresponding to the Diels-Alder reaction to all nonequivalent bonds of the endohedral compound $Xe_2@C_{60}$. The reaction energies (in black), activation barriers (in red, between brackets) have also been represented. The most favorable addition sites have been marked in boldface.

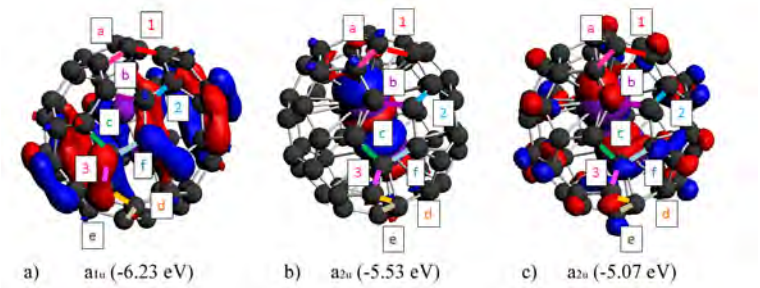

Figure 8.5: The HOMO orbitals for $He_2@C_{60}$ (a), $Kr_2@C_{60}$ (b), $Xe_2@C_{60}$ (c) are represented. Isosurface values are -0.03 au. All nonequivalent bonds have been marked following the coloring scheme used in Figure 1.

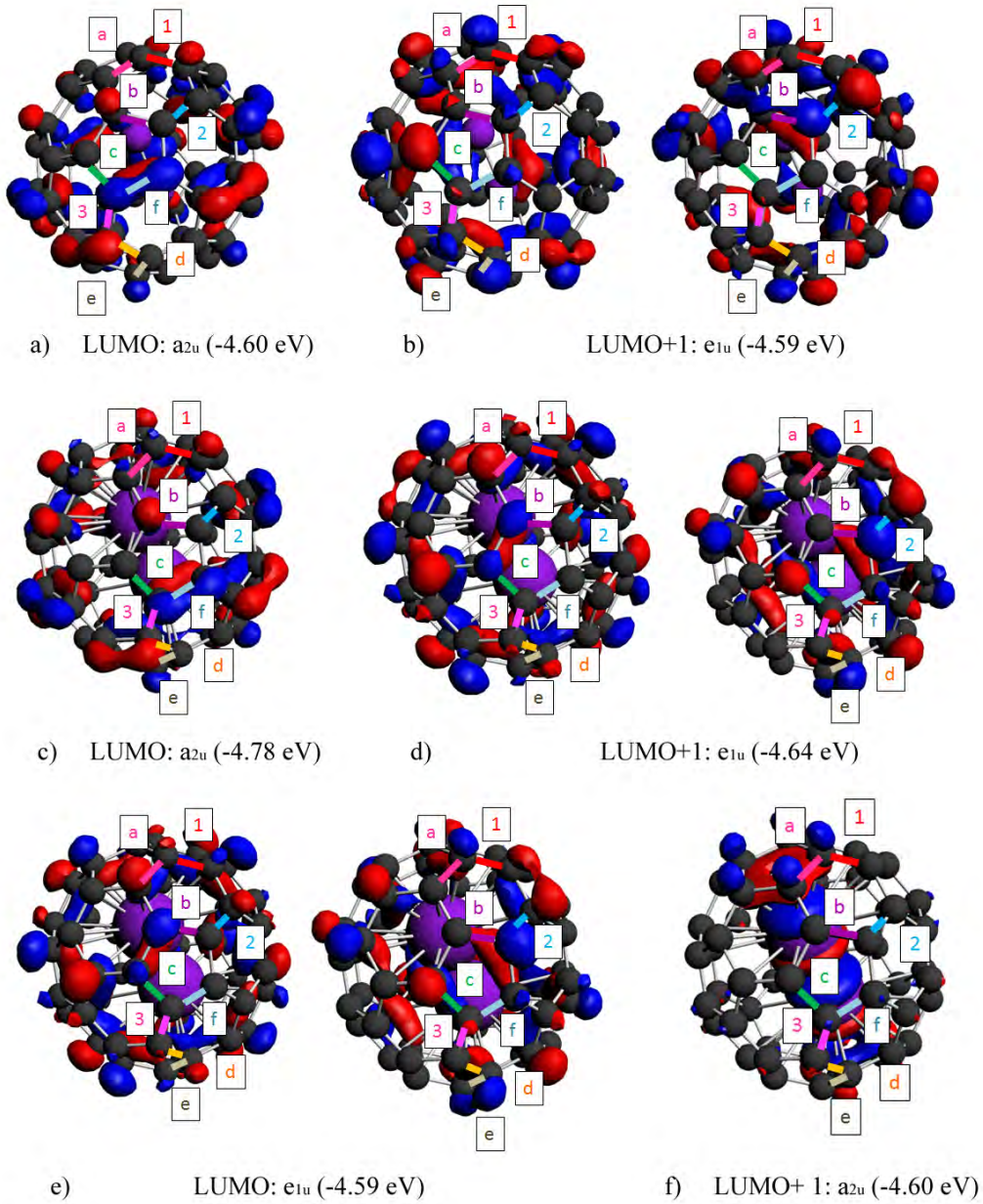

Figure 8.6: The LUMO orbitals for $He_2@C_{60}$ (a-b), $Kr_2@C_{60}$ (c-d), $Xe_2@C_{60}$ (e-f) are represented. Isosurface values are -0.03 au. All nonequivalent bonds have been marked following the coloring scheme used in Figure 1

Chapter 9

Diels-Alder reaction between cyclopentadiene and C_{60}: An analysis of the performance of the ONIOM method for the Study of Chemical reactivity in fullerenes and nanotubes

S. Osuna, J. Morera, M. Cases, K. Morokuma, M. Solà. “Diels−Alder Reaction between Cyclopentadiene and C_{60}: An Analysis of the Performance of the ONIOM Method for the Study of Chemical Reactivity in Fullerenes and Nanotubes”. *Journal of Physical Chemistry A.* Vol. 113, issue 35 (2009) : p. 9721-9726.

http://dx.doi.org/10.1021/jp904294y

Departament de Química, Universitat de Girona, 17071, Girona, Spain
Institut de Química Computacional, Universitat de Girona, 17071, Girona, Spain

Received: May 8, 2009; Revised Manuscript Received: July 16, 2009; Publication Date (Web): August 7, 2009

Abstract

In this article, we theoretically analyze the Diels−Alder cycloaddition between cyclopentadiene and C_{60} for which experimental results on energy barriers and reaction energies are known. The comparison of the results obtained with the two-layered ONIOM approach using different partitions for the high- and low-level layers with those obtained employing the B3LYP/6-31G(d) method for the entire system allows us to conclude that the partition including a pyracylene unit of C_{60} in the description of the high-level layer is enough to get excellent results. Using this partition in the two-layered ONIOM approach, we have computed the energy barriers and reaction energies for this Diels−Alder reaction for different functionals, and we have compared them with experimental data. From this comparison, both the ONIOM2(M06-2X/6-31G(d):SVWN/STO-3G) and the M06-2X/6-31G(d)//ONIOM2(B3LYP/6-31G(d):SVWN/STO-3G) methods are recommended as reliable and computationally affordable approaches to be exploited for the study of the chemical reactivity of [6,6]-bonds in fullerenes and nanotubes.

Chapter 10

On the mechanism of the thermal retrocycloaddition of pyrrolidinofullerenes (retro-Prato reaction)

S. Filippone, M. Izquierdo Barroso, Á. Martín-Domenech, S. Osuna, M. Solà, N. Martín. “On the Mechanism of the Thermal Retrocycloaddition of Pyrrolidinofullerenes (Retro-Prato Reaction)”. *Chemistry : a European journal*. Vol. 14, issue 17 (Jun. 2008) : p. 5198-5206.

http://dx.doi.org/10.1002/chem.200800096

Departament de Química, Universitat de Girona, 17071, Girona, Spain
Institut de Química Computacional, Universitat de Girona, 17071, Girona, Spain

Received: 17 January 2008; Published Online: Apr 25 2008

Abstract

In contrast to *N*-methyl or N-unsubstituted pyrrolidinofullerenes, which efficiently undergo the retrocycloaddition reaction to quantitatively afford pristine fullerene, *N*-benzoyl derivatives do not give this reaction under the same experimental conditions. To unravel the mechanism of the retrocycloaddition process, trapping experiments of the in-situ thermally generated azomethine ylides, with an efficient dipolarophile were conducted. These experiments afforded the respective cycloadducts as an *endo*/*exo* isomeric mixture. Theoretical calculations carried out at the DFT level and by using the two-layered ONIOM (our own *n*-layered integrated molecular orbital and molecular mechanics) approach underpin the experimental findings and predict that the presence of the dienophile is not a basic requirement for the azomethine ylide to be able to leave the fullerene surface under thermal conditions. Once the 1,3-dipole is generated in the reaction medium, it is efficiently trapped by the dipolarophile (maleic anhydride or *N*-phenylmaleimide). However, for N-unsubstituted pyrrolidinofullerenes, the participation of the dipolarophile in assisting the 1,3-dipole to leave the fullerene surface throughout the whole reaction pathway is also a plausible mechanism that cannot be ruled out.

Keywords: density functional calculations • fullerenes • nanostructures • reaction mechanisms • retrocycloaddition

Chapter 11

Cycloaddition reactions of butadiene and 1,3-dipoles to curved arenes, fullerenes, and nanotubes: Theoretical evaluation of the role of distortion energies on activation barriers

S. Osuna, K. N. Houk. “Cycloaddition Reactions of Butadiene and 1,3-Dipoles to Curved Arenes, Fullerenes, and Nanotubes: Theoretical Evaluation of the Role of Distortion Energies on Activation Barriers”. *Chemistry : a European journal*. Vol. 15, issue 47 (Dec. 2009) : p. 13219-13231.

http://dx.doi.org/10.1002/chem.200901761

Departament de Química, Universitat de Girona, 17071, Girona, Spain
Institut de Química Computacional, Universitat de Girona, 17071, Girona, Spain

Received: 25 June 2009; Published Online: Oct 28 2009

Abstract

Diels-Alder cycloadditions of butadiene and 1,3-dipolar cycloadditions of azomethine ylide, fulminic acid, and the parent nitrone to polyacenes, fullerenes, and nanotubes have been investigated with density functional theory and ONIOM methods. Activation barriers obtained for cycloaddition reactions on planar and curved systems have been shown to be highly correlated to the energy needed to distort the reactants to the geometry of the transition state (TS).

Keywords: cycloaddition • density functional calculations • Diels-Alder reactions • distortion/interaction theory • Marcus theory • ONIOM

SUPPORTING INFORMATION

Cycloaddition reactions of butadiene and 1,3-dipoles to curved arenes, fullerenes, and nanotubes: Theoretical evaluation of the role of distortion energies on activation barriers

Sílvia Osuna[a,b] and K. N. Houk [a*]

a) Department of Chemistry and Biochemistry, University of California, Los Angeles, Los Angeles, CA 90095-1569 USA
b) Institut de Química Computacional and Departament de Química, Universitat de Girona, Campus Montilivi, 17071 Girona, Catalonia, Spain

	ΔE_R	$\Delta E^{\ddagger}$	R_{CC}		$\Delta E_d^{\ddagger}$
Benzene endo	-24.3	15.0	2.294	2.294	22.0
Benzene exo	-26.2	14.7	2.287	2.287	21.4
Naphthalene 1	9.2	28.7	1.905	2.527	35.8
Naphthalene 2	-4.4	17.4	1.932	3.018	19.7
Naphthalene 3	-37.6	9.5	2.279	2.438	16.5
Naphthalene 4	-13.9	19.8	1.877	2.770	24.7
Anthracene 1	18.5	31.5	1.718	2.530	48.2
Anthracene 2	3.2	16.5	1.923	3.128	19.0
Anthracene 3	-41.4	7.3	2.315	2.463	14.6
Anthracene 4	-8.0	19.8	1.685	2.714	38.2
Anthracene 5	-17.5	11.5	2.075	3.063	14.5
Hexacene 1	28.9	38.3	1.713	2.846	70.6
Hexacene 2	-17.3	4.7	2.241	3.149	8.6
Hexacene 3	-45.3	5.4	2.485	2.343	13.1
Hexacene 4	-2.3	17.7	1.848	3.218	19.6
Cycloheptacene 1	-83.5	0.0	-	-	-
Cycloheptacene 2	-60.2	0.0	-	-	-
Coronene 1	13.9	28.5	1.730	2.490	48.2
Coronene 2	4.6	24.8	1.860	2.597	34.7
Coronene 3	-2.2	19.3	1.846	3.182	22.3
Coronene 4	-37.6	8.9	2.359	2.359	16.1
Curved coronene 1	-5.0	10.3	1.959	3.153	13.9
Curved coronene 2	-26.9	5.1	2.228	2.525	14.6
Curved coronene 3	-18.2	8.0	2.018	3.132	12.8
Curved coronene 4	-27.3	2.6	2.253	2.495	11.9
Corannulene 1	-22.6	11.8	2.015	2.848	14.9
Corannulene 2	-24.3	7.6	2.124	2.651	14.3
Corannulene 3	-10.9	11.4	2.005	3.038	13.9
Corannulene 4	-49.9	3.4	2.451	2.451	10.3
Curved Corannulene 1	-34.3	2.1	2.200	3.114	6.7
Curved Corannulene 2	-48.4	-2.6	2.583	2.846	2.6
Curved Corannulene 3	-28.1	4.7	2.115	3.120	8.8
Curved Corannulene 4	-45.3	-2.1	2.540	2.540	6.0
C_{60} [6,6]	-53.5	-4.1	3.000	3.000	1.7
C_{60} [5,6]	-34.4	1.5	2.152	3.223	4.4
(5,5) SWCNT 1	-26.3	4.3	2.143	2.730	9.0
(5,5) SWCNT 2	-26.1	5.1	2.088	2.984	5.4
(6,6) SWCNT 1	-17.2	9.7	2.073	2.781	15.5
(6,6) SWCNT 2	-8.2	10.7	1.636	2.614	31.1

Table 11.1: Reaction energies (ΔE_R in $kcal.mol^{-1}$), activation barriers ($\Delta E^{\ddagger}$ in $kcal.mol^{-1}$), distortion energies ($\Delta E_d^{\ddagger}$ in $kcal.mol^{-1}$), and distances (R_{CC} in Å) for the bonds being formed at the TS for the 1,3-dipolar cycloaddition with azomethine ylide are represented.

	ΔE_R		$\Delta E^{\ddagger}$	R_{CC}	$\Delta E_d^{\ddagger}$
Benzene exo	2.4	38.2	2.117	2.117	43.8
Naphthalene 1	39.4	60.7	2.038	2.038	66.1
Naphthalene 2	21.0	49.4	1.720	2.336	70.2
Naphthalene 3	-13.5	32.3	2.068	2.265	38.7
Naphthalene 4	15.8	45.4	2.061	2.063	50.6
Anthracene 1	49.0	67.2	1.912	2.095	73.1
Anthracene 2	27.3	51.7	2.255	1.679	80.0
Anthracene 3	-18.0	29.8	2.081	2.296	37.4
Anthracene 4	22.0	48.6	1.836	2.234	57.6
Anthracene 5	7.9	38.1	1.679	2.461	69.9
Hexacene 1	64.5	77.1	1.803	2.072	85.7
Hexacene 2	8.2	23.1	1.904	3.371	27.7
Hexacene 3	-21.5	27.9	2.107	2.303	35.4
Hexacene 4	27.9	51.5	2.228	1.750	66.4
Cycloheptacene 1	5.0	26.8	2.539	2.539	28.4
Cycloheptacene 2	-30.9	6.6	2.162	3.338	10.5
Coronene 1	52.7	66.2	1.841	2.146	77.4
Coronene 2	41.3	59.0	2.173	1.897	68.0
Coronene 3	22.7	52.0	1.735	2.316	71.3
Coronene 4	-13.2	32.6	2.164	2.164	39.1
Curved coronene 1	30.7	48.8	1.764	2.280	63.3
Curved coronene 2	8.2	34.2	2.273	2.008	41.1
Curved coronene 3	14.9	39.6	1.756	2.420	55.5
Curved coronene 4	6.3	31.5	2.154	2.154	41.0
Corannulene 1	9.2	37.7	1.771	2.428	50.1
Corannulene 2	9.2	34.3	1.790	2.410	47.7
Corannulene 3	21.2	41.9	1.700	2.334	65.2
Corannulene 4	-19.7	24.9	2.206	2.207	32.0
Curved Corannulene 1	-3.0	28.2	1.734	2.566	43.6
Curved Corannulene 2	-15.8	19.8	1.947	2.613	26.9
Curved Corannulene 3	4.9	32.0	1.726	2.504	50.0
Curved Corannulene 4	-13.2	21.6	2.215	2.215	30.0
C_{60} [6,6]	-21.7	17.8	2.233	2.233	26.5
C_{60} [5,6]	-3.0	29.2	1.752	2.572	42.3
(5,5) SWCNT 1	10.5	33.4	1.750	2.461	49.5
(5,5) SWCNT 2	8.8	35.5	1.788	2.462	48.1
(6,6) SWCNT 1	19.7	40.5	1.756	2.402	57.0
(6,6) SWCNT 2	35.8	48.5	1.761	2.354	62.0

Table 11.2: Reaction energies (ΔE_R in $kcal.mol^{-1}$), activation barriers ($\Delta E^{\ddagger}$ in $kcal.mol^{-1}$), distortion energies ($\Delta E_d^{\ddagger}$ in $kcal.mol^{-1}$), and distances (R_{CC} in Å) for the Diels-Alder reaction with s-cis-1,3-butadiene are represented.

	1,3-dipolar: methylene nitrone				
	ΔE_R	$\Delta E^{\ddagger}$	$\Delta E_d^{\ddagger}$	R_{OC}	R_{CC}
Benzene exo	7.9	27.8	37.6	1.907	2.160
Naphthalene 3	-2.6	21.8	30.7	2.225	1.969
Naphthalene 3_2	-3.0	22.9	31.1	2.138	2.022
Anthracene 3	-6.8	19.6	28.4	2.236	2.002
Anthracene 3_2	-7.1	20.8	28.9	2.141	2.058
Hexacene 3	-12.2	18.0	26.4	2.241	2.031
Hexacene 3_2	-12.0	19.1	27.1	2.155	2.081
Coronene 4	-4.9	21.8	30.7	2.181	2.000
Curved coronene 2	5.7	20.8	31.2	2.138	1.981
Curved coronene 2_2	6.6	21.2	32.9	2.191	1.928
Curved coronene 4	6.6	20.7	32.2	2.208	1.939
Corannulene 1	9.5	24.0	34.5	1.833	2.257
Corannulene 2	6.0	25.5	34.1	1.994	2.031
Corannulene 2_2	9.3	19.2	30.7	2.290	1.878
Corannulene 4	-16.0	16.1	23.7	2.077	2.192
Curv corannulene 1	-0.5	17.2	25.5	2.416	1.851
Curv corannulene 2	-14.3	10.4	17.6	2.353	2.044
Curv corannulene 2_2	-14.7	11.3	19.2	2.210	2.023
Curv corannulene 3	5.6	19.9	30.0	2.635	1.771
Curv corannulene 3_2	3.5	20.7	32.6	2.346	1.835
Curved corannulene 4	-14.3	13.1	21.0	2.204	2.084
C_{60} [6,6]	-15.8	8.8	14.5	2.138	2.154
C_{60} [5,6]	0.0	18.0	27.0	2.340	1.869
(5,5) SWCNT 1	6.1	18.4	30.1	2.203	1.884
(5,5) SWCNT 2	5.4	22.0	37.8	2.266	1.821
(6,6) SWCNT 1	14.8	24.6	40.7	2.167	1.823
(6,6) SWCNT 2	24.5	34.3	54.7	2.088	1.766

Table 11.3: Reaction energies (ΔE_R in $kcal.mol^{-1}$), activation barriers ($\Delta E^{\ddagger}$ in $kcal.mol^{-1}$), distortion energies ($\Delta E_d^{\ddagger}$ in $kcal.mol^{-1}$), and distances (R_{CC} and R_{OC} in Å) for the bonds being formed at the 1,3-dipolar cycloadditions with methylene nitrone.

	1,3-dipolar: fulminic acid				
	ΔE_R	$\Delta E^{\ddagger}$	$\Delta E_d^{\ddagger}$	R_{OC}	R_{CC}
Benzene exo	-5.2	22.9	30.8	2.52	1.930
Naphthalene 3	-16.1	18.9	26.4	2.543	2.010
Naphthalene 3_2	-16.1	20.5	27.7	2.488	2.022
Anthracene 3	-20.5	17.6	24.7	2.548	2.046
Anthracene 3_2	-20.3	19.2	26.2	2.486	2.058
Hexacene 3	-23.9	16.6	23.5	2.546	2.076
Hexacene 3_2	-23.5	18.1	24.8	2.499	2.086
Coronene 4	-16.3	19.4	27.1	2.013	2.534
Curved coronene 2	-4.8	19.0	24.3	2.664	1.958
Curved coronene 2_2	-3.0	20.7	26.5	2.566	1.943
Curved coronene 4	-7.9	18.3	24.5	2.566	2.001
Corannulene 1	-1.4	19.5	24.4	2.765	1.868
Corannulene 2	-4.1	17.5	23.7	2.676	1.940
Corannulene 2_2	-0.7	23.8	29.2	2.465	1.957
Corannulene 4	-26.9	15.7	22.1	2.509	2.096
Curv corannulene 1	-11.3	14.1	16.3	2.918	1.917
Curv corannulene 2	-24.8	11.8	15.2	2.692	2.071
Curv corannulene 2_2	-25.9	11.8	18.1	2.541	2.111
Curv corannulene 3	-3.8	12.9	20.2	2.916	1.904
Curv corannulene 3_2	-6.6	17.8	22.4	2.802	1.908
Curved corannulene 4	-24.6	13.1	18.5	2.583	2.100
C_{60} [6,6]	-28.5	11.9	16.6	2.546	2.118
C_{60} [5,6]	-10.5	15.2	16.8	2.853	1.914
(5,5) SWCNT 1	-2.9	17.9	21.1	2.679	1.907
(5,5) SWCNT 2	-5.9	17.2	21.9	2.743	1.896
(6,6) SWCNT 1	5.8	23.0	29.0	2.662	1.871
(6,6) SWCNT 2	12.9	24.5	32.0	2.752	1.797

Table 11.4: Reaction energies (ΔE_R in $kcal.mol^{-1}$), activation barriers ($\Delta E^{\ddagger}$ in $kcal.mol^{-1}$), distortion energies ($\Delta E_d^{\ddagger}$ in $kcal.mol^{-1}$), and distances (R_{CC} and R_{OC} in Å) for the bonds being formed at the 1,3-dipolar cycloadditions with nitrile oxide.

Chapter 12

On the mechanism of action of fullerene derivatives for superoxide dismutation

S. Osuna, M. Swart, M. Solà. “On the Mechanism of Action of Fullerene Derivatives in Superoxide Dismutation”. Chemistry : a European journal. Vol. 16, issue 10 (Mar. 2010) : 3207 – 3214.

http://dx.doi.org/10.1002/chem.200902728

Departament de Química, Universitat de Girona, 17071, Girona, Spain
Institut de Química Computacional, Universitat de Girona, 17071, Girona, Spain

Received: 4 October 2009; Published Online: 29 Jan 2010

Abstract

We have studied the mechanism of the antioxidant activity of C_{60} derivatives at the BP86/TZP level with inclusion of solvent effects (DMSO) by using the COSMO approach. The reaction studied here involves degradation of the biologically relevant superoxide radical ($O_2^{\cdot -}$), which is linked to tissue damage in several human disorders. Several fullerene derivatives have experimentally been shown to be protective in cell culture and animal models of injury, but precisely how these compounds protect biological systems is still unknown. We have investigated the activity of tris-malonyl C_{60} (also called C_3), which efficiently removes the superoxide anion with an activity in the range of several biologically effective, metal-containing superoxide dismutase mimetics. The antioxidant properties of C_3 are attributed to the high affinity of C_{60} to accept electrons. Our results show that once the superoxide radical is in contact with the surface of C_3, its unpaired electron is transferred to the fullerene. This process, which converts the damaging $O_2^{\cdot -}$ to neutral oxygen O_2, is the rate-determining step of the reaction. Afterwards, another superoxide radical reacts with $C_3^{\cdot -}$ to form hydrogen peroxide and in the process takes up the additional electron that was transferred in the first step. The overall process is clearly exothermic and, in general, involves reaction steps with relatively low activation barriers. The capability of C_3 to degrade a highly reactive oxygen species that is linked to several human diseases is of immediate interest for future applications in the field of biology and medicine.

Keywords: antioxidants • density functional calculations • fullerenes • radicals • radical reactions

Chapter 13

Results and Discussion

Hereafter, the most important results from chapters 6-12 will be briefly summarized.

13.1 Chemical reactivity of D_{3h} C_{78} (metallo)fullerene: Regioselectivity changes induced by Sc_3N encapsulation

Although the exohedral reactivity of free fullerenes is quite well-understood, how TNT endohedral metallofullerenes react is still unclear as different factors counteract. An increase of the reactivity might be expected taking into account that the insertion of the TNT unit leads to a higher pyramidalization of some carbon atoms. The more pyramidalized the C-C bond being attacked, the closer to the final sp^3 situation of the final adduct and the lower the deformation energy of the cage. On the other hand, the electronic transfer produced from the TNT unit to the fullerene reduces the electron affinity of the cage which implies that a reduction of the reactivity might be produced. Moreover, the LUMO orbitals of the endohedral compound are destabilized because of the charge transfer of six electrons from the metal cluster to the fullerene cage, thus disfavoring the interaction with the HOMO of the diene. In contrast to C_{80}, the rotation of the TNT unit encapsulated inside the C_{78} cage is highly impeded,[337] and therefore the study of how the reactivity of the different bonds is affected by the metal insertion can be directly investigated. The Diels-Alder [4+2] reaction has been studied at BP86/TZP//BP86/DZP over the thirteen non-equivalents bonds of the $D_{3h} - C_{78}$ and $Sc_3N@D_{3h} - C_{78}$ compounds (see Figure 13.1). In Figure 13.1, all non-equivalents bonds are marked in the fullerene compound, as well as the activation barriers obtained for every addition site. C_{78} has seven non-equivalent [6,6] type bonds which can be classified in three subtypes, (1) Pyracylenic or type A (Bonds called **1** and **7** (figure 13.1)), (2) Type B (Bonds **3**, **4**, **5** and **6**) and (3) Pyrenic or type C (Bond **2**); and six coranulenne or type D [5,6] bonds (**a-f**). We will refer to each different bond according to this nomenclature, where for example number **1** is used to denote the pyracylenic or type A bond situated in the position indicated in figure 13.1.

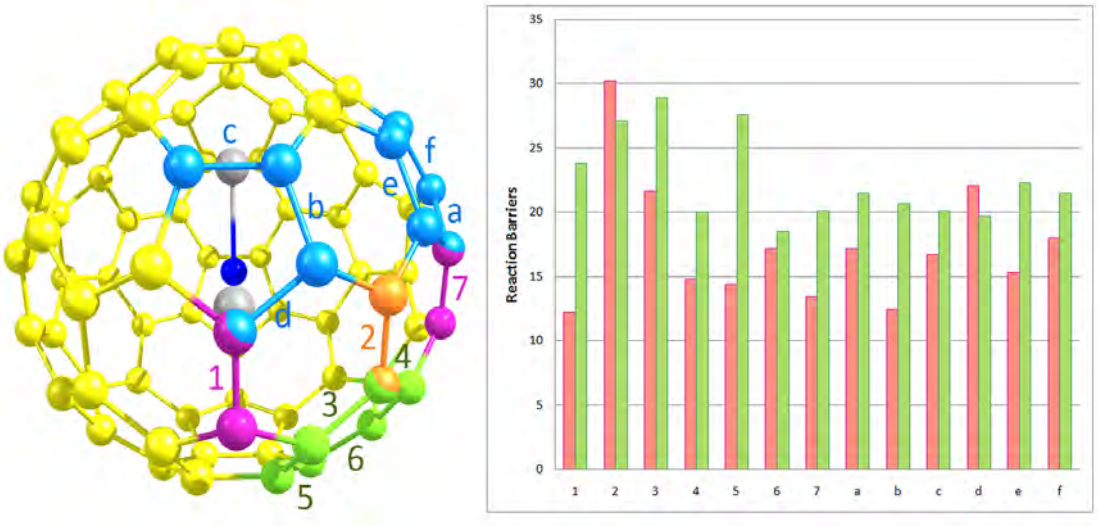

Figure 13.1: Representation of all non-equivalents bonds of the $Sc_3N@C_{78}$ endohedral fullerene, and the activation barriers obtained for the Diels-Alder reaction on the free C_{78} (represented in red) and the $Sc_3N@C_{78}$ (represented in green)compounds. All energies are represented in $kcal.mol^{-1}$

The Diels-Alder reaction on the free $D_{3h} - C_{78}$ cage is basically favored over a [5,6] bond called **b** and two type A [6,6] bonds (bonds **1** and **7**). Coranulenne or type D [5,6] bond **b** presents a reaction energy of -23.9 $kcal.mol^{-1}$ and an activation barrier of 12.5 $kcal.mol^{-1}$. However, pyracylenic type-A bonds called **1** and **7** do also present favorable reaction and activation barriers (for bond **1**: ΔE_R=-16.0 $kcal.mol^{-1}$, $\Delta E^{\ddagger}$=12.2 $kcal.mol^{-1}$, and for bond 7: ΔE_R=-18.8 $kcal.mol^{-1}$, $\Delta E^{\ddagger}$=13.5 $kcal.mol^{-1}$). It is important to remark here that pyracylene bonds correspond to the most favorable addition sites for C_{60} (see chapter 8), and that is indeed the case for the free $D_{3h} - C_{78}$ cage.

The encapsulation of the scandium based metal cluster inside the $D_{3h} - C_{78}$ cage (i.e. $Sc_3N@D_{3h} - C_{78}$) involves a change in the regioselectivity of the reaction. The most reactive bonds are two type B [6,6] bonds called **6** and **4**, and one [5,6] type D bond called **c**. The reaction energies obtained are -12.7, -9.7 and -10.4 $kcal.mol^{-1}$ for the addition over **6**, **4** and **c**, respectively. Furthermore, a huge destabilization is produced after the TNT encapsulation, as most of the considered bonds become less reactive by approximately 12-20 $kcal.mol^{-1}$. A high destabilization is observed for those bonds situated close to the scandium atoms (specially for **1** and **b**). The only case where the cycloaddition reaction is enhanced after the encapsulation is over bond **6** which is stabilized by ca. 17 $kcal.mol^{-1}$. Interestingly, the lowest ac-

tivation barrier is found for bond **6** (18.5 $kcal.mol^{-1}$), which also presents the most exothermic reaction energy. It should be noted that the most favorable addition site in $Sc_3N@D_{3h} - C_{78}$ presents an activation barrier which is 6.3 $kcal.mol^{-1}$ higher in energy than the lowest found for the free cage (18.5 $kcal.mol^{-1}$ for bond **6** in $Sc_3N@D_{3h} - C_{78}$ as compared to 12.2 $kcal.mol^{-1}$ for bond **1** in $D_{3h} - C_{78}$). However, the reaction becomes less regioselective as bonds **4**, **7**, **b**, **c**, and **d** present activation barriers within the range of 19.7-20.7 $kcal.mol^{-1}$. Interestingly, the 1,3-dipolar cycloaddition reaction on $Sc_3N@D_{3h} - C_{78}$ yielded two cycloaddition products corresponding to the addition to the [6,6] bonds called **6** and **4**.[255] Although our calculations indicate that the reaction might also be favorable over bond **c** (**7** and **b** could also be formed even though they present less exothermic reaction energies), our calculations are in good agreement with the experimental findings.

The reactivities found for the free cage and its endohedral derivative can be described in terms of C-C bond distances, pyramidalization angles, and shapes of the lowest-lying unoccupied molecular orbitals. The most favorable addition sites present short C-C bond distances, that is indeed the case for bonds **1**, **7**, and **b** for $D_{3h}-C_{78}$. Similarly, bond **2** presents the longest C-C bond distance and gives a significantly endothermic reaction energy. However, there are some bonds that present similar bond distances and their reaction energies are exothermic (for instance bond **c**). The most reactive bond in the case of $Sc_3N@D_{3h}-C_{78}$ does also present the shortest C-C bond distance, but for instance bond **7** has the same C-C distance and its reaction energy is approximately 5 $kcal.mol^{-1}$ less exothermic. In the case of the endohedral compound, the longest bond (**2**) does not possess the least favorable reaction energy. Hence, there is not an overall correlation between C-C bond distances and reaction energies, apart from the fact that the most reactive bonds do exhibit short C-C bond distances.

As it happens with bond distances, the prediction of the fullerene reactivity in terms of the pyramidalization angles is not straightforward. The most reactive sites exhibit from moderately to high values, however a large pyramidalization angle does not always correspond to an enhanced reactivity of the bond. The encapsulation of the Sc_3N moiety inside the cage leads to an increase of the pyramidalization angles, especially for those bonds situated close to the scandium influence. For instance, bond **1** in $Sc_3N@D_{3h} - C_{78}$ presents the highest pyramidalization angle (13.80^o), but the cycloaddition reaction over it is endothermic by 4 $kcal.mol^{-1}$. Therefore, the use of pyramidalization angles to predict fullerene reactivity does not always lead to the correct answer.

Finally, the cycloaddition reaction between 1,3-cis-butadiene and the fullerene compounds might also be understood in terms of the molecular orbitals of both reacting species. The most prominent interaction occurs between the HOMO of the diene and the LUMO of the fullerene, therefore those bonds presenting suitable shaped orbitals to interact with the HOMO of the diene might be the most favorable addition

sites. In C_{78}, bonds **1**, **7** and **b** present suitable orbitals to interact, and are indeed the most reactive sites of the fullerene compound. However, several bonds present similar suitable antibonding orbitals to react with diene **1**, **2**, **3**, **4**, **6**, **7**, **c**, and **e** in the case of $Sc_3N@C_{78}$. Among all bonds with suitable orbitals to interact only **6**, **4**, **7** and **c** present favorable reaction and activation energies. Moreover bond **d** does not possess suitable shaped orbitals and its reaction and activation barriers are substantially favorable. Hence, the predictions of reactivity for fullerene compounds using the LUMO orbitals are too imprecise, as one finds many bonds suitable to interact.

Although the previously mentioned descriptors do not give accurate results for describing the exohedral reactivity of the cages, the combination of all three descriptors C-C bond distances, pyramidalization angles and molecular orbital analysis give quite successful results. Only bonds **1**, **7** and **b** in the case of C_{78}, and bonds **4**, **6**, **7**, and **c** in $Sc_3N@C_{78}$ fulfill the three criteria. They exhibit short C-C bond distances, relatively high pyramidalization angles and suitable orbitals to interact with diene. And in fact, our thermodynamic and kinetic study indeed shows these bonds to be most reactive.

13.2 The Diels-Alder reaction on endohedral $Y_3N@C_{78}$: The importance of the fullerene strain energy

In some experimental studies, it was observed that the exohedral reactivity of the TNT endohedral metallofullerenes is highly affected by the nature of the encapsulated cluster.[88] Our initial study involving the Diels-Alder reaction on the endohedral scandium based fullerene compound has been extended to directly compare how the reactivity is affected by encapsulating either scandium or yttrium inside the cage. In the first part of this section, the preferred addition sites for the $Y_3N@D_{3h}-C_{78}$ molecule will be throughly described as well as compared to the previously reported $Sc_3N@D_{3h}-C_{78}$ and $D_{3h}-C_{78}$. Finally, an insight into the exohedral reactivity of the most favorable isomer for the encapsulation of the large Y_3N unit is presented.

13.2.1 The Diels-Alder reaction on the D_{3h} cage

The large yttrium based TNT cluster is forced to adopt a pyramidal configuration inside the $D_{3h}-C_{78}$ cage, and two clearly differentiated areas are present (see Figure 13.2): the so-called *up* region, which is more influenced by the nitrogen atom, and the *down* part which has the yttrium atoms in close contact.
In every region, thirteen non equivalent bonds might be considered to take into account all possible addition sites: two type A [6,6] bonds (**1** and **7**), four type B [6,6] bonds (**3**, **4**, **5**, **6**), one type C [6,6] bond (**2**), and 6 type D [5,6] bonds (**a-f**). The study of the Diels-Alder reaction at BP86/TZP//BP86/DZP on both faces of the fullerene indicates that both areas are equally reactive with energy differences of at

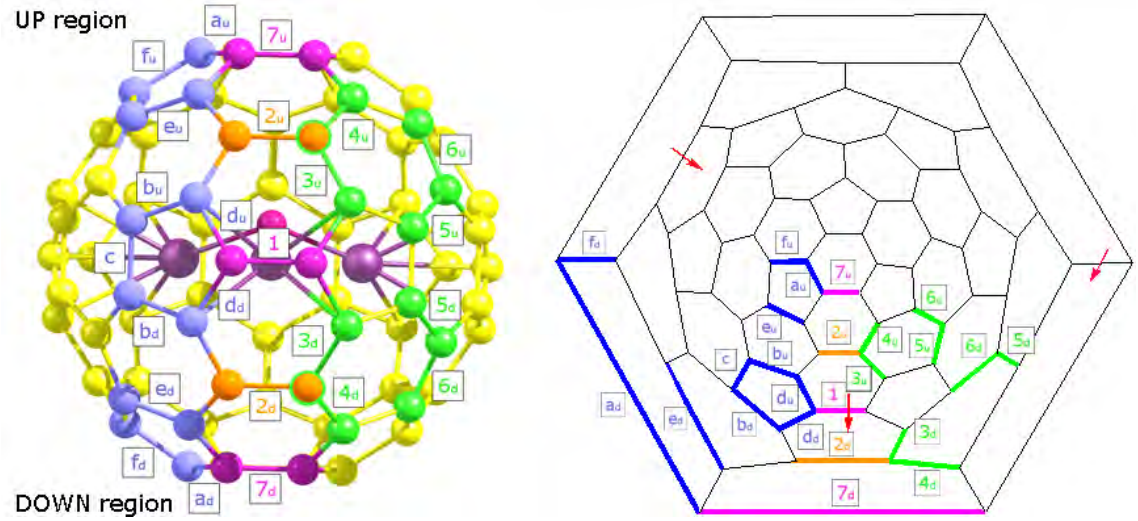

Figure 13.2: Representation of all non-equivalents bonds of the $Y_3N@D_{3h}-C_{78}$. The Schlegel diagram of the fullerene (2D representation) is also depicted where the non-equivalent bonds are marked. The Y_3N cluster presents a pyramidal configuration and therefore two clearly differentiated areas exist. The up region is more affected by the nitrogen atom, whereas the down area is more influenced by the yttrium atoms.

most 1.6 $kcal.mol^{-1}$. The most stable regioisomer for the Diels-Alder cycloaddition reaction over the endohedral compound $Y_3N@D_{3h}-C_{78}$ is shown to be favored over the [5,6] bond **d** that exhibits the longest bond distance in the initial fullerene (ΔE_R=-15.0 $kcal.mol^{-1}$, $\Delta E^{\ddagger}$=17.1 $kcal.mol^{-1}$). As far as we know, this is the first case of a cycloaddition reaction where the most stable addition is obtained over one of the longest C-C bonds in the cage. This observation is of significance as those bonds with the shortest bond distances are usually related with the most reactive positions. Therefore, bond distances cannot be considered a predictor of fullerene reactivity anymore, and as a consequence those studies where only short bonds were investigated might not give the correct picture of the reactivity of endohedral fullerene compounds. The second most favorable regioisomer corresponds to the addition over a type B [6,6] bond called **6** (ΔE_R=-11.0 $kcal.mol^{-1}$, $\Delta E^{\ddagger}$=18.3 $kcal.mol^{-1}$). Finally, although the reaction energy for the cycloaddition reaction to the [5,6] bond called **e** is hardly exothermic (-4.1 $kcal.mol^{-1}$), it does present a low activation barrier (17.2 $kcal.mol^{-1}$). Moreover, there is a difference of 4.1 $kcal.mol^{-1}$ between the activation barrier of bond **e** situated in the *down* and *up* areas. The enhanced reactivity of bond **e** situated in the down region is basically attributed to the presence of suitable shaped orbitals to interact with diene at lower energy. Moreover, the cycloaddition reaction over bond e_u (i.e. situated in the up region) is disfavored as it breaks a bonding interaction between the N atom and this e_u bond.

By comparing the same Diels-Alder reaction over the related compounds $D_{3h}-C_{78}$, $Sc_3N@D_{3h}-C_{78}$, and $Y_3N@D_{3h}-C_{78}$ different reactivity patterns are observed (see Figure 13.3). For the free cage, the reaction is favored over the [5,6] bond called **b**. The second and third most stable regiosiomers correspond to the addition to the pyracylenic [6,6] bonds called **7** and **1**, respectively. Once the scandium based TNT cluster is encapsulated inside, the addition is basically preferred to the type B [6,6] bond called **6**. The other favorable interactions are over the type B [6,6] bond **4** and the type D [5,6] **c**. It should be emphasized here, that the most reactive bonds in $Sc_3N@D_{3h}-C_{78}$ exhibit short C-C bond distances, relatively high pyramidalization angles and are situated far away from the scandium influence. In contrast to $Sc_3N@D_{3h}-C_{78}$, the reaction in the case of $Y_3N@D_{3h}-C_{78}$ is basically favored over those bonds with one of the yttrium atoms in close contact. This preference for reacting with bonds situated close to the yttrium atoms is due to two different factors. First, the D_{3h} cage is extremely deformed, especially in the pyracylenic areas situated close to the yttrium atoms which contain the most reactive bonds, thus the attack reduces the strain energy of the cage. Second, in the final adduct the Y_3N cluster gets additional space to adopt a more planar configuration. The C-C bond of the attacked bond **d** is practically broken and an open fulleroid is obtained. The addition to bond **d** is preferred as the diene has to be deformed less to react (in the case of bonds **1** and **3** situated close to the yttrium atoms, the deformation of the diene is approximately 22 $kcal.mol^{-1}$, whereas only 14 in the case of **d**). As observed in the previous section, the encapsulation of Sc_3N inside the D_{3h} cage produces a decrease of the exohedral reactivity. It is basically explained by the electronic charge transfer from the TNT to the fullerene that leads to LUMOs higher in energy. Most of the considered bonds in the case of $Y_3N@D_{3h}-C_{78}$ slightly decrease their reactivity, which is consistent with the relatively larger HOMO-LUMO gap found for $Y_3N@D_{3h}-C_{78}$ (1.26 and 1.22 eV for the yttrium and scandium based metallofullerenes, respectively) and the higher electron transfer produced in the case of yttrium.

13.2.2 The Diels-Alder reaction on the $C_2:22010$ cage

The most favorable C_{78} cage to encapsulate the large Y_3N cluster is the non-IPR $C_2:22010$ isomer where the TNT moiety can adopt a planar configuration. The difference in energy between $Y_3N@D_{3h}-C_{78}$ and $Y_3N@C_2-C_{78}$ is 20.2 $kcal.mol^{-1}$ at BP86/TZP//BP86/DZP. The latter is similar to the difference of 21.1 $kcal.mol^{-1}$ between the two synthesized and exohedrally functionalized D_{5h} and I_h cages of the C_{80} fullerene, which are both experimentally attainable.[70] Among all non-equivalent bonds of the $C_2:22010$ cage, ten bonds were selected on the basis of the reactivity trends observed in the D_{3h} cage: one type E [5,5] bond only present in the non-IPR cages (called C_2-E), one type F [5,6] bond (C_2-F), two type B [6,6] bonds with short bond distances and situated far away from the metals (C_2-B1, C_2-B2), another type B [6,6] bond situated near one of the yttrium atoms (C_2-B3), one type D [5,6] bond with large C-C bond distances and positioned close to the yttrium

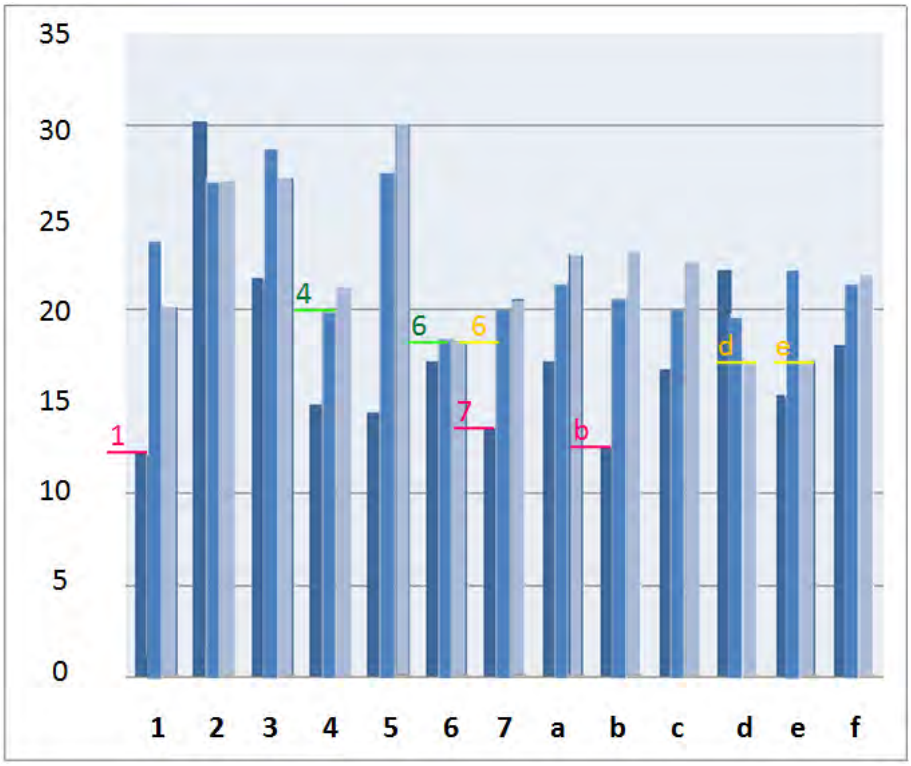

Figure 13.3: The activation barriers obtained for $D_{3h}-C_{78}$ (represented in dark blue), $Sc_3N@D_{3h}-C_{78}$ (in blue), $Y_3N@D_{3h}-C_{78}$ (in light blue). The most reactive bonds for all studied fullerene molecules are marked using different colors: the preferred addition sites for $D_{3h}-C_{78}$ are marked in pink, for $Sc_3N@D_{3h}-C_{78}$ in green, and for $Y_3N@D_{3h}-C_{78}$ in yellow.

metal ($C_2 - Dl$), another type D [5,6] bond with short bond distance and situated far away from the yttrium influence ($C_2 - Ds$), and finally one pyracylene [6,6] bond called $C_2 - A$ close to the yttrium atom (see Figure 13.4).

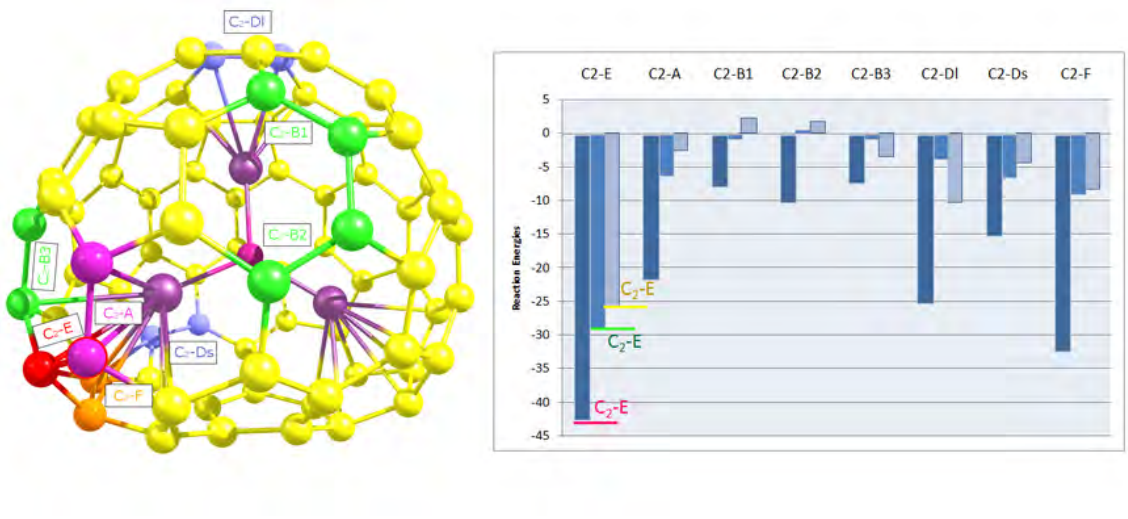

Figure 13.4: Representation of the selected bonds of the $Y_3N@C_2 - C_{78}$ compound. The reaction energies obtained for the different cases studied: $C_2 - C_{78}$ (represented in dark blue), $Sc_3N@C_2 - C_{78}$ (in blue), and $Y_3N@C_2 - C_{78}$ (in light blue) are represented in $kcal.mol^{-1}$. The preferred addition sites for all compounds have been marked in pink for the free cage, and in green and yellow for the scandium and yttrium based endohedral metallofullerenes, respectively.

Interestingly, the Diels-Alder reaction on $Y_3N@C_2 - C_{78}$ is favored over the [5,5] bond called $C_2 - E$ which presents one of the yttrium atoms directly faced. As far as we know, the reactivity of these [5,5] bonds was never assessed before. Although Campanera and coworkers predicted a low reactivity of these non-IPR bonds on the basis of the Mayer Bond Order analysis,[239] our theoretical findings indicate that the reaction is substantially exothermic (-25.9 $kcal.mol^{-1}$) and highly stereoselective. The reaction over the rest of the considered bonds is from 15.6 to 28.1 $kcal.mol^{-1}$ less favorable. This observed tendency to react with those bonds situated close to the metal atoms might either be influenced by the presence of the yttrium atoms or be dictated by the C_2 cage. Hence, the Diels-Alder reaction was also assessed in the case of the free C_2 and the scandium based endohedral derivative. Interestingly, the reaction is found to be favored over the [5,5] bond called $C_2 - E$ in both $C_2 - C_{78}$ and $Sc_3N@C_2 - C_{78}$ compounds (the reaction energies obtained are -42.6 and -28.9 $kcal.mol^{-1}$, respectively). Therefore, our theoretical calculations indicate that the exohedral functionalization of the recently synthesized $Tm_3N@C_{78}$,[71] $Dy_3N@C_{78}$,[72] and $Gd_3N@C_{78}$[27] might be stereoselectively produced over the [5,5] bonds.

13.3 Reactivity and regioselectivity of noble gas endohedral fullerenes $Ng@C_{60}$ and $Ng_2@C_{60}$ (Ng=He-Xe)

Krapp and Frenking performed a theoretical study about the noble gas dimers endohedral fullerenes $Ng_2@C_{60}$ (Ng=He-Xe).[130] Interestingly, they observed that an electron transfer of 1-2 electrons is produced in the case of the larger noble gas homologues specially for the Xe_2 dimer. Free noble gas dimers are rarely observed, however a genuine chemical bond is formed once the Xe_2 unit is trapped inside the fullerene moiety. In addition to that, the encapsulation of Ar_2, Kr_2 and Xe_2 was found to affect the C-C bond distances of the C_{60} compound as well as the pyramidalization angles. Therefore, a change on the exohedral reactivity might be observed. In this study, the Diels-Alder reaction is studied in detail either in the single noble gas endohedral compounds $Ng@C_{60}$ (Ng=He-Xe) and the noble gas dimers endohedral fullerenes $Ng_2@C_{60}$ at the BP86/TZP level of theory.

13.3.1 Study of the Diels-Alder reaction on the single noble gas endohedral compounds

The Diels-Alder reaction between 1,3-cis-butadiene and C_{60} has been studied as a reference. The reaction is basically favored over the pyracylene [6,6] bond that presents a reaction energy of -20.7 $kcal.mol^{-1}$ and an activation barrier of 12.7 $kcal.mol^{-1}$. [5,6] bonds are substantially less reactive as the reaction and activation energies obtained are 15.4 and 8.3 $kcal.mol^{-1}$ less favorable. The noble gas encapsulation hardly affects the exohedral reactivity of the cage, as the reaction energies obtained corresponding to the [6,6] addition are approximately equal to the ones for the free cage (-20.5, -20.3, -20.2, -20.3, and -20.5 $kcal.mol^{-1}$ for $Ng@C_{60}$ Ng= He, Ne, Ar, Kr, and Xe, respectively). The effect of substituting He by Xe in $Ng@C_{60}$ is small with energy differences of less than 0.1 $kcal.mol^{-1}$. This low reactivity difference has also been observed in experiment, however an slight preference for $He@C_{60}$ with respect to $Xe@C_{60}$ was described.[257] Similarly, the activation barriers obtained for the addition to the [6,6] bond are approximately equal to the ones for C_{60} (13.0, 13.4, 13.3, 13.1, 12.9 $kcal.mol^{-1}$ for $Ng@C_{60}$ Ng= He, Ne, Ar, Kr, and Xe, respectively). The activation barrier corresponding to the [5,6] addition has only been calculated for the $Kr@C_{60}$ compound which is only 0.6 $kcal.mol^{-1}$ higher than for C_{60}, but substantially less favorable than for the [6,6] addition.

13.3.2 Study of the Diels-Alder reaction on the noble gas dimers endohedral compounds

More interesting results are obtained for the case of the noble gas dimer encapsulation. Krapp and Frenking studied the cage isomerism of the noble gas endohedral derivatives and observed that the most stable structure was the D_{3d} for He-Kr, and the D_{5d} for Xe.[130] However, the energy differences between the different isomers was found to be very low. We decided to study the Diels-Alder reaction on the D_{5d} iso-

mer for all noble gases for many reasons. First, the comparison of the different bonds can only be done considering the same isomer for all cases studied. Second, the most interesting compound to study is the xenon-based endohedral fullerene because of the electron transfer produced. Finally, the energy differences found for the encapsulation of the He-Kr atoms inside D_{5d} was less than 2 $kcal.mol^{-1}$ less stable (at SCS-MP2/TZVPP//BP86/TZVPP) than in D_{3d}.[130] For the D_{5d} symmetry there are six non-equivalent type D [5,6] bonds (called **a**, **b**, **c**, **d**, **e**, and **f**) and three type A [6,6] bonds (called **1**, **2** and **3**) (see Figure 13.5).

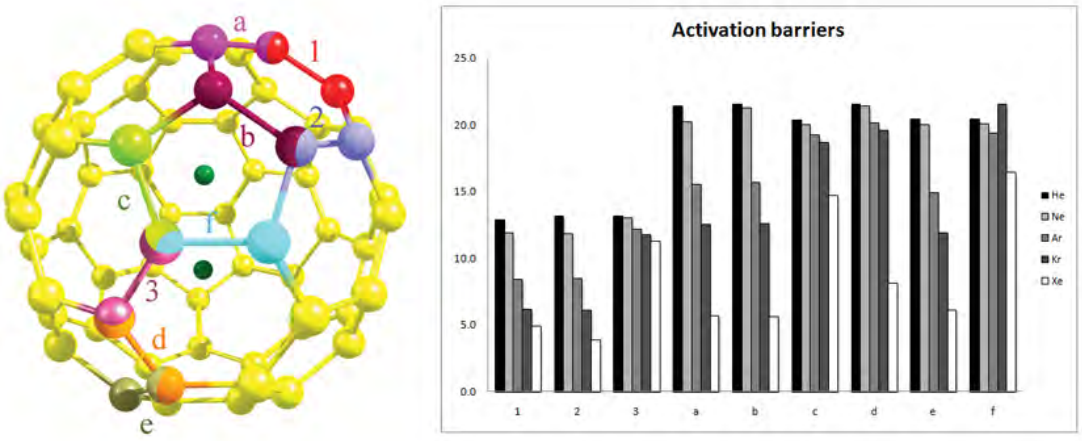

Figure 13.5: Representation of all non-equivalent bonds of the $Ng_2@C_{60}$ compound. The activation energies (in $kcal.mol^{-1}$) corresponding to the Diels-Alder cycloaddition reaction between 1,3-butadiene and all non-equivalent bonds for all considered noble gas endohedral compounds $Ng_2@C_{60}$ has been represented on the right. A grey scale has been used to represent the different noble gases endohedral compounds: black color is used to represent the helium-based fullerene, light grey for neon, medium grey for argon, dark grey for krypton, and white for xenon.

The Diels-Alder reaction produced on the lighter noble gas dimer compounds (i.e. $He_2@C_{60}$ and $Ne_2@C_{60}$) does present reaction and activation barriers that are not far from the ones obtained for free C_{60}. The reaction energies for the most reactive bond **1** are 0.2 and 2.4 $kcal.mol^{-1}$ more favorable for the helium and neon noble gas compounds, respectively. The activation barrier for the addition to bond **1** is 12.8 $kcal.mol^{-1}$ and 11.9 $kcal.mol^{-1}$ for the $He_2@C_{60}$ and $Ne_2@C_{60}$ cases, respectively. The rest of the [6,6] bonds present reaction and activation energies close to the values obtained for **1**, whereas [5,6] bonds are much more less reactive. It is important to remark that the addition of 1,3-butadiene produces a rotation of the noble gas dimer which is reoriented during the course of the reaction from the initial position

to face the attacked bond. Once Ar_2 and Kr_2 are inserted inside C_{60}, the reaction becomes substantially more exothermic (-32.2 and -39.9 $kcal.mol^{-1}$ for bonds **1** and **2** of $Ar_2@C_{60}$ and $Kr_2@C_{60}$, respectively), and the activation barriers are largely reduced (ca. 8 and 6 $kcal.mol^{-1}$ for Ar_2 and Kr_2 compounds, respectively). The addition to the [6,6] bond **3** is less favored, as the noble gas moiety is not totally reoriented to face the attacked bond. Of course, the larger the noble gas atom, the more impeded the rotation of the noble gas dimer inside the cage. Hence, for the larger noble gas endohedral compounds the addition is favored over those bonds situated close to the C_5 axis where the dimer is initially contained. This lack of rotation leads to substantially less favored reaction and activation barriers.

The preferred addition site for the xenon based compound corresponds to the [6,6] bond called **1** (-44.9 $kcal.mol^{-1}$), however the [5,6] bonds **a**, **b** and **e** do also present favorable reaction energies (-44.6, -44.5, and -45.5 $kcal.mol^{-1}$, respectively). The lowest activation energy is found for the [6,6] bond **2** (3.8 $kcal.mol^{-1}$), nonetheless bonds **1**, **a**, **b**, and **e** also present low energy barriers (4.9, 5.7, 5.6, 6.1 $kcal.mol^{-1}$, respectively). Therefore, the reaction is no longer regioselective as 5 regioisomers might be formed during the reaction between 1,3-butadiene and $Xe_2@C_{60}$.

The enhanced reactivity observed along the series $He_2@C_{60} < Ne_2@C_{60} < Ar_2@C_{60} < Kr_2@C_{60} < Xe_2@C_{60}$ might be attributed to several factors. First, the HOMO-LUMO gap is reduced from 1.63 eV for $He_2@C_{60}$ to 0.75 eV for $Xe_2@C_{60}$ (for the free cage it is 1.66 eV), which is basically produced by a slight stabilization of the LUMO and a major destabilization of the HOMO. The latter is a complex situation as the HOMO for the lighter noble gas compounds (a_{1u} orbital, for He-Ar) is different to that of xenon and krypton fullerenes (a_{2u} orbital that primarily presents antibonding σ^* orbitals in the noble gas dimer unit). The destabilization of the a_{2u} orbital increases from He to Xe because of the reduction of the Ng-Ng distance along the series. Second, the deformation energy of the cage also plays an important role. The encapsulation of He_2 and Ne_2 inside C_{60} hardly affects the cage as the calculated deformation energies are 0 and less than 1 $kcal.mol^{-1}$, respectively. However, the insertion of the larger Ar_2, Kr_2, and Xe_2 leads to a deformation energy of 11.2, 22.5 and 34.1 $kcal.mol^{-1}$, respectively. The high deformation energy found, especially for the xenon-based compound, leads to a highly strained cage where all [5,6] and [6,6] bonds situated close to the initial position of the Xe_2 dimer are equally reactive. The reaction is then extremely exothermic and unselective as the strain of the cage is partially released after reaction. Finally, the Ng-Ng bond distance elongation does also contribute to the enhanced reactivity for the heavier noble gas compounds. After reaction, the Ng-Ng distance is increased by 0.028, 0.043, 0.040, 0.035, and 0.054 Å along the $He_2 - Xe_2@C_{60}$ series which corresponds to an stabilization of -0.2, -1.0, -4.1, -5.3, and -10.4 $kcal.mol^{-1}$. This decompression represents an important contribution to the exothermicity of the reaction for those bonds where the Ng dimer is reoriented facing the attacked bond.

13.4 Diels-Alder reaction between cyclopentadiene and C_{60}: An analysis of the performance of the ONIOM method for the study of chemical reactivity in fullerenes and nanotubes

The ONIOM approach is one of the most commonly used computational strategies to study the reactivity of fullerene, nanotubes and related compounds. The system is partitioned in different layers, usually two (i.e. ONIOM2), the so-called *high* layer which contains those atoms that are directly involved in the reaction and are treated using a higher level of theory, and the *low* layer where the rest of the system is contained. In this project, different partitioning schemes are investigated for studying the Diels-Alder reaction with C_{60} and cyclopentadiene. Finally, different DFT functionals are tested within the ONIOM approach to find the combination that better describes the experimental results.

13.4.1 ONIOM partitions

We have considered 4 different partitions of the fullerene compound: the simplest model is obtained including in the high layer the C-C bond that is being attacked and the cyclopentadiene molecule (model I), model II contains a naphthalene fragment, model III a pyracylene unit, and finally model IV a buckybowl fragment $C_{26}H_{12}$ (see Figure 13.6). B3LYP together with the standard basis set 6-31G(d) has been the

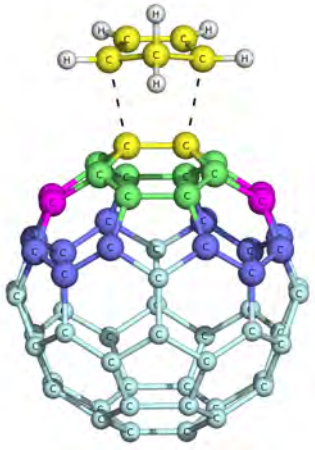

Figure 13.6: Scheme of the different partitioning models of C_{60}. Model I is the simplest model marked in yellow and contains the attacked C-C bond, model II is a naphthalene fragment of the fullerene and adds the green atoms to the yellow ones. Model III contains the pyracylene unit (model II plus pink carbon atoms), and model IV contains the previous model plus the blue carbon atoms.

method chosen for the high level layer, with either the semiempirical AM1 or the LDA (SVWN) DFT-method in conjuction with the minimal basis set STO-3G for the low level layer. The SVWN functional gives in all considered models a more accurate description for the reaction and activation energies with deviations compared to the full B3LYP result of less than 6.1 $kcal.mol^{-1}$ for the reaction energy, and less than 2 $kcal.mol^{-1}$ for the activation barrier. The best performance is obtained for models III and IV with small differences of less than 0.5 $kcal.mol^{-1}$ for both the reaction and activation energies. The optimized geometries using model III and IV are also much closer to the B3LYP result. However a slightly asynchronous TS structure is found for model IV (the difference in energy between the synchronous/asynchronous TSs is just 0.2 $kcal.mol^{-1}$ with the asymmetric configuration lower in energy). Therefore, our calculations indicate that model III is the best ONIOM partition for describing either energies or geometries of cycloaddition reactions of fullerene compounds at a low computational cost.

13.4.2 Performance of different functionals

The Diels-Alder cycloaddition reaction between cyclopentadiene and C_{60} has been experimentally achieved. The estimated reaction enthalpy is -19.8±2.2 $kcal.mol^{-1}$, and the activation barrier 6.9 $kcal.mol^{-1}$. The comparison of experimental data and full B3LYP results (ΔH_R=-6.6 $kcal.mol^{-1}$, $\Delta H^{\ddagger}$=18.0 $kcal.mol^{-1}$) shows that B3LYP errors are larger than 10 $kcal.mol^{-1}$. This unexpected overestimation of B3LYP is not studied here but it might be related to the reduction of the HOMO-LUMO gap in curved species as compared to the planar ones. The use of the full MPW1K/6-31G(d) improved the obtained results (ΔH_R=-23.9 $kcal.mol^{-1}$, $\Delta H^{\ddagger}$=12.5 $kcal.mol^{-1}$), although differences in the activation barriers of more than 5 $kcal.mol^{-1}$ are still found. As observed in the previous section, full MPW1K results are close to the model III ONIOM2(MPW1K/6-31G(d):SVWN/STO-3G) with small variations of less than 1.6 $kcal.mol^{-1}$. Other pure DFT functionals BP86, BPW91, OPBE, and the hybrid O3LYP have been used instead of B3LYP for the high level method to compute the reaction and activation energies. Among the functionals tested, the methods with the highest and lowest errors are ONIOM2(O3LYP/6-31G(d):SVWN/STO-3G) and ONIOM2(BP86/6-31G(d):SVWN/STO-3G), respectively. Interestingly, single point (SP) calculations of the latter functionals at the optimized ONIOM2 B3LYP geometry (SP ONIOM2(B3LYP/6-31G(d):SVWN/STO-3G)) give the same results that when geometry optimization is allowed (with differences of less than 1 $kcal.mol^{-1}$ in all cases). Taking advantage of this evidence and performing only SP calculations, the recently defined meta-hybrid functionals PW6B95, PWB6K, M05, M05-2X, M06, and M06-2X as the high level method have been tested either using the ONIOM approach (i.e. ONIOM2(X/6-31G(d):SVWN/STO-3G)//ONIOM(B3LYP/6-31G(d):SVWN/STO-3G)) or computing full DFT SP (i.e. X/6-31G(d)//ONIOM2(B3LYP/6-31G(d):SVWN/STO-3G)). Results indicate small differences between the SP DFT and the SP ONIOM calculations of less than 2.5 and 2.2 $kcal.mol^{-1}$ for the reaction and activation energies, respectively in all considered cases. The combina-

tion of DFT functionals that accurately describes the reaction and activation barriers according to the experimental values are M06/6-31G(d)//(ONIOM2(B3LYP/6-31G(d):SVWN/STO-3G) and M06-2X/6-31G(d)//ONIOM2(B3LYP/6-31G(d):SVWN/STO-3G). The former method performs better for reaction energies (the error is 1.5 $kcal.mol^{-1}$) and the latter for energy barriers, which are overestimated by only 0.2 $kcal.mol^{-1}$.

Our theoretical findings indicate that the best model within the ONIOM approach to describe fullerene reactivity is model III which consists of a pyracylene fragment of the C_{60} compound and cyclopentadiene. Finally, the DFT functionals M06 and M06-2X are recommended for accurately describing the reaction energies and activation barriers obtained experimentally.

13.5 On the mechanism of the thermal retrocycloaddition of pyrrolidinofullerenes (retro-Prato reaction)

The 1,3-dipolar cycloaddition reaction involving fullerene compounds is a suitable procedure for fullerene functionalization as final cycloaddition products are considered to be pretty stable. However, in a preliminary communication by Martín and coworkers the retro-Prato reaction was experimentally achieved in the presence of a large excess of dipolarophile.[218] In this study, the mechanism by which the retro-Prato reaction is achieved has been investigated in collaboration with the experimental organic group of Prof. Martín. Although the project presents both experimental and theoretical sections, only a summary of the most important theoretical findings will be hereafter presented. In the previous section, the best ONIOM2 approach for studying cycloaddition reactions was found to be B3LYP/6-31G(d) for the high layer (a pyracylene fragment and the dipole), and SVWN/STO-3G for the rest of the system. Hence, the latter has been the selected strategy to theoretically assess the mechanism of the retro-cycloaddition process.

13.6 Retrocycloaddition without maleic anhydride

Under thermal treatment and in the presence of reagent excess of some dipolarophile such as maleic anhydride, the retro-cycloaddition reaction can be efficiently produced. The retro-Prato reaction of N-methylpyrrolidinofullerene to give C_{60} and azomethine ylide is assessed in the presence of maleic anhydride as a dipolarophile. In Figure 13.7 the reaction profile of the retro-cycloaddition reaction is represented. The retro-reaction converting the pyrrolidinofullerene into C_{60} and azomethine ylide (**4b** $\rightarrow$ C_{60} + **6a**) presents a highly endothermic reaction energy (53.2 and 34.0 $kcal.mol^{-1}$ in terms of electronic and free Gibbs energies, respectively). Moreover, an extremely high activation barrier is found (45.4 $kcal.mol^{-1}$). The fact that the first transition state of the reaction (**TS1a**) is lower in energy than final products shows that a minimum structure should exist. Unfortunately, all attempts to find the

latter reaction intermediate failed leading to either initial reactants or final products suggesting the presence of a very shallow minimum structure close to the TS.

The second reaction mechanism analyzed is for the azomethine ylide dipole bearing an ester substituent (R= -$COOCH_3$) on one of the terminal carbons. The introduction of this substituent leads to a less endothermic retro-Prato reaction (with reaction energies of 38.7 and 21.0 $kcal.mol^{-1}$ in terms of electronic and free Gibbs energies, respectively, see Figure 13.8). The transition state for the retro-cycloaddition (**TS1b**) presents an activation energy of 35.9 $kcal.mol^{-1}$ which is lower in energy than final products (C_{60} + **6b**). In contrast with the unsubstituted case, a reaction intermediate has been located (**int1b**, 33.4 $kcal.mol^{-1}$). The ester substituent reduces the activation barrier by 10 $kcal.mol^{-1}$ and the reaction energy by 15 $kcal.mol^{-1}$ which might be attributed to the electron-withdrawing character from both inductive and resonance effects of the $COOCH_3$. Still, the reaction is highly disfavored to be produced experimentally.

13.7 Retrocycloaddition assisted by maleic anhydride

The dipolarophile maleic anhydride could improve the process either reducing the activation barrier of the retro-reaction or stabilizing the final generated 1,3-dipole. Both possibilities have been assessed theoretically and have been represented in Figures 13.7, 13.8, 13.9, 13.11.

As it can be seen in Figure 13.9, once the maleic anhydride is present the overall reaction energy is converted from highly endothermic to substantially exothermic (-16.4 $kcal.mol^{-1}$ as compared to 53.2 $kcal.mol^{-1}$). However, a high activation barrier is found for the transition state (**TS3a**) (40.8 $kcal.mol^{-1}$). As it can be seen in figure 13.10, three molecules are interacting simultaneously at **TS3a**. Once the C-C bond of the pyrrolidino ring is being broken releasing the azomethine ylide, the dipole reacts with maleic anhydride to form the new cycloaddition product. The latter barrier is approximately 5 $kcal.mol^{-1}$ lower than the non-assisted one (**TS1a**, 45.39 $kcal.mol^{-1}$). However, since the entropy of the system is decreased when going from **4a**+ **5** to **TS3a** the Gibbs free energy activation barrier is 4.5 $kcal.mol^{-1}$ higher than the electronic one. Hence, the presence of maleic anhydride does not improve the efficiency of the reaction by reducing the barrier of the retro-cycloaddition reaction, instead the effect is more thermodynamic as the overall reaction energy is clearly enhanced.

Another possibility might be the assistance of maleic anhydride only at the last stage of the reaction (see Figure 13.7). The latter implies that the retro-Prato reaction is first produced (**4a** + **5** $\rightarrow$ C_{60} + **6a** + **5**), and afterwards the generated ylide is stabilized reacting with the new dipolarophile (i.e. maleic anhydride). Neither the transition state (**TS2a**) leading to the formation of the cycloaddition product between maleic anhydride and azomethine ylide (**7a**) nor the reaction intermediate

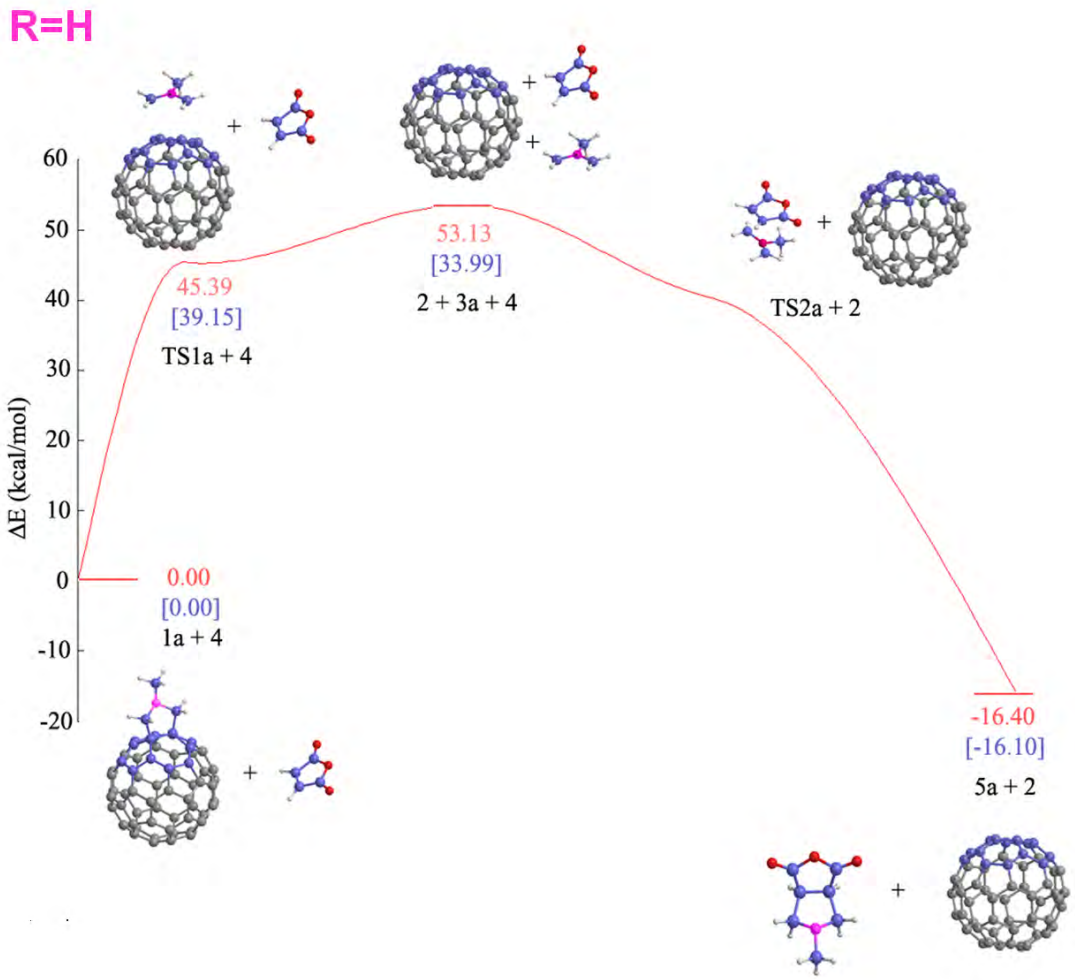

Figure 13.7: Reaction energy profile for the retro-Prato reaction of the unsubstituted system (R= H) without the assistance of maleic anhydride in the first step of the reaction. Gibbs free energies are represented in square brackets.

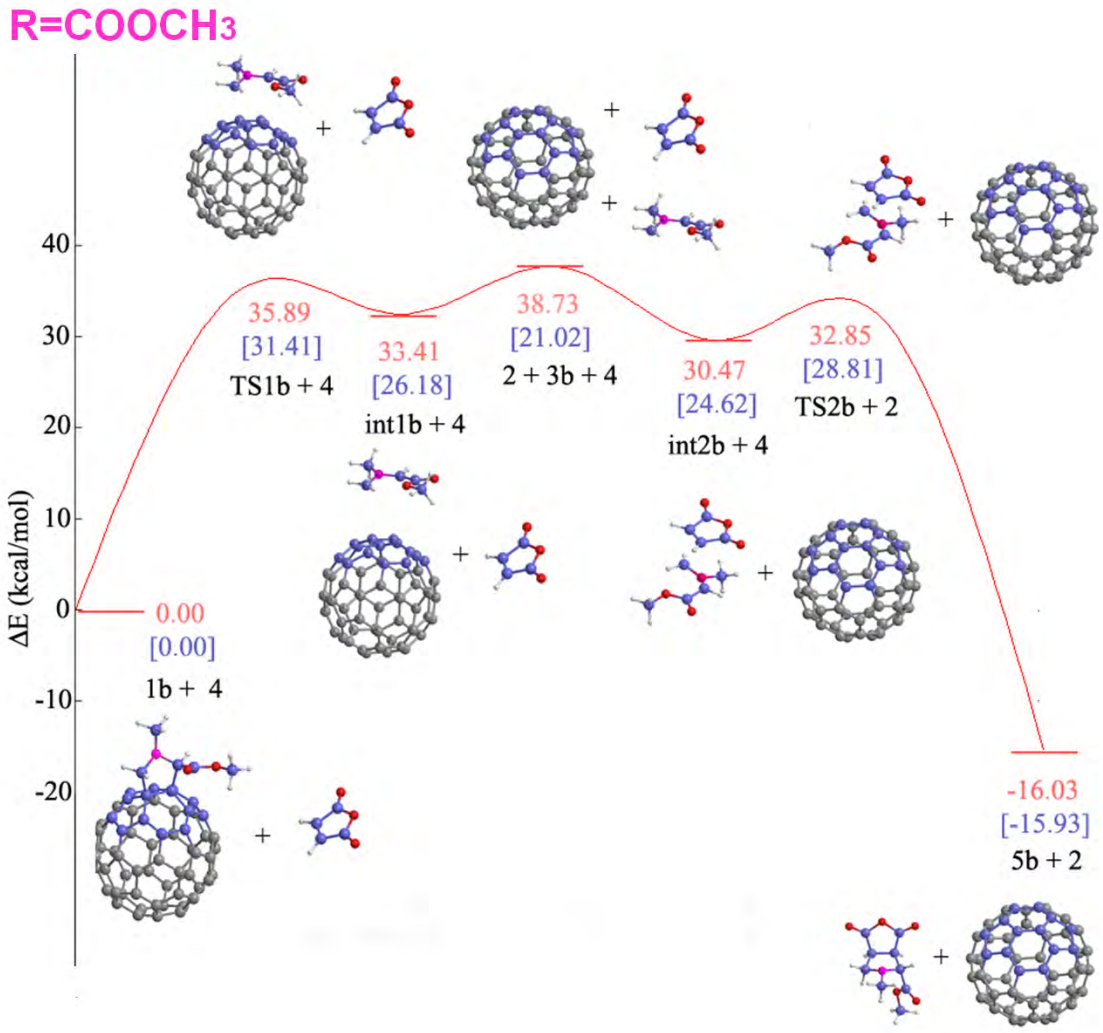

Figure 13.8: Reaction energy profile for the retro-Prato reaction of the substituted system (R= $COOCH_3$) without the assistance of maleic anhydride in the first step of the reaction. Gibbs free energies are represented in square brackets.

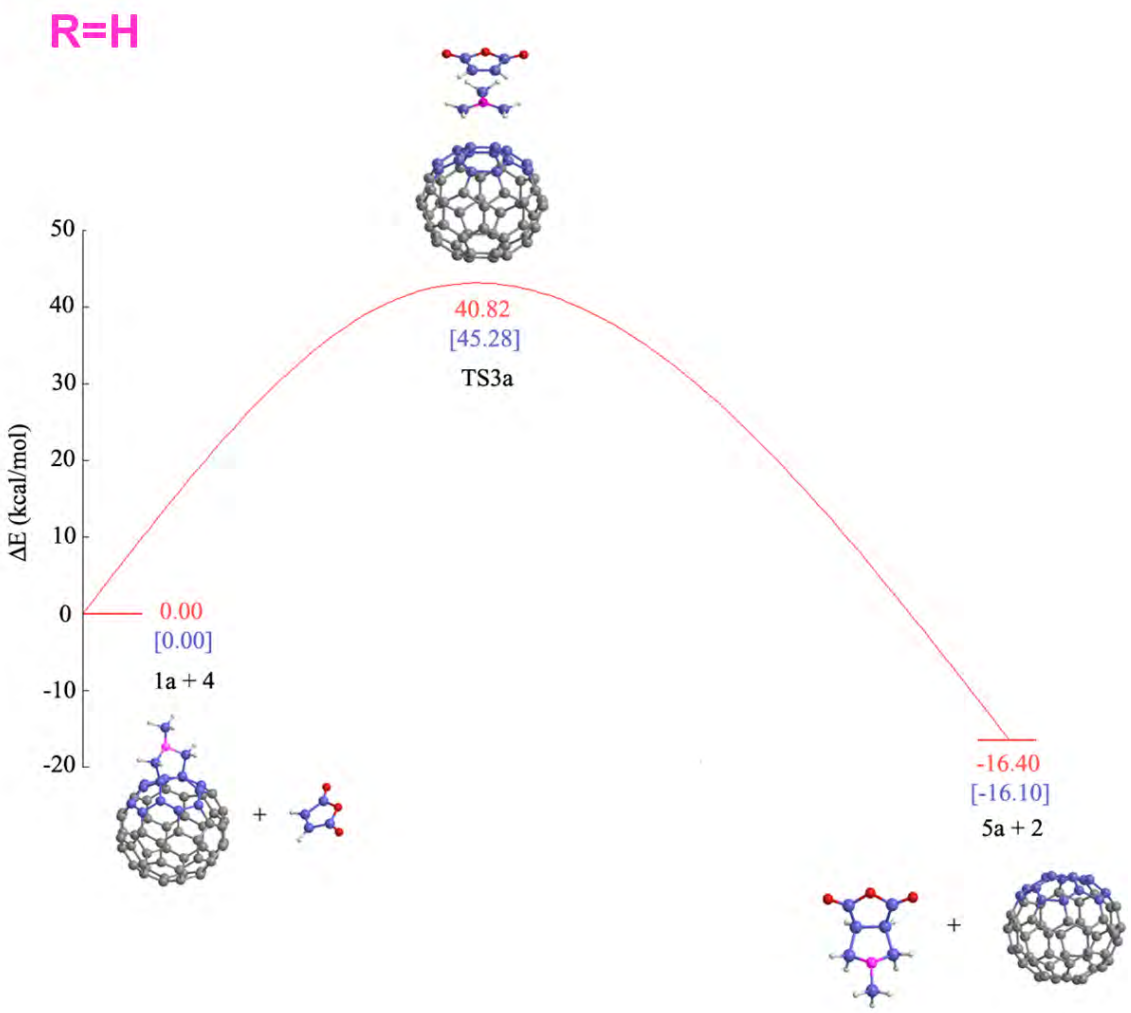

Figure 13.9: Reaction energy profile for the retro-Prato reaction of the unsubstituted system (R= H) assisted by the dipolarophile maleic anhydride. Gibbs free energies are represented in square brackets.

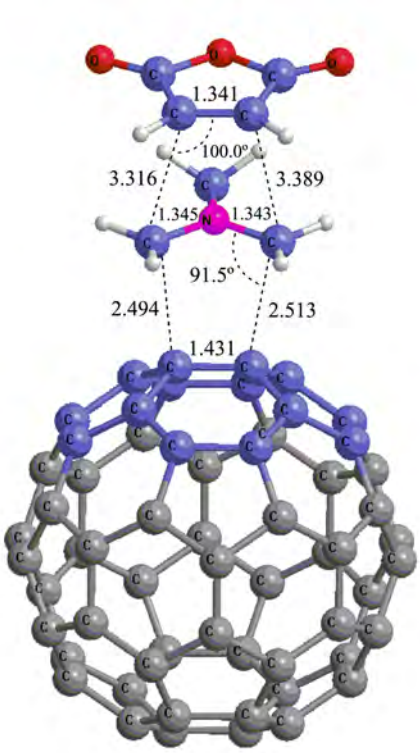

Figure 13.10: ONIOM2(B3LYP/6-31G(d):SVWN/STO-3G) optimized geometry for the assisted transition state **TS3a**. Most relevant distances and angles are represented in Å and degrees, respectively.

could be located. This fact indicates that the process is barrierless and that once the azomethine ylide is produced it immediately reacts with maleic anhydride. The activation barriers obtained show that both assisted and non-assisted mechanisms could be followed under intense heating due to the slight differences in the activation barriers obtained (the electronic energies favor the assisted mechanism, whereas free Gibbs energies the non-assisted one).
The same mechanisms have been considered for the substituted case (R= -$COOCH_3$). The assisted TS (**TS3b**) presents a lower activation barrier (28.4 $kcal.mol^{-1}$) as compared to the unassisted one (**TS1b**, 35.9 $kcal.mol^{-1}$), although the Gibbs free energies are similar (see Figure 13.11). After the latter TS, two reaction intermediates (**int3b** and **int4b**) where the C-C bonds of the azomethine ylide are no longer attached to the fullerene surface but are interacting with maleic anhydride are found. Although a TS should be located between **int3b** and **int4b**, no energy maxima was obtained performing a linear transit. This basically indicates the existence of a very shallow plateau. The rate-determining step of the assisted mechanism relies on the last transition state of the reaction (**TS5b**), where the terminal carbon atoms of the azomethine ylide are interacting with the double bond of the maleic anhydride rather than with C_{60}. The activation barrier for the last step of the reaction is 46.9 $kcal.mol^{-1}$ and 51.7 $kcal.mol^{-1}$ in terms of electronic and Gibbs free energies, respectively. Finally, the mechanism where the dipolarophile is only involved at the last stage of the reaction has also been considered. After the retro-1,3-dipolar is produced, the reaction intermediate (**int2b**) where the generated azomethine ylide is interacting with maleic anhydride is obtained. This intermediate presents an energy of 30.5 $kcal.mol^{-1}$, and is ca. 8.4 $kcal.mol^{-1}$ lower in energy than isolated products for the retro-reaction (C_{60} + **6b** + **5**). Nevertheless, Gibbs free energies are somewhat higher (24.6 $kcal.mol^{-1}$) due to the reduction of the entropy of the system. The TS involving the cycloaddition reaction between azomethine ylide and maleic anhydride (**TS2b**) presents an activation barrier of 32.9 $kcal.mol^{-1}$ (or 28.9 $kcal.mol^{-1}$ in free Gibbs energies) which is 14 $kcal.mol^{-1}$ (or 23 $kcal.mol^{-1}$ in Gibbs free energies) lower in energy than the one found for the assisted mechanism (**TS5b**). Therefore, the mechanism where the assistance of the maleic anhydride is produced only at the last stage of the reaction is clearly preferred, which contrasts with the unsubstituted case where both mechanisms are equally favored.

13.8 Cycloaddition reactions of butadiene and 1,3-dipoles to curved arenes, fullerenes, and nanotubes: Theoretical evaluation of the role of distortion energies on activation barriers

Since the discovery of cycloaddition reactions, the mechanism by which these reactions are performed has been intensively debated. It is now widely accepted that a concerted mechanism is followed, the stepwise process usually being higher in energy.

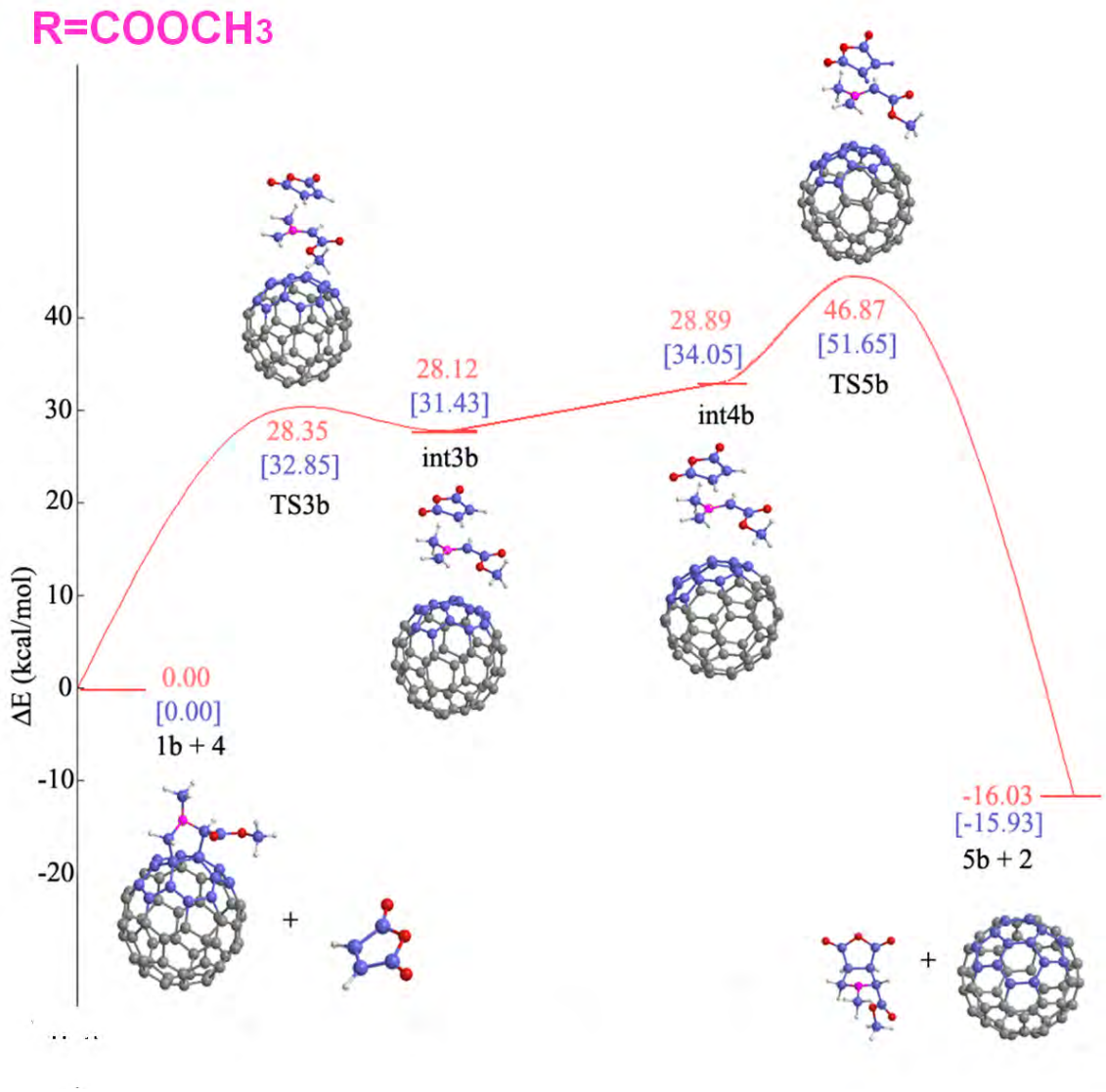

Figure 13.11: Reaction energy profile for the retro-Prato reaction of the substituted system (R=$-COOCH_3$) assisted by the dipolarophile maleic anhydride. Gibbs free energies are represented in square brackets.

The development of the frontier molecular orbital (FMO) theory allowed the prediction of reactivity and regioselectivity of cycloaddition reactions. However, there are some cases described in the literature where the latter theory fails to describe the chemical reactivity of certain compounds, for instance the reactivity of PAHs. Therefore, the possibility of finding other models to understand the mechanism of pericyclic reactions is still highly appealing. This section corresponds to the last cycloaddition study included in this thesis, where the role of distortion energy in the latter reactions involving large compounds such as fullerenes and nanotubes is hereafter discussed in detail.

13.8.1 The Diels-Alder and 1,3-dipolar with 1,3-cis-butadiene and azomethine ylide

The cycloaddition reactions have been studied at B3LYP/6-31G(d) in several positions of a wide variety of organic compounds ranging from planar hydrocarbons: benzene, naphthalene, anthracene, hexacene and coronene to cycloheptacene, fullerene and nanotube compounds (see Figure 13.12). In addition, some models for fullerene, carbon nanotubes and graphene have been considered too. The latter correspond to the introduction of pentagonal rings that induce curvature to coronene and coranulene (called *curved coronene* and *curved coranulene*). The ONIOM2 approach has been used to treat the large carbon nanotube systems studied (B3LYP/6-31G(d)//ONIOM2(B3LYP/6-31G(d):SVWN/STO-3G)).
The most favorable addition site for naphthalene, anthracene, and hexacene corresponds to the addition to bond **3** that present reaction energies of -37.6, -41.4, -45.3 $kcal.mol^{-1}$ for the 1,3-dipolar and -13.5, -18.0, -21.5 $kcal.mol^{-1}$ for the reaction with 1,3-cis-butadiene. The lowest activation barrier is found for the addition to bond **3**, with the exception of hexacene where an slightly more favored activation energy is obtained for bond **2**. This preference for reacting with position **3** might be understood in terms of the aromaticity disruption of the molecule rings. The aromaticity of a single benzene unit is modified after reaction with bond **3**, whereas half or the whole system is altered once the addition is produced to bond **2** or the rest of the considered bonds, respectively.

A high reactivity is observed for the cycloaddition reactions to cycloheptacene (species e in Figure 13.12). The highly pyramidalized structure presents highly exothermic reaction energies and extremely low activation barriers (no barrier was obtained for the 1,3-dipolar addition). A preliminary study where the reactions were studied in distorted ethylene indicated that no TS was located for a dihedral angle lower than 166^o, and that is indeed the case for cycloheptacene (the C-C-C-C dihedral is 155^o).

The same reactions studied in a graphene model, i.e. coronene (species f in Figure 13.12), indicated that the best addition site corresponds to bond **4** which is situated on the periphery of the molecule (the reaction energy is -37.6 and -13.2 $kcal.mol^{-1}$, and the activation barrier 8.9 and 32.6 $kcal.mol^{-1}$ for the 1,3-dipolar

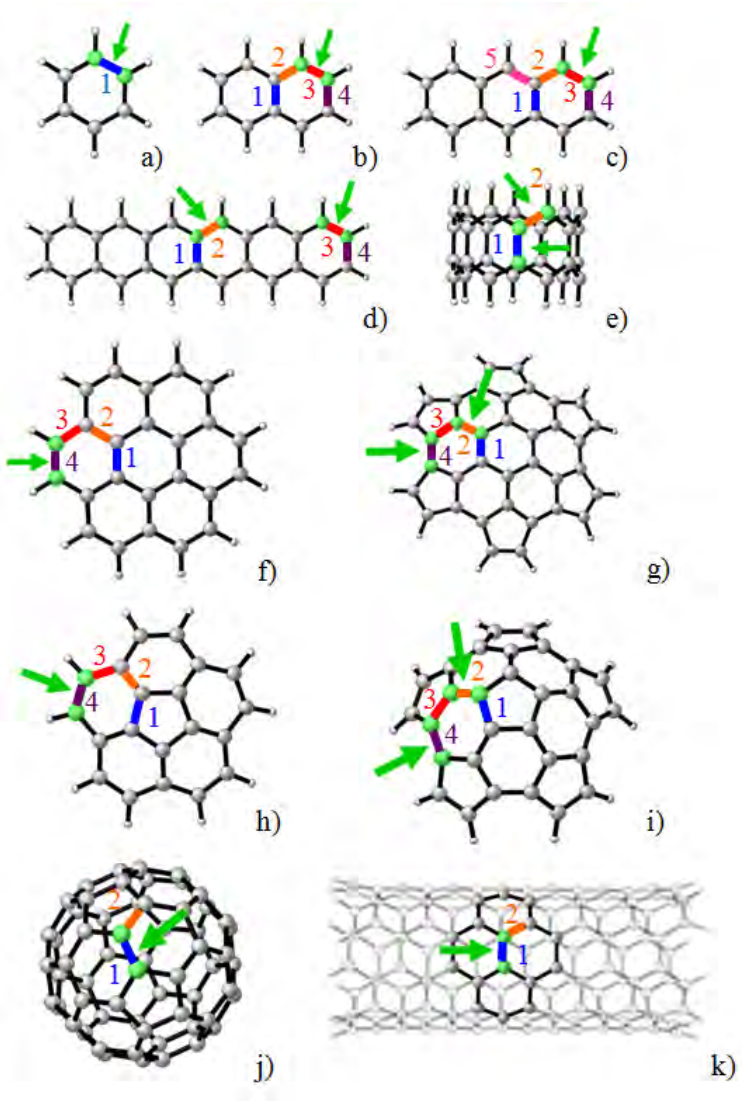

Figure 13.12: The molecules (a-k) to which cycloadditions have been studied. All considered addition sites are marked using the following coloring scheme: bond **1** in blue, **2** in orange, **3** in red, and **4** in lilac. An additional bond **5** (in pink) has been considered for anthracene. Green arrows represent the preferred addition sites for the cycloaddition reactions considered.

and Diels-Alder reaction, respectively). The same tendency is observed for corannulene (species h), where the addition is also preferred for bond **4**. This preference might be attributed to the location of bond **4** at the outer edge of the molecule where the pyramidalizaton of the attacked carbon atoms is more easily accommodated.

The introduction of pentagonal rings around the periphery of the coronene molecule induces some curvature. Therefore, *curved coronene* (species g) might be considered a possible model to mimic the reactivity of carbon nanotubes as they are formed by curved coronene patches. Although the addition to bonds **4** and **2** present similar reaction energies (-27.3 and 6.3 $kcal.mol^{-1}$ for the addition of $CH_2N(H)CH_2$ and C_4H_6 for bond **4** as compared to -26.9 and 8.2 $kcal.mol^{-1}$ for bond **2**), the addition to **4** is preferred as the activation barrier is somewhat lower in energy (2.6 and 31.5 $kcal.mol^{-1}$ for the 1,3-dipolar and Diels-Alder, respectively for position **4**, and 5.1 and 34.2 $kcal.mol^{-1}$ for bond **2**). The reaction and activation energies found for the model are in agreement with the nanotube results, especially for the more curved (5,5) structure. The addition to the most favorable position (**1**) has a reaction energy for the 1,3-dipolar cycloaddition of -26.3 and -17.3 for the (5,5) and (6,6) carbon nanotubes and an activation barrier of 4.3 and 9.7 $kcal.mol^{-1}$, respectively. It should be noted here that in a previous study by Lu and coworkers the 1,3-dipolar cycloaddition reaction involving the same dipole and using the same methodology (i.e. ONIOM) was assessed. However, main differences rely on the selected method for the low level calculations. In our case, the LDA DFT method SVWN together with the minimal basis set STO-3G has been used, whereas Lu *et al.* employed the semiempirical AM1. Interestingly, their reported reaction energy was 13 $kcal.mol^{-1}$ more exothermic and the activation barrier approximately 1 $kcal.mol^{-1}$ lower. In order to test the validity of our results, SP calculations using the AM1 method instead of SVWN have been performed. Interestingly, differences of 20 and 3 $kcal.mol^{-1}$ for the reaction and activation energy, respectively as compared to the full B3LYP SP are found. Therefore, the use of AM1 within the ONIOM approach leads to an underestimation of both reaction and activation energies compared to the full high level calculation and is no longer recommended for studying the chemical reactivity of nanotube compounds.

The Diels-Alder reaction is not favorable for any of the nanotubes considered. Again, the comparison of our estimated reaction and activation energies with the previously reported by Lu and coworkers using the ONIOM(B3LYP/6-31G(d):AM1) approach shows large deviations either in the reaction or in the activation energies, thus providing strong evidence that the use of AM1 as the low level method for ONIOM calculations is not appropriate for the study of these large systems.

As it happens in any buckybowl structure, different bond types (i.e. [6,6] and [5,6]) are present on the model *curved corannulene* (species i). Interestingly, the preferred addition site corresponds to a [6,6] bond with reaction and activation energies that are close to the ones obtained for C_{60}. Actually, the geometries of the transition

state are also in close agreement. For instance, in the case of the Diels-Alder, the reaction and activation energies found for bond called **2** ([6,6]) are -15.8 and 19.8 $kcal.mol^{-1}$ for the model and -21.7 and 17.8 $kcal.mol^{-1}$ for the real structure. Even closer values are obtained if the addition to the [5,6] bond is considered (-34.3 and 2.1 $kcal.mol^{-1}$ as compared to the C_{60} values of -34.4 and 1.5 $kcal.mol^{-1}$).

13.8.2 Other 1,3-dipolar cycloaddition reactions involving methylene nitrone and fulminic acid

Other dipoles such as the parent methylene nitrone ($CH_2 = N(H) - O^-$) and fulminic acid ($HC \equiv N - O^-$) have been studied but only considering the preferred addition sites found for the Diels-Alder and azomethine ylide cases. Reactivities obtained decrease along the series: formoazomethine ylide > fulminic acid > methylene nitrone. As a general rule, the reaction energies are reduced by 20-30 $kcal.mol^{-1}$ between each pair in the series, while this is 11-14 $kcal.mol^{-1}$ for the activation energies. The higher reactivity observed for azomethine ylide is not surprising as it exhibits the lowest HOMO-LUMO gap (3.62 eV as compared to 5.52 and 6.80 eV for nitrone and nitrile oxide). As it happens with the Diels-Alder and 1,3-dipolar cycloadditions, the obtained reaction and activation energies for *curved coranulenne* are in close agreement with the C_{60} results. This is not unexpected in view of previous studies.[338] Finally, it should be emphasized that the addition of methylene nitrone and nitrile oxide to (5,5) and (6,6) nanotubes is nearly thermoneutral and present much higher activation barriers compared to the highly reactive azomethine ylide case.

13.8.3 Thermodynamic and distortion/interaction models applied to cycloaddition reactions

Thermodynamical models such as Bell-Evans-Polanyi (BEP), Brönsted, and Marcus theory that correlate the reaction energy with the activation barrier have been satisfactorily applied to study chemical reactivity.[339] Houk and coworkers considered the possibility of applying these models to cycloaddition reactions.[174] The BEP relationship (or Marcus curve) for nearly thermoneutral reactions can be simplified to the Dimroth equation: $\Delta\Delta E^{\ddagger} = \frac{1}{2}\Delta\Delta E_{rx}$. In Figure 13.13, the linear correlations performed between the electronic reaction energies (ΔE_{rx}) and the activation barriers ($\Delta E^{\ddagger}$) for all Diels-Alder and 1,3-dipolar cycloadditions have been represented. In the case of the Diels-Alder and 1,3-dipolar with azomethine ylide, the ΔE_{rx} seems to be correlated to $\Delta E^{\ddagger}$, although a correlation coefficient lower than 0.90 is obtained in both cases. However, the latter relationship is no longer fulfilled once the 1,3-dipolar cycloaddition reactions involving methylene nitrone and nitrile oxide are considered. Although the linear Dimroth approximation should only be applicable to nearly thermoneutral reactions, the fit to the second order polynomial curve (i.e. Marcus equation, see Reactivity chapter) does not improve the results (see Figure 13.14). Moreover, the second order term was found to be close to 0, thus indicating

that the linear approximation to the Marcus curve still remains valid.

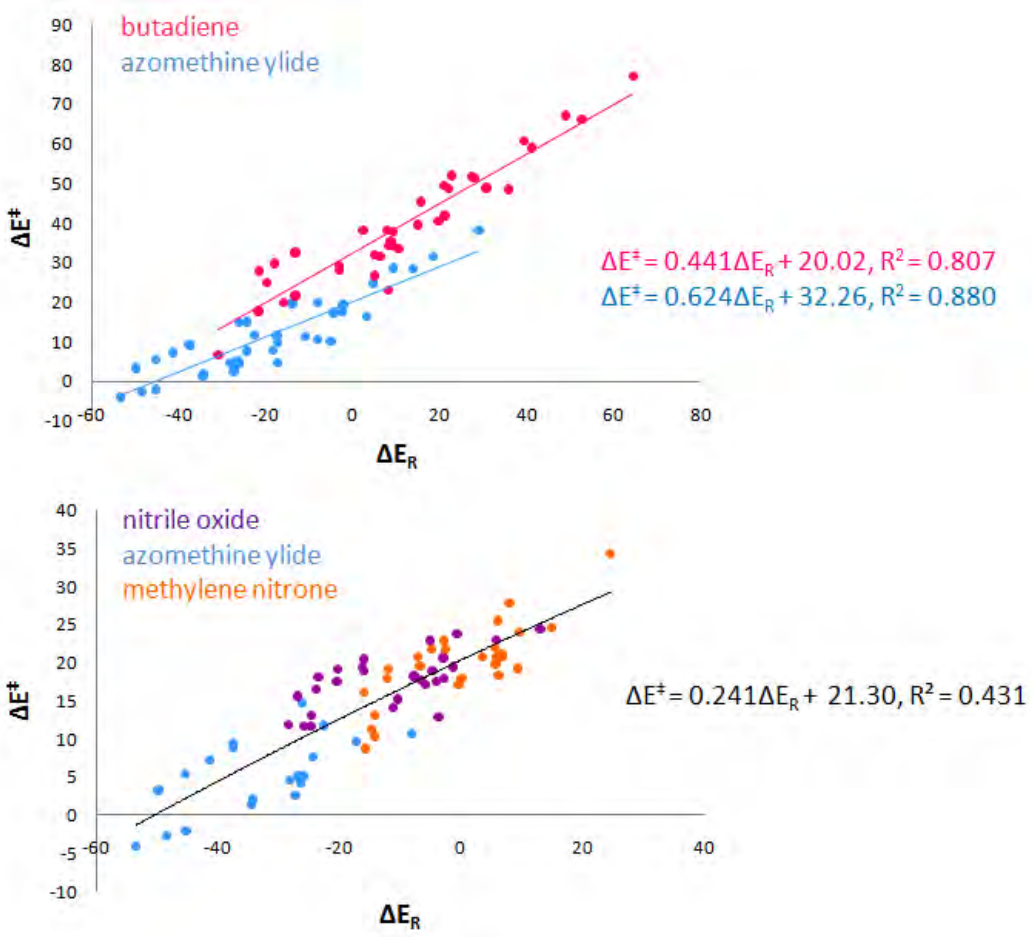

Figure 13.13: Plot of the B3LYP/6-31G(d) activation energies ($\Delta E^{\ddagger}$) versus reaction energies (ΔE_{rx}) for the Diels-Aler (in pink) and 1,3-dipolar with azomethine ylide (in blue) for all planar and curved organic compounds studied.

The distortion/interaction model by Houk was shown to give surprisingly accurate linear correlations between the activation barrier of cycloaddition reactions and the distortion energies (i.e. the energy required to deform initial reactants to the geometry they present at the TS). However, the latter model was only assessed considering small molecules such as acetylene, ethylene, and small PAHs.[173,174,181] In Figure 13.15, the linear correlations performed between the the activation barrier ($\Delta E^{\ddagger}$) and the distortion energy ($\Delta E_d^{\ddagger}$) for all Diels-Alder and 1,3-dipolar cycloadditions have been represented. As it can be seen in Figure 13.15, the distortion/interaction model is fulfilled in all considered cases, and more importantly is that in those systems where the BEP principle is not obeyed (i.e. for methylene nitrone and nitrile oxide) the

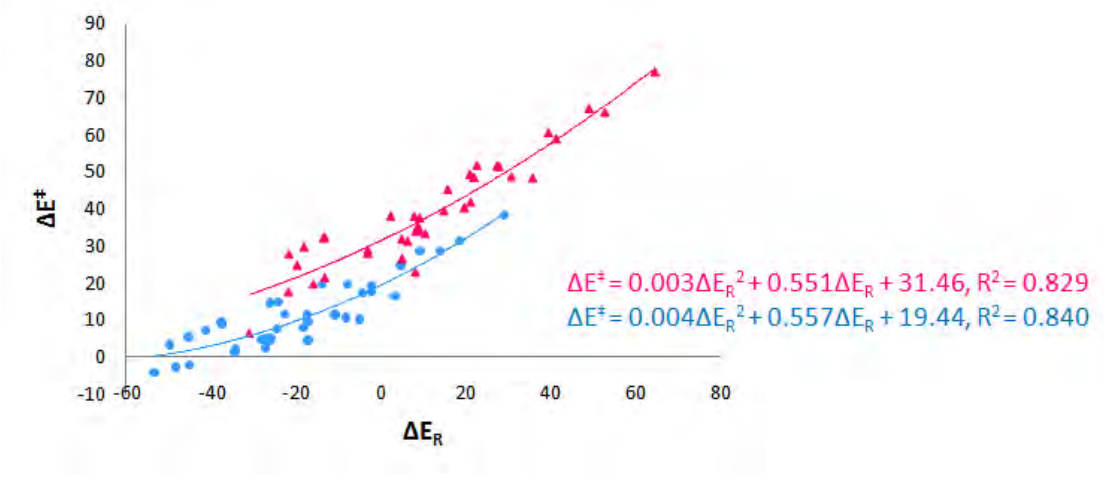

Figure 13.14: Plot of the B3LYP/6-31G(d) activation energies ($\Delta E^{\ddagger}$) versus reaction energies (ΔE_{rx}) for the Diels-Alder (in pink) and 1,3-dipolar with azomethine ylide (in blue) for all planar and curved organic compounds studied adjusted to a second order curve.

distortion/interaction model succeeds. Although the distortion/interaction model has the limitation that the TS needs to be known, the correlations found between barriers and distortion energies are still of interest. The most important contribution to the activation barrier for cycloadditions comes from the higher distortion energy required for the reaction to be produced. The latter is valid for systems ranging from relatively small compounds (acetylene, ethylene, benzene) but also for large molecules such as fullerene and nanotube compounds. The distortion/interaction model might then provide an important tool for understanding the mechanism and the preferred addition sites for cycloaddition reactions on fullerene and nanotube compounds.

13.9 On the mechanism of action of fullerene derivatives for superoxide dismutation

Fullerenes have usually been considered *radical sponges*. The latter characteristic is of significance as they are potential antioxidants to treat a wide variety of disorders related to oxidative stress (i.e. an over-production of reactive oxygen species (ROS) (such as the superoxide anion $O_2^{\cdot -}$) is produced due to an unbalanced situation between those processes responsible for the generation and those for the removal). Some biological and medical studies have been performed during the last decades to further investigate the *in vivo* and *in vitro* antioxidant capabilities of carboxyl and hydroxyl fullerene compounds. Among active fullerene compounds, the so-called C_3 which consists of three malonyl groups attached to the fullerene surface is one of

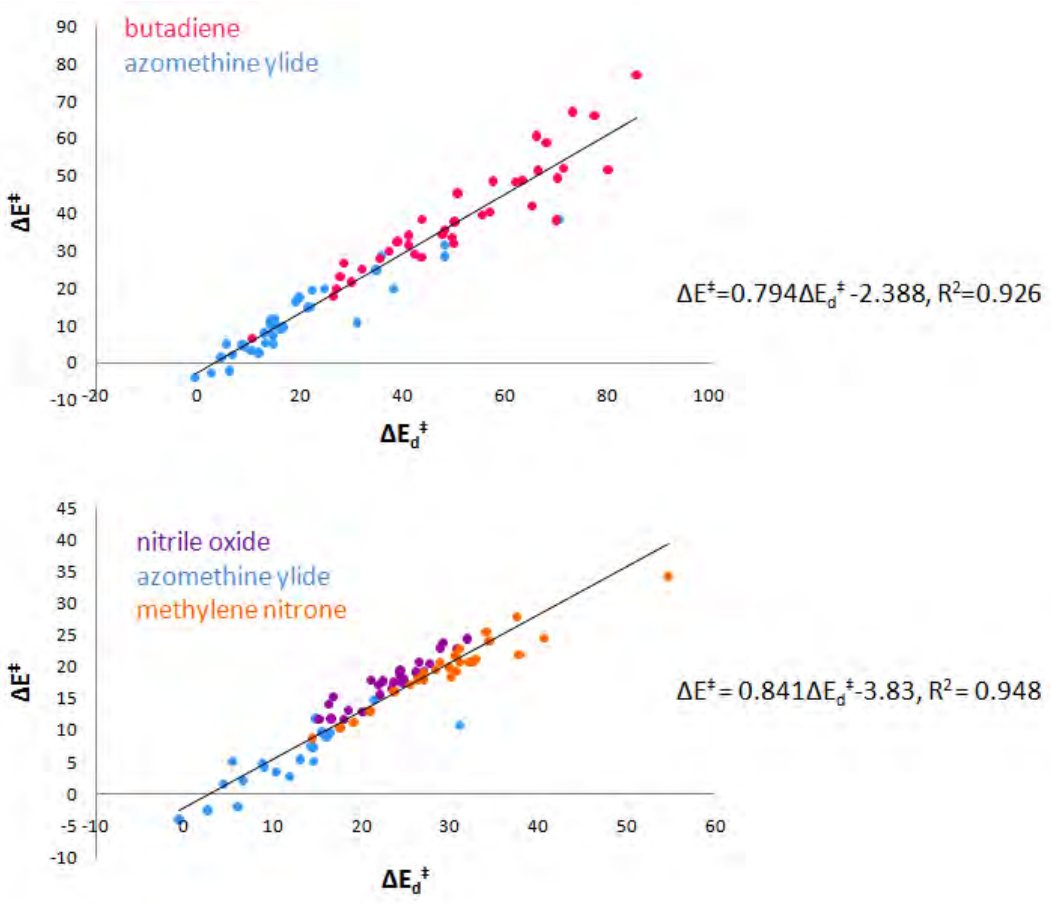

Figure 13.15: Plot of the B3LYP/6-31G(d) activation energies ($\Delta E^{\ddagger}$) versus distortion energies (ΔE_d) for the 1,3-dipolar cycloadditions with azomethine ylide (in blue), methylene nitrone (in orange), and fuminic acid (in lilac) for all planar and curved organic compounds studied.

the archetypal compounds. The mechanism through the antioxidant properties of C_3 and its derivatives is still an open issue, and as far as we know there are no theoretical studies where the latter mechanism is investigated in detail. Hereafter, the theoretical investigation at BP86/TZP for the mechanism of superoxide removal ($O_2^{\cdot -}$) involving the C_3 compound is presented (see Figure 13.16).

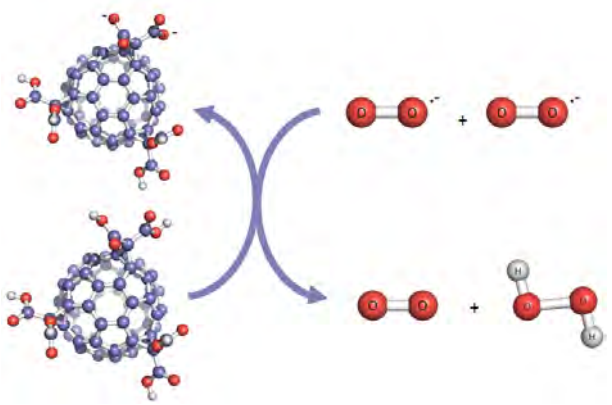

Figure 13.16: Scheme of the overall dismutation process involving the C_3 compound. Two superoxide radicals are converted into molecular oxygen and hydrogen peroxide.

In Figure 13.17, the relative energies of the localized intermediate structures, TSs and products are depicted for the whole process. The first intermediate of the mechanism (**int1**) corresponds to the interaction of a superoxide anion with the fullerene cage, six water molecules and a potassium cation (K^+) coming from the initial KO_2. It should be mentioned that we have considered the same experimental conditions reported in Liu and coworkers study (a large excess of KO_2 in DMSO containing 0.06% of water).[294] Therefore, all stationary points have been optimized including DMSO as solvent using the COSMO model,[340,341] and introducing a K^+ cation and six water molecules. In intermediate **int1**, the unpaired electron of the superoxide moiety has not been transferred yet. The formation of **int1** has associated with it an stabilization of -46.1 $kcal.mol^{-1}$ as compared to isolated reactants (C_3+ KO_2 + $6H_2O$). The electron transfer is produced in the second intermediate (**int2**) of the process where the superoxide anion has been converted to molecular oxygen and the fullerene cage has accepted the unpaired electron (C_3+ KO_2 + $6H_2O \rightarrow$ **int2** + O_2). The latter transfer presents a reaction energy of -23.6 $kcal.mol^{-1}$. Although a TS should be located here, the TS search involving electron transfer processes is not an straightforward procedure. Therefore, the activation barrier for the process has been estimated to be equal to the reaction energy of the reaction (22.5 $kcal.mol^{-1}$). Hence, the process (**int1** $\rightarrow$ **int2** + O_2) has a relatively high activation barrier and is actually the rate-determining step of the reaction. The electron transfer produced from the superoxide anion to the fullerene cage might be described considering the HOMO orbitals of the superoxide radical and the LUMO of the fullerene compound.

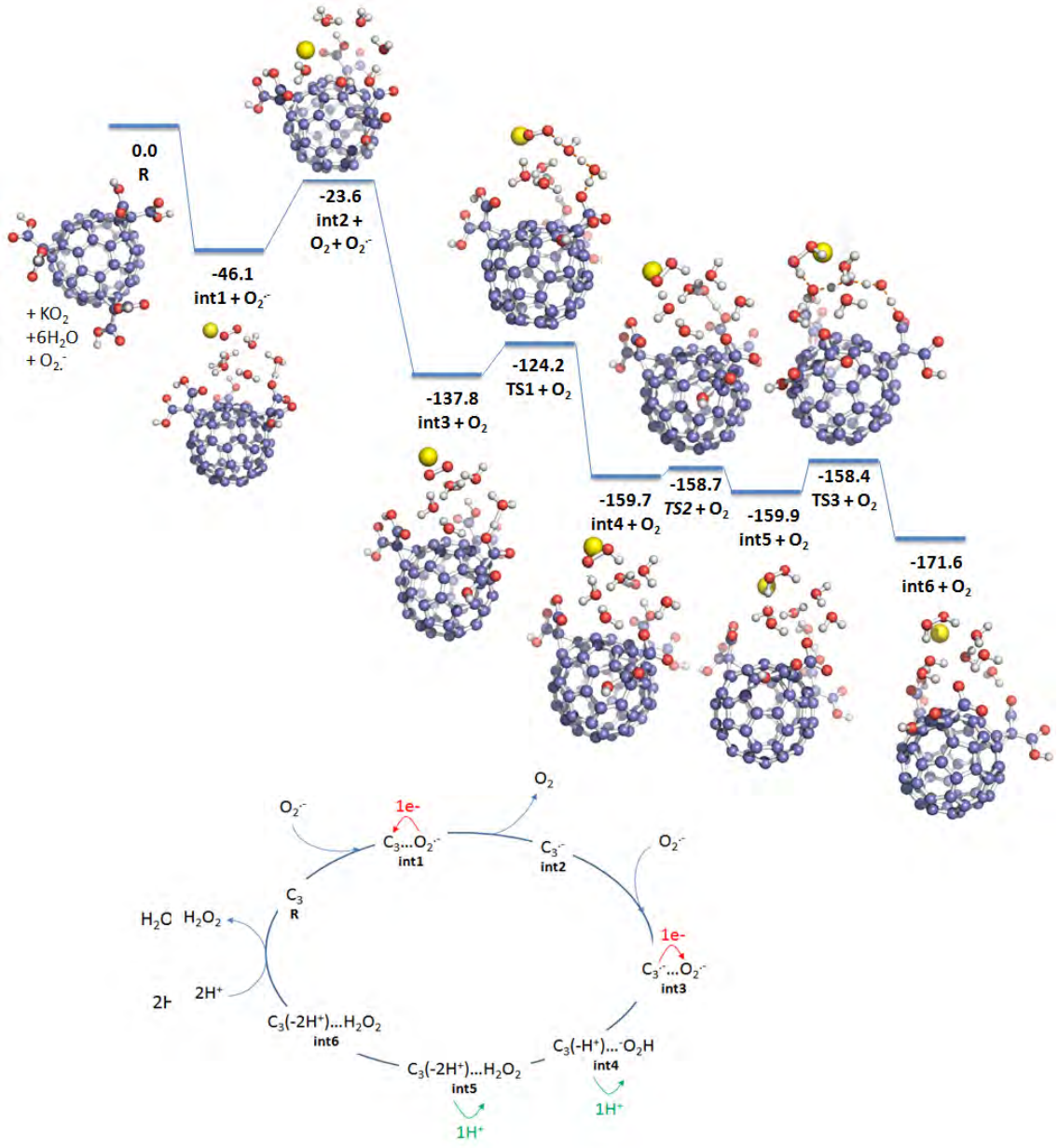

Figure 13.17: Reaction mechanism for the SOD removal involving the C_3 compound. All energies are expressed in $kcal.mol^{-1}$

The LUMOs of C_3 are 0.09 eV higher in energy than the HOMO of the superoxide (see Figure 13.18). That is the main reason for the relatively small difference between **int1** and **int2**. Liu and coworkers observed a higher antioxidant activity for those fullerene compounds with higher reduction potentials.[294] Of course, a higher reduction potential implies a higher affinity for accepting electrons which leads to more stabilized HOMO and LUMO orbitals. An stabilization of the LUMO orbitals of the fullerene compound favors the transference of one of the two electrons of the HOMO of the KO_2 to the more stabilized LUMO orbital of the C_3 molecule.

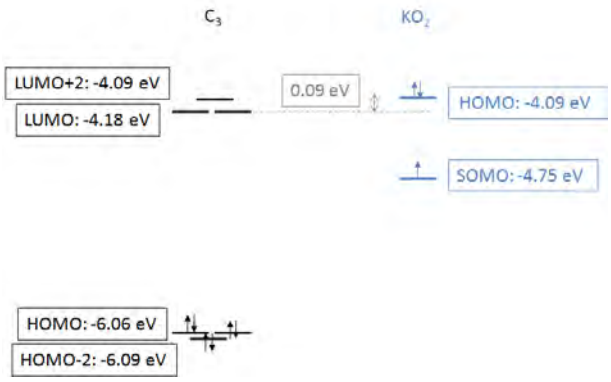

Figure 13.18: Representation of the frontier orbitals of the superoxide radical and the LUMO of the fullerene compound. All energies are expressed in eV.

In the third intermediate (**int3**), another superoxide radical is interacting with the fullerene but now bearing an extra electron (C_3^{-}) transferred in the last step of the reaction. The latter intermediate could present either a singlet or a triplet spin state configuration corresponding to the anti-parallel or parallel alignment of the unpaired electrons of O_2^{-} and C_3^{-} compounds. However, the difference in energy between both configurations is rather small (0.1 $kcal.mol^{-1}$) as the superoxide radical and that of the fullerene compound are not in close contact.

In **int4**, a proton has already been transferred to the superoxide moiety and presents a reaction energy of -159.7 $kcal.mol^{-1}$ with respect to initial reactants. Again two possible spin configurations might be considered. However, the singlet spin state was found to be 36.8 $kcal.mol^{-1}$ more stable than the triplet which can be attributed to the preference of hydrogen peroxide (and related species) for a singlet ground state (in the case of H_2O_2 the singlet is 37.2 $kcal.mol^{-1}$ more stable). Three proton transfers are involved in the corresponding TS (**int3** $\rightarrow$**TS1** $\rightarrow$ **int4**) from one of the COOH groups of C_3 to the superoxide radical through two interconnected water molecules. This process has an activation barrier of 13.6 $kcal.mol^{-1}$ (with respect to the previous intermediate **int3**). After this barrier is surmounted another intermediate (**int4**) is detected where the hydroperoxide anion (^{-}OOH) is formed. The subsequent barrier that has to be surmounted (**TS2**) to finally obtain the hydrogen

peroxide molecule (H_2O_2) (**int5**) is less than 1 $kcal.mol^{-1}$. Finally, the last transition state (**TS3**) has to be overcome in order to protonate the water molecule that gave up its proton to the hydrogen peroxide in **TS2**. This process has an activation barrier of 1.5 $kcal.mol^{-1}$ (compared to **int5**) and involves three interconnected water molecules. One of the carboxyl groups of the fullerene surface is deprotonated to transfer its hydrogen atom to a water molecule that, at the same time, transfers another proton to a second water. Additionally, a third proton transfer is produced from the latter water molecule to the unprotonated water that already transferred one hydrogen in **TS2** (see Figure 13.19). In the last intermediate of the reaction (**int6**), hydrogen peroxide is interacting with the surrounding water molecules and the fullerene compound presenting two of the carboxyl groups deprotonated, and is actually -171.6 $kcal.mol^{-1}$ more stable than the initial reactants (C_3 + KO_2 $+6H_2O$).

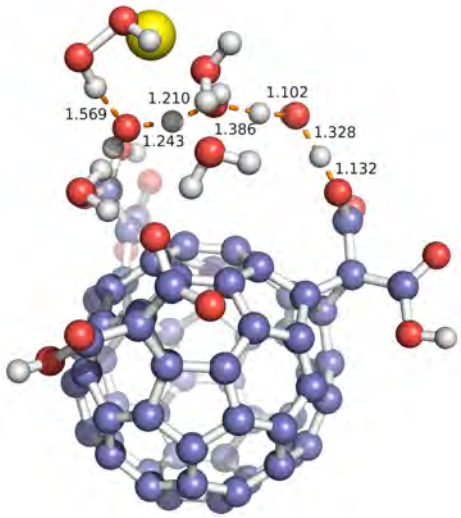

Figure 13.19: BP86/TZP optimized structure for the transition state **TS3** that involves the proton transfer from one of the carboxyl groups of the fullerene compound to the deprotonated water molecule that in **TS2** transferred one of its protons to the hydrogen peroxide. Distances are represented in Å.

At this point, the reaction could either continue following the same mechanism described as the fullerene compound still presents four protonated carboxyl groups, or start the reaction again after protonation of the two carboxyl groups of the C_3. In the first case, six superoxide radicals might be converted to three oxygen molecules and three hydrogen peroxide compounds. The reaction for the whole process (C_3 + $6O_2^{\cdot -}$ $\rightarrow$ $3O_2$ + $3H_2O_2$ + $C_3(-6H^+)$) is -128.6 $kcal.mol^{-1}$. Therefore, a high antioxidant activity is observed as only one fullerene molecule is capable of removing six dam-

aging superoxide radicals. The knowledge of the mechanism behind the superoxide removal involving fullerenes is highly appealing due to the potential application of these compounds to treat those diseases related to oxidative stress.

Chapter 14

Conclusions

The most important conclusions taken out from the previous studies involving fullerene compounds will be briefly summarized.

First:

The study of the Diels-Alder reaction involving the free fullerene cage C_{78} and the scandium based endohedral derivative $Sc_3N@C_{78}$ has shown that the regioselectivity of the reaction is highly modified upon encapsulation. Main reactivity differences are due to the changes on the physical properties caused by the metal cluster trapped inside the fullerene cage, which first of all reduces the compound reactivity and second, favors the reaction over different bonds. Thermodynamic and kinetic results have shown that the Diels-Alder reaction on the endohedral compound is preferred over the type B [6,6] bonds called **6** and **4** and the type D [5,6] **c**. It should be emphasized here that the 1,3-dipolar cycloaddition on $Sc_3N@C_{78}$ was assessed experimentally. In line with our theoretical predictions, the two cycloaddition products detected corresponded to the addition over bonds **6** and **4**. In the C_{78} case, the reaction is favored over type D [5,6] bond called **b**, and over type A [6,6] bonds **7** and **1**. Interestingly, there is a general reduction of the exohedral reactivity of the endohedral compound especially for those bonds situated close to the scandium atoms that are highly deactivated.

The reactivity patterns obtained do not correlate well with the predictions from C-C bond distances, pyramidalization angles, and molecular orbitals. However, those bonds presenting short C-C bond distances, from moderate to high pyramidalization angles, and suitable shaped LUMO orbitals to interact with diene will surely correspond to the preferred addition sites.

Second:

The Diels-Alder cycloaddition reaction has been studied for the yttrium based fullerene compounds $Y_3N@D_{3h}-C_{78}$ and $Y_3N@C_2-C_{78}$. The metal cluster encapsulated inside the relatively small $D_{3h}-C_{78}$ cage is forced to adopt a pyramidal structure,

thus producing two differentiated zones in the fullerene cage: the area more influenced by the nitrogen atom *up* and the *down* region more affected by the yttrium atoms. Although both sides are not equivalent, a similar reactivity is observed for the two faces of the fullerene compound. The TNT encapsulation of yttrium-based metal cluster produces a global decrease of the exohedral reactivity of the fullerene cage. Interestingly, the preferred addition site is over the type D [5,6] bond called **d** which is situated close to one of the yttrium atoms and exhibits one of the largest C-C bond distances in the initial fullerene structure. The latter is of significance as it corresponds to the first case of cycloaddition reaction where the most stable addition is obtained over an extremely long C-C bond.

A change on the regioselectivity of the Diels-Alder reaction is observed for the different metal based endohedral fullerenes $X_3N@D_{3h}-C_{78}$ (X= Sc, Y). It has been shown in the previous study that the preferred addition sites for the case of $Sc_3N@D_{3h}-C_{78}$ are two [6,6] type B bonds and one type D [5,6] that exhibit short C-C bond distances and are situated far away from the scandium influence. However, the encapsulation of the yttrium based TNT unit clearly favors the addition over extremely long C-C bonds situated close to the metal atoms. This preference is attributed to two different factors. First, the $D_{3h}-C_{78}$ cage is highly deformed and the fullerene strain is highly released after reaction with those bonds situated close to the Y. Second, a more planar configuration of the TNT unit can be adopted thanks to the additional space gained after the reaction.

The most stable cage for encapsulating the large Y_3N cluster is the $C_2(22010)-C_{78}$ cage. In this non-IPR isomer, the yttrium unit can adopt a planar configuration. Although $Y_3N@C_2-C_{78}$ presents more than 60 non-equivalent bonds, 10 bonds have been selected on the basis of the reactivity patterns observed for the $D_{3h}-C_{78}$ cage. The preferred addition site corresponds to the addition to the type E [5,5] bond which is present only in non-IPR structures. Interestingly, the same reactivity pattern is observed for $Sc_3N@C_2-C_{78}$ and C_2-C_{78} suggesting that the exohedral reactivity of the recently synthesized $Dy_3N@C_2-C_{78}$, $Tm_3N@C_2-C_{78}$, and $Gd_3N@C_2-C_{78}$ might be produced on these highly reactive [5,5] bonds.

Third:

The exohedral reactivity of the endohedral compounds $Ng@C_{60}$ and $Ng_2@C_{60}$, Ng= He, Ne, Ar, Kr and Xe has been investigated in detail. In particular, we have studied the [4+2] Diels-Alder cycloaddition for all different reactive bonds of the noble gas endohedral fullerenes. The reactivity of the single noble gas endohedral fullerenes is hardly affected by the noble gas unit, and the activation and reaction energies obtained are close to those for the free C_{60} compound. A similar reactivity to the free fullerene cage is also observed for the lighter noble gas dimer homologues $He_2@C_{60}$ and $Ne_2@C_{60}$, although the reaction is slightly more favored for the latter compound. The preferred addition sites correspond to the addition to the [6,6] bonds. In the lighter dimer homologues, the Ng_2 unit is in some cases reoriented

to face the attacked C-C bond. An enhanced reactivity is observed for $Ar_2@C_{60}$, $Kr_2@C_{60}$, and especially for $Xe_2@C_{60}$. For Ar_2 and Kr_2 endohedral compounds, the addition is preferred over those [6,6] bonds situated close to the C_5 axis where the noble gas dimer is initially contained (**1** and **2**). Of course, the larger the noble gas atoms the more impeded the rotation of the dimer to face the attacked bond. In the xenon fullerene, an electronic transfer of 1-2 electrons from the noble gas moiety to the fullerene cage is produced, and a genuine chemical bond between both xenon atoms is formed. A decrease of the reactivity might be expected from the fact that a reduction of the electron affinity is produced. However, the exohedral reactivity of $Xe_2@C_{60}$ is highly enhanced and the reaction becomes no longer regioselective as both [6,6] and [5,6] bonds are equally reactive.

The increased reactivity found for the heaviest homologues might be understood considering three different factors. First, the LUMO energy of the endohedral compound is reduced as a consequence of the noble gas encapsulation. Second, the insertion of large noble gas dimers inside the small C_{60} cage leads to a highly strained fullerene cage. The latter strain is partially released after reaction due to the increase in the pyramidalization of the attacked C-C bonds. Finally, the elongation of the Ng-Ng distance in the final adduct compared to the initial fullerene structure leads to substantially more exothermic reaction energies.

Fourth:
The performance of the two-layered ONIOM approach for studying cycloaddition reactions involving fullerene compounds has been assessed. Full B3LYP results have been compared to those obtained using ONIOM and considering different fragments for the high level calculations. The smallest fragment considered is made up by a single [6,6] C-C bond, and the largest the $C_{26}H_{12}$ buckybowl species. Partition III involving a pyracylene unit of C_{60} and the diene provides the best compromise between accuracy and computational cost. The Diels-Alder reaction between C_{60} and cyclopentadiene has been experimentally assessed, and therefore the reaction and activation barriers have been estimated. Taking advantage of that, we have studied the reaction using several DFT functionals in order to obtain the best DFT combination for describing cycloaddition reactions on fullerene compounds. Our results indicate that the ONIOM2(M06-2X/6-31G(d):SVWN/STO-3G) and the M06-2X/6-31G(d)//ONIOM2(B3LYP/6-31G(d):SVWN/STO-3G) approaches are among the most reliable and computationally efficient methods for describing the activation barriers and reaction energies, respectively of cycloaddition reactions of fullerenes and related compounds such as carbon nanotubes.

Fifth:
The mechanism behind the retro-cycloaddition reaction of pyrrolidinofullerenes has been investigated in detail at the DFT level of theory using the ONIOM approach. The presence of another dipolarophile such as maleic anhydride in the reaction mixture, facilitates the retro-process converting the reaction from highly endothermic

to substantially exothermic. However, two different mechanisms can be followed at the experimental conditions. The first possibility corresponds to the assistance of the maleic anhydride during the retro-process. Therefore, once the pyrrolidino ring is being broken the generated azomethine ylide is simultaneously interacting with maleic anhydride. The other possible mechanism corresponds to the assistance of maleic anhydride at the last stage of the reaction. That basically implies that the retro-reaction is produced leading to the formation of C_{60} and azomethine ylide, and afterwards the generated dipole reacts with maleic anhydride to form the corresponding cycloaddition product. In the case of the unsubstituted azomethine ylide, both mechanisms are approximately equally favored (electronic energies favor the assisted mechanism, whereas Gibbs-free energies the non-assisted path). However, the non-assisted reaction is substantially more favored when an ester substituent is introduced in one of the terminal carbons of the azomethine ylide (the highest activation barrier that has to be surmounted is approximately 10 $kcal.mol^{-1}$ lower in energy than that for the assisted process).
The mechanism of the retro-1,3-dipolar cycloaddition involving azomethine ylide bearing two different substituents has been unraveled. The latter is of significance due to the possible application of this kind of reactions as a new efficient protection-deprotection protocol in fullerene science.

Sixth:
The Diels-Alder and the 1,3-dipolar cycloaddition reactions involving different dipoles (azomethine ylide, methylene nitrone, and fulminic acid) have been studied over a wide range of organic compounds including fullerenes and carbon nanotube compounds. The preferred addition site for naphthalene, anthracene, and hexacene has been found to be over bond called **3** as it only disrupts the aromaticity of a single benzene unit, whereas for coronene and corannulene the most favorable addition corresponds to bond **4**, which is situated at the periphery of the molecule where pyramidalization is more easily accommodated. In the case of the model systems, *curved coronene* still reacts preferentially at bond **4**, but reactions of **2** are more favorable for *curved corannulene*. The reaction and activation barriers obtained for these model systems are quite similar to the ones obtained in the real fullerene and nanotube systems. Of course, all cycloaddition reactions studied over the [6,6] bond of the fullerene compound lead to the most favorable addition. The 1,3-dipolar cycloadditions produced on the (5,5) nanotube involving azomethine ylide and fulminic acid are exothermic, whereas in the rest of the cases studied the reaction is unfavorable. For the study of the nanotube compounds, we have used the ONIOM2 approach using the B3LYP level of theory together with the standard 6-31G(d) for the high-level (a coronene patch) and the SVWN functional with the minimal basis set STO-3G for the rest of the system. The reaction and activation barriers obtained are very similar to those performing full SP calculations at the high level of theory. However, we have detected that the use of AM1 for the low level calculations within the ONIOM approach gives surprisingly underestimated values as compared to the full high-level predictions.

Finally, we have investigated the applicability of the recently proposed distortion/ interaction model for describing cycloaddition reactions. In all cases studied, the activation barriers for the cycloaddition reactions are highly correlated to the energy required to distort initial reactants to that of the transition state (i.e. distortion energy).

Seventh:
The mechanism for the superoxide removal involving the so-called C_3 fullerene compound has been studied in detail at the DFT level of theory. In general, all activation barriers that have to be surmounted are low, except for the first step of the reaction. The latter corresponds to the rate-determining step of the process and involves the electron transfer of the unpaired electron of the superoxide radical to the fullerene surface. The activation barrier for the electronic transfer is primilarly related to the LUMO energy of the C_3 compound. The lower the energy of the LUMO, the more favorable the transfer of the unpaired electron as the difference in energy between the LUMO of C_3 and the HOMO of KO_2 is reduced or even negative (the LUMO orbital of the fullerene may be more stable than the HOMO orbital of the superoxide). Therefore, it is not surprising that those derivatives of the C_3 compound that present lower reduction potentials exhibit higher antioxidant activity in experiment. Once the unpaired electron has been transferred, a second superoxide can react with the fullerene radical ($C_3^{\cdot -}$) removing the extra electron from the fullerene and forming hydrogen peroxide (H_2O_2). The formation of H_2O_2 involves the deprotonation of two of the carboxyl groups attached to the fullerene compound. The latter is achieved through several interconnected water molecules. The first transition state (**TS1**) has an activation barrier of 13 $kcal.mol^{-1}$, whereas the rest of the TSs (**TS2** and **TS3**) present reaction barriers of less than 1.6 $kcal.mol^{-1}$. After the hydrogen peroxide is formed, the reaction could either continue as the C_3 still presents four protonated carboxyl groups or start the reaction again protonating the deprotonated carboxyl groups. In the first case, one single fullerene molecule might be able to convert six superoxide radicals into three oxygen molecules and three hydrogen peroxide compounds. This capability of the fullerene derivatives of removing the highly reactive oxygen species linked to several human diseases is extremely interesting for future applications of these compounds in (bio)medicine.

Chapter 15

Full list of publications

1. Osuna, S.; Poater, J.; Bofill, J. M.; Alemany, P.; Solà, M., Are nucleus-independent (NICS) and $^1H - NMR$ chemical shifts good indicators of aromaticity in π-stacked polyfluorenes? *Chem. Phys. Lett.* **2006**, 428, 191-195.

2. Izquierdo, M.; Osuna, S.; Filippone, S.; Martín-Domenech, A.; Solà, M.; Martín, N., H-bond-assisted regioselective (cis-1) intramolecular nucleophilic addition of the hydroxyl group to [60]Fullerene. *J. Org. Chem.* **2009**, 74, 1480-1487.

3. Dachs, A.; Torrent, A.; Roglans, A.; Parella, T.; Osuna, S.; Solà, M., Rhodium-(I)-Catalysed Intramolecular [2+2+2] Cyclotrimerizations of 15-, 20- and 25-Membered Azamacrocycles: Experimental and Theoretical Mechanistic Studies. *Chem. Eur. J.* **2009**, 15, 5289-5300.

4. Osuna, S.; Torrent-Sucarrat, M.; Ewels, C. P.; Solà, M.; Geerlings, P.; Van Lier, G., Local Aromaticity of Pristine and Fluorinated Carbon Nanotubes. *J. Nanosci. Nanotechnol.* **2009**, 9, 6078-6083.

5. Osuna, S.; Swart, M.; Baerends, E. J.; Bickelhaupt, F. M.; Solà, M., Homolytic versus Heterolytic Dissociation in Diatomic Alkalimetal Halides. The effect of microsolvation. *ChemPhysChem.* **2009**, 10, 2955-2967.

6. Izquierdo, M., Osuna, S., Filippone, S., Martín-Domenech, A., Solà, M. and Martín, N., Regioselective intramolecular nucleophilic addition of alcohols to C_{60}: one-step formation of a cis-1 bicyclic-fused fullerene, *J. Org. Chem.* **2009**, 74, 6253-6259.

7. Dachs, A.; Osuna, S.; Roglans, A.; Solà, M., A Density Functional Theory Study of the [2+2+2] Cyclotrimerization of Acetylene Catalyzed by the Wilkinson's Catalyst, $RhCl_3(PPh_3)_3$. The effect of replacing PPh_3 for PH_3, *Submitted for publication* **2009**.

8. Delgado, J. L.; Osuna, S.; Bouit, P. A.; Martínez-Alvarez, R.; Espíldora, E.; Solà, M.; Martín, N. Competitive Retro-Cycloaddition Reaction in Fullerene

Dimers connected through Pyrrolidino-pyrazolino Rings. *J. Org. Chem.* **2009**, 74, 8174-8180.

9. Swart, M.; Solà, M.; Osuna, S.; Poater, J., Metales, disolventes, proteínas: la importancia del entorno químico, *LifeSciencesLab* **2009**, 5, 50-53.

10. Izquierdo, M.; Osuna, S.; Filippone,S.; Martín-Domenech, A.; Solà, M.; Martín, N. On the regioselective intramolecular nucleophilic addition of thiols to C_{60}. *Eur. J. Org. Chem.* **2009**, 6231-6238.

11. Osuna, S.; Torrent-Sucarrat, M.; Solà, M.; Geerlings, P.; Ewels, C. P.; Van Lier, G. New hybrid carbon nanotubes, *Submitted for publication* **2009**.

The thesis is based on the following papers:

1. Osuna, S.; Swart, M.; Campanera, J. M.; Poblet, J. M.; Solà, M., Chemical reactivity of D_{3h} C_{78} (metallo) fullerene: regioselectivity changes induced by Sc_3N encapsulation. *J. Am. Chem. Soc.* **2008**, 130, 6206-6214.

2. Osuna, S.; Swart, M.; Solà, M., The Diels Alder reaction on the endohedral $Y_3N@C_{78}$: the importance of the fullerene strain energy. *J. Am. Chem. Soc.* **2009**, 131, 129-139.

3. Osuna, S.; Swart, M.; Solà, M., Reactivity and regioselectivity of noble gas endohedral fullerenes $Ng@C_{60}$ and $Ng_2@C_{60}$ (Ng = He-Xe). *Chem. Eur. J.* **2009**, 15, 13111-13123.

4. Osuna, S.; Morera, J.; Cases, M.; Morokuma, K.; Solà, M., The Diels-Alder Reaction between Cyclopentadiene and C_{60}: An analysis of the performance of the ONIOM method for the study of chemical reactivity in fullerenes and nanotubes. *J. Phys. Chem. A* **2009**, 113, 9721-9726.

5. Filippone, S.[§]; Barroso, M. I.; Martín-Domenech, A.; Osuna, S.[§]; Solà, M.; Martín, N., On the mechanism of the thermal retrocycloaddition of pyrrolidinofullerenes (retro-prato reaction). *Chem. Eur. J.* **2008**, 14, 5198-5206. ([§]: The authors equally contributed to the work: Correction. *Chem. Eur. J.* **2008**, 14, 5709).

6. Osuna, S.; Houk, K. N., Cycloaddition reactions of butadiene and 1,3-dipoles to curved arenes, fullerenes, and nanotubes: Theoretical evaluation of the role of distortion energies on activation barriers. *Chem. Eur. J.* **2009**, 15, 13219-13231.

7. Osuna, S.; Swart, M.; Solà, M., On the mechanism of the superoxide dismutation involving fullerene derivatives. *Chem. Eur. J. Accepted for publication* **2009**.

Chapter 16

Acknowledgments

Voldria començar els agraïments donant les gràcies als meus directors de tesi, en Miquel i en Marcel.
Agraeixo moltíssim la paciència, l'entusiasme i l'interès que sempre Miquel has mostrat. Sempre aprenc un munt de coses i per qualsevol problema que pugui sorgir sempre tens una bona solució. Moltes gràcies per tota l'ajuda, el suport, els ànims i per encomanar-me de les teves ganes de treballar. No sé què faria sense l'ajuda d'en Marcel, el gran avanç en la realització d'aquesta tesi ha estat gràcies a ell, i estic segura que sense el seu programa QUILD encara estaríem buscant els TSs. Valoro molt la paciència que tens, les ganes de treballar, també l'interès i el suport. Moltes gràcies Marcel per les teves explicacions i per ajudar-me amb tot.

No em vull oblidar dels meus companys de despatx amb qui tinc un munt d'anècdotes per recordar: en Ferran (alias *Fala*, una mica de vodka amb "regalís"?), en Pata (ja saps el pròxim cop que vagis a Suècia protecció solar 60!), en Juanma (a quin joc juguem?), la Cristina (has comentat els abstracts amb en MF?), la Mireia (els fem creure a tots!), l'Anna Dachs (alias *Dachs*, fusionem àtoms?), l'Eloy (alias *Ramos-Cordoba*, com tens l'angewandte?), l'Eugene (alias *Horba*, no obris la finestra!), en Lluís (alias *Rambo*, on has deixat el rambo mòbil?). Però tampoc d'en Jordi, en Pedro, en Quansong (alias *Quantum Li*), l'Edu, l'Albert, la Díaz, en Samat, en Quim, en Sergi, la Laia, en Dani, l'Hugas, en Miquel Torrent, la Montse Cases, en Rafael i la Montse. Moltes gràcies a tots per les bones estones que passem, pels sopars, les festes, però també per l'ajuda i suport.

No sé què faria (i en general, què faríem) sense la Carme, perquè sense ella, l'IQC seria un caos. Moltes gràcies per tota l'ajuda amb la paperassa i també per les xerrades i els farts de riure que ens fèiem als esmorzars.

Vull agrair a en Miquel Duran que me donés l'oportunitat de fer el doctorat, però també vull donar les gràcies a tots els membres de l'IQC, entre tots formem una gran familia, que per sort i que així duri durant molts anys va creixent i creixent sense

parar. A tots vosaltres gràcies per tot.

Mama i papa, gràcies per tot el que feu per a mi, per ajudar-me i animar-me sempre. Aquesta tesi està dedicada a vosaltres. No em vull oblidar de l'avi Florenci, que tot i que a vegades li falla la memòria sé que també n'estaria ben orgullós. Tampoc em vull deixar l'àvia Concha, la tia Carme, els meus "germanets" en Joan i en Xavier, l'oncle Joan, la tia Carmen i el tiet Francisco, en Marc, en Daniel i l'Isaac.

Aquesta tesi també està dedicada a tu Narcís, no sé què faria sense tu i tampoc m'ho vull imaginar. Gràcies per ajudar-me, per animar-me i fer-me riure en els moments difícils, per recolzar-me i ajudar-me sempre. A més, vull donar les gràcies a l'Imma, en Narcís i l'Aida.

Voldria agrair a la Marta, en Sergi i en Marc per les bones estones que passem (sopars, jocs, partits de futbol, padel, festes, excursions..) i pel seu suport moral.

Tot sembla indicar que les molècules d'estudi d'aquesta tesi, els ful.lerens, podrien ser útils per al tractament d'algunes malalties neurodegeneratives. Tot i que qualsevol contribució en aquest sentit és lluny encara de tenir una implicació real en el món de la medicina, el fet de pensar en que les "meves" molècules podrien ajudar a curar a totes aquelles persones malaltes, persones com l'àvia o l'avi, és realment encoratjador. No hi ha res més desesperant que veure com la malaltia se t'emporta dia a dia, poc a poc i sense fre a aquella persona del teu costat, i a la vegada no hi ha res més motivador que tenir l'esperança de poder fer-hi alguna cosa. Avi, aquesta tesi està dedicada a tu perquè sé que ningú més hagués valorat tot l'esforç i el treball. M'imagino donant-te la tesi, tu posant-te les ulleres i intentant llegint-la amb gran interès. Sé que n'estaries orgullós igual com jo n'estic i n'estaré sempre de tu.

El temps passa i és el mateix temps el principal responsable de l'oblit, fa temps que no ets aquí amb mi, però no et pensis que t'he oblidat. Mai tindré prou paraules per poder agrair-te tot el que vas fer per mi, i mai podré oblidar-ho. Àvia, a tu també et dedico la tesi perquè ningú s'ho mereix tant com tu, sempre seràs el meu exemple i sempre estaràs dins el meu cor.

List of Figures

List of Tables

Bibliography

[1] Kroto, H. W.; Heath, J. R.; O'Brien, S. C.; Curl, R. F.; Smalley, R. E. *Nature* **1985**, *318*, 162.

[2] Jones, D. E. H. *New Sci.* **1966**, 245.

[3] Osawa, E. *Kagaku* **1970**, *25*, 854.

[4] Bochvar, D.; Gal'pern, E. G. *Proc. Acad. Sci. USSR* **1973**, *209*, 239.

[5] Davidson, R. A. *Theor. Chim. Acta* **1981**, *58*, 193.

[6] Haymet, A. D. *J. Chem. Phys. Lett.* **1985**, *122*, 421.

[7] Dietz, T. G.; Duncan, M. A.; Powers, D. E.; Smalley, R. E. *J. Chem. Phys.* **1981**, *74*, 6511.

[8] Rohlfing, E. A.; Cox, D. M.; Kaldor, A. *J. Chem. Phys.* **1984**, *81*, 3322.

[9] Bloomfield, L. A.; Geusic, M. E.; Freeman, R. R.; Brown, W. L. *Chem. Phys. Lett.* **1985**, *121*, 33.

[10] Krätschmer, W.; Lamb, L. D.; Fostiropoulos, K.; Huffman, D. R. *Nature* **1990**, *347*, 354.

[11] Taylor, R.; Hare, J. P.; Abdul-Sada, A. K.; Kroto, H. W. *J. Chem. Soc., Chem. Commun.* **1990**, 1423.

[12] Schmalz, G. T.; Seitz, A.; Klein, D. J.; Hite, G. E. *J. Am. Chem. Soc.* **1988**, *110*, 1113.

[13] Fowler, P. W.; Cremona, J. E.; Steer, J. I. *Theor. Chim. Acta* **1988**, *73*, 1.

[14] Fowler, P. W.; Manoloupoulus, D. E. *An Atlas of Fullerenes*; Oxford University Press: Oxford, 1995.

[15] Haddon, R. C. *Science* **1993**, *261*, 1545.

[16] Kroto, H. *Nature* **1987**, *329*, 529.

[17] Tan, Y. Z.; Liao, Z. J.; Qian, Z. Z.; Chen, R. T.; Wu, X.; Liang, H.; Han, X.; Zhu, F.; Zhou, S. J.; Zheng, Z.; Lu, X.; Xie, S. Y.; Huang, R. B.; Zheng, L. S. *Nat. Mater.* **2008**, *7*, 790.

[18] Diederich, F.; Whetten, C.; Thilgen, C.; Ettle, R.; Chao, I.; Alvarez, M. M. *Science* **1991**, *254*, 1768.

[19] Kikuchi, K.; Nakahara, N.; Wakabayashi, T.; Suzuki, S.; Shiromaru, H.; Miyake, Y.; Saito, K.; Ikemoto, I.; Kainosho, M.; Achiba, Y. *Nature* **1992**, *357*, 142.

[20] Taylor, R.; Langley, G. J.; Dennis, T. J. S.; Kroto, H. W.; Walton, D. R. M. *J. Chem. Soc., Chem. Commun.* **1992**, 1043.

[21] Shustova, N. B.; Kuvychko, I. K.; Bolskar, R. D.; Seppelt, K.; Strauss, S. H.; Popov, A. A.; Boltalina, O. V. *J. Am. Chem. Soc.* **2006**, *128*, 15793.

[22] Shustova, N. B.; Newell, B. S.; Miller, S. M.; Anderson, O. P.; Bolskar, R. D.; Seppelt, K.; Popov, A. A.; Boltalina, O. V.; Strauss, S. H. *Angew. Chem. Int. Ed.* **2007**, *46*, 4111.

[23] Kareev, I. E.; Popov, A. A.; Kuvychko, I. V.; Shustova, N.; Lebedkin, S. F.; Bubnov, V. P.; Anderson, O. P.; Seppelt, K.; Strauss, S. H.; Boltalina, O. V. *J. Am. Chem. Soc.* **2008**, *130*, 13471.

[24] Simeonov, K. S.; Amsharov, K. Y.; Krokos, E.; Jansen, M. *Angew. Chem. Int. Ed.* **2008**, *47*, 6283.

[25] Simeonov, K. S.; Amsharov, K.; Yu.,; Jansen, M. *Chem. Eur. J.* **2008**, *14*, 9585.

[26] Raghavachari, K.; Rohlfing, C. M. *Chem. Phys. Lett.* **1993**, *208*, 436.

[27] Beavers, C. M.; Chaur, M. N.; Olmstead, M. M.; Echegoyen, L.; Balch, A. L. *J. Am. Chem. Soc.* **2009**, *131*, 11519.

[28] Katritzky, A.; Jug, K.; Oniciu, D. *Chem. Rev.* **2001**, *101*, 1421.

[29] Cyrański, M. K.; Krygowski, T. M.; Katritzky, A.; Schleyer, P. *J. Org. Chem* **2002**, *67*, 1333.

[30] Katritzky, A. R.; Barczynski, P.; Musumarra, G.; Pisano, D.; Szafran, M. *J. Am. Chem. Soc.* **2002**, *111*, 7.

[31] Hirsch, A.; Chen, Z.; Jiao, H. *Angew. Chem. Int. Ed.* **2000**, *39*, 3915.

[32] Krygowski, T. M.; Ciesielski, A. J. *J. Chem. Inf. Comp. Sci.* **1995**, *35*, 1001.

[33] Bühl, M. *Chem. Eur. J.* **1998**, *4*, 734.

[34] Poater, J.; Fradera, X.; Duran, M.; Solà, M. *Chem. Eur. J.* **2002**, *9*, 1113.

[35] Matito, E.; Salvador, P.; Duran, M.; Solà, M. *J. Phys. Chem. A* **2006**, *110*, 5108.

[36] Poater, J.; Duran, M.; Solà, M. *Int. J. Quantum Chem.* **2004**, *98*, 361.

[37] Pradeep, T.; Vijayakrishnan, V.; Santra, A. K.; Rao, C. N. R. *J. Phys. Chem.* **1991**, *85*, 7564.

[38] Branz, W.; Billas, I. M. L.; Malinowski, N.; Tast, F.; Heinebrodt, M.; Martin, T. P. *J. Chem. Phys.* **1998**, *109*, 3425.

[39] Hawkins, J. M.; Meyer, A.; Lewis, T. A.; Loren, S.; Hollander, F. J. *Science* **1991**, *252*, 312.

[40] Heath, J. R.; O'Brien, S. C.; Zhang, Q.; Liu, Y.; Curl, R. F.; Kroto, H. W.; Tittel, F. K.; Smalley, R. E. *J. Am. Chem. Soc.* **1985**, *107*, 7779.

[41] Chai, Y.; Guo, T.; Jin, C.; Haufler, R. E.; Chibante, L. P. F.; Fure, J.; Wang, L.; Alford, J. M.; Smalley, R. E. *J. Phys. Chem.* **2002**, *95*, 7564.

[42] Wang, C. R.; Kai, T.; Tomiyama, T.; Yoshida, T.; Kobayashi, Y.; Nishibori, E.; Takata, M.; Sakata, M.; Shinohara, H. *Angew. Chem. Int. Ed.* **2001**, *40*, 397.

[43] Stevenson, S.; Rice, G.; Glass, T.; Harich, K.; Cromer, F.; Jordan, M. R.; Craft, J.; Hadju, E.; Bible, R.; Olmstead, M. M.; Maitra, K.; Fischer, A. J.; Balch, A. L.; Dorn, H. C. *Nature* **1999**, *401*, 55.

[44] Stevenson, S.; Mackey, M. A.; Stuart, M. A.; Phillips, J. P.; Easterling, M. L.; Chancellor, C. J.; Olmstead, M. M.; Balch, A. L. *J. Am. Chem. Soc.* **2008**, *130*, 11844.

[45] Liu, S.; Suna, S. *J. Organomet. Chem.* **2000**, *599*, 74.

[46] Shinohara, H. *Rep. Prog. Phys.* **2000**, *63*, 843.

[47] Akasaka, T.; Nagase, S. *Endofullerenes: A new Family of Carbon Clusters*; Kluwer Academic Publishers: Dordrecht, 2002.

[48] Chaur, M.; Melin, F.; Ortiz, A. L.; Echegoyen, L. *Angew. Chem. Int. Ed.* **2009**, *48*, 7514.

[49] Wang, T. S.; Chen, N.; Xiang, J. F.; Li, B.; Wu, J. Y.; Xu, W.; Jiang, L.; Tan, K.; Shu, C. Y.; Lu, X.; Wang, C. R. *J. Am. Chem. Soc.* **2009**, *131*, 16646.

[50] Cioslowski, J. *J. Am. Chem. Soc.* **1991**, *113*, 4139.

[51] Saunders, M.; Cross, R. J.; Jiménez-Vázquez, H. A.; Shimshi, R.; Khong, A. *Science* **1996**, *271*, 1693.

[52] Dunsch, L.; Krause, M.; Noack, J.; Georgi, P. *J. Phys. Chem. Solids* **2004**, *65*, 309.

[53] Stevenson, S.; Thompson, M. C.; Coumbe, H. L.; Mackey, M. A.; Coumbe, C. E.; Phillips, J. P. *J. Am. Chem. Soc.* **2007**, *129*, 16257.

[54] Chaur, M. N.; Athans, A. J.; Echegoyen, L. *Tetrahedron* **2008**, *64*, 11387.

[55] Krause, M.; Popov, A.; Dunsch, L. *Chem. Phys. Chem.* **2006**, *7*, 1734.

[56] Campanera, J. M.; Bo, C.; Poblet, J. M. *Angew. Chem. Int. Ed.* **2005**, *44*, 7230.

[57] Olmstead, M. H.; de Bettencourt-Dias, A.; Duchamp, J. C.; Stevenson, S.; Marciu, D.; Dorn, H. C.; Balch, A. L. *Angew. Chem. Int. Ed.* **2001**, *40*, 1223.

[58] Stevenson, S.; Fowler, P. W.; Heine, T.; Duchamp, J. C.; Rice, G.; Glass, T.; Harich, K.; Hajdu, E.; Bible, R.; Dorn, H. C. *Nature* **2000**, *408*, 427.

[59] Olmstead, M. H.; de Bettencourt-Dias, A.; Duchamp, J. C.; Stevenson, S.; Dorn, H. C.; Balch, A. L. *J. Am. Chem. Soc.* **2000**, *122*, 12220.

[60] Stevenson, S.; Lee, H. M.; Olmstead, M. M.; Kozikowski, C.; Stevenson, P.; Balch, A. L. *Chem. Eur. J.* **2002**, *8*, 4528.

[61] Beavers, C. M.; Zuo, T.; Duchamp, J. C.; Harick, K.; Dorn, H. C.; Olmstead, M. M.; Balch, A. L. *J. Am. Chem. Soc.* **2006**, *128*, 11352.

[62] Stevenson, S.; Phillips, J. P.; Reid, J. E.; Olmstead, M. M.; Rath, S. P.; Balch, A. L. *Chem. Commun.* **2004**, 2814.

[63] Yang, S.; Troyanov, S. I.; Popov, A.; Krause, M.; Dunsch, L. *J. Am. Chem. Soc.* **2006**, *128*, 16733.

[64] Echegoyen, L.; Chancellor, C. J.; Cardona, C.; Elliott,; Rivera, J.; Olmstead, M.; Balch, A. L. *Chem. Commun.* **2006**, 2653.

[65] Cao, B.; Wakahara, T.; Tsuchiya, T.; Kondo, M.; Maeda, Y.; Rahman, G. M. A.; Akasaka, T.; Kobayashi, K.; Nagase, S.; Yamamoto, K. *J. Am. Chem. Soc.* **2004**, *126*, 9164.

[66] Cao, B.; Nikawa, H.; Nakahodo, T.; Tsuchiya, T.; Maeda, Y.; Akasaka, T.; Sawa, H.; Slanina, Z.; Mizorogi, N.; Nagase, S. *J. Am. Chem. Soc.* **2007**, *130*, 983.

[67] Yamada, M.; Wakahara, T.; Tsuchiya, T.; Maeda, Y.; Kako, M.; Akasaka, T.; Yoza, K.; Horn, E.; Mizorogi, N.; Nagase, S. *Chem. Commun.* **2008**, 558.

[68] Yumura, T.; Sato, Y.; Suenaga, K.; Iijima, S. *J. Phys. Chem. B* **2005**, *109*, 20251.

[69] Hino, S.; Kato, D.; Yoshimura, D.; Moribe, H.; Umemoto, H.; Ito, Y.; Sugai, T.; Shinohara, H.; Otani, M.; Yoshimoto, Y.; Okada, S. *Phys. Rev. B* **2007**, *75*, 125418.

[70] Popov, A. A.; Dunsch, L. *J. Am. Chem. Soc.* **2007**, *129*, 11835.

[71] Krause, M.; Wong, J.; Dunsch, L. *Chem. Eur. J.* **2005**, *11*, 706.

[72] Popov, A. A.; Krause, M.; Yang, S.; Wong, J.; Dunsch, L. *J. Phys. Chem. B* **2007**, *111*, 3363.

[73] Greenwood, N. N.; Earnshaw, A. *Chemistry of the Elements*; Pergamon: Oxford, U.K, 1984.

[74] Mercado, B. Q.; Beavers, C. M.; Olmstead, M. M.; Chaur, M. N.; Walker, K.; Holloway, B. C.; Echegoyen, L.; Balch, A. L. *J. Am. Chem. Soc.* **2008**, *130*, 7854.

[75] Zuo, T.; Walker, K.; Olmstead, M. M.; Melin, F.; Holloway, B. C.; Echegoyen, L.; Dorn, H. C.; Chaur, M. N.; Chancellor, C. J.; Beavers, C. M.; Balch, A. L.; Athans, A. J. *Chem. Commun.* **2008**, 1067.

[76] Wakahara, T.; Nikawa, H.; Kikuchi, T.; Nakahodo, T.; Rahman, G. M. A.; Tsuchiya, T.; Maeda, Y.; Akasaka, T.; Yoza, K.; Horn, E.; Yamamoto, K.; Mizorogi, N.; Slanina, Z.; Nagase, *J. Am. Chem. Soc.* **2006**, *128*, 14228.

[77] Kato, H.; Taninaka, A.; Sugai, T.; Shinohara, H. *J. Am. Chem. Soc.* **2003**, *125*, 7782.

[78] Lu, X.; Nikawa, H.; Nakahodo, T.; Tsuchiya, T.; Ishitsuka, M. O.; Maeda, Y.; Akasaka, T.; Toki, M.; Sawa, H.; Slanina, Z.; Mizorogi, N.; Nagase, *J. Am. Chem. Soc.* **2008**, *130*, 9129.

[79] Lu, X.; Nikawa, H.; Tsuchiya, T.; Maeda, Y.; Ishitsuka, M. O.; Akasaka, T.; Toki, M.; Sawa, H.; Slanina, Z.; Mizorogi, N.; Nagase, S. *Angew. Chem., Int. Ed.* **2008**, *47*, 8642.

[80] Yang, S.; Popov, A. A.; Dunsch, L. *J. Phys. Chem. B* **2007**, *111*, 13659.

[81] Wang, C.-R.; Kai, T.; Tomiyama, T.; Yoshida, T.; Kobayashi, Y.; Nishibori, E.; Takata, M.; Sakata, M.; Shinohara, H. *Nature* **2000**, *408*, 426.

[82] Yang, S.; Popov, A. A.; Dunsch, L. *Angew. Chem. Int. Ed.* **2007**, *46*, 1256.

[83] Olmstead, M. M.; Lee, H. M.; Duchamp, J. C.; Stevenson, S.; Marciu, D.; Dorn, H. C.; Balch, A. L. *Angew. Chem. Int. Ed.* **2003**, *42*, 900.

[84] Shi, Z. Q.; Wu, X.; Wang, C. R.; Lu, X.; Shinohara, H. *Angew. Chem. Int. Ed.* **2006**, *45*, 2107.

[85] Park, S. S.; Liu, D.; Hagelberg, F. *J. Phys. Chem. A* **2005**, *109*, 8865.

[86] Bendjaballah, S.; Kahal, S.; Costuas, K.; Bévillon, E.; Saillard, J. Y. *Chem. Eur. J.* **2006**, *12*, 2048.

[87] Summerscales, O. T.; Cloke, F. G. N. *Coord. Chem. Rev.* **2006**, *250*, 1120.

[88] Cardona, C. M.; Kitaygorodskiy, A.; Echegoyen, L. *J. Am. Chem. Soc.* **2005**, *127*, 10448.

[89] Aihara, J. *J. Am. Chem. Soc.* **1995**, *117*, 4130.

[90] Agnoli, A. L.; Jungmann, D.; Lochner, B. *Neurosurg. Rev.* **1987**, *10*, 25.

[91] Harisinghani, M. G.; Jhaveri, K. S.; Weissleder, R.; Schima, W.; Saini, S.; Hahn, P. F.; Mueller, P. R. *Clinical Radiology* **2001**, *56*, 714.

[92] Mikawa, M.; Kato, H.; Okumura, M.; Narazaki, M.; Kanazawa, Y.; Miwa, N.; Shinohara, H. *Bioconjugate Chem.* **2001**, *12*, 510.

[93] Wolf, M.; Müller, K. H.; Skourski, Y.; Eckert, D.; Georgi, P.; Krause, M.; Dunsch, L. *Angew. Chem. Int. Ed.* **2005**, *44*, 3306.

[94] Wu, J.; Hagelberg, F. *J. Phys. Chem. C* **2008**, *112*, 5770.

[95] Lu, X.; Zhang, L. L.; Xu, X.; Wang, N. Q.; Zhang, Q. N. *J. Phys. Chem. B* **2002**, *106*, 2136.

[96] Fatouros, P. P.; Corwin, F. D.; Chen, Z.; Broaddus, W. C.; Tatum, J. L.; Kettenmann, B.; Ge, Z.; Gibson, H.; Russ, J. L.; Leonard, A. P.; Duchamp, J. C.; Dorn, H. C. *Radiology* **2006**, *240*, 756.

[97] Wilson, L. J.; Cagle, D. W.; Thrash, T. P.; Kennel, S. J.; Mirzadeh, S.; Alford, J. M.; Ehrardt, G. J. *Coord. Chem. Rev.* **1999**, *190*, 199.

[98] Schinazi, R. F.; Sijbesma, R.; Srdanov, G.; Hill, C. L.; Wudl, F. *Antimicrob. Agents Chemother.* **1993**, *37*, 1707.

[99] Moussa, F.; Trivin, F.; Céolin, R.; Hadchouel, M.; Sizaret, P. Y.; Geugny, V.; Fabre, C.; Rassat, A.; Szwarc, H. *Fullerene Sci. Technol.* **1996**, *4*, 21.

[100] Kobayashi, K.; Kuwano, M.; Sueki, K.; Kikuchi, K.; Achiba, Y.; Nakahara, H.; Kananishi, N.; Wanatanabe, M.; Tomura, K. *J. Radioanal. Nucl. Chem.* **1995**, *192*, 81.

[101] Caldwell, K. A.; Giblin, D. E.; Gross, M. L. *J. Am. Chem. Soc.* **1992**, *114*, 3743.

[102] DiCamillo, B. A.; Hettich, R. L.; Guiochon, G.; Compton, R. N.; Saunders, M.; Jiménez-Vázquez, H. A.; Khong, A.; Cross, J. *J. Phys. Chem.* **1996**, *100*, 9197.

[103] Yamamoto, K.; Saunders, M.; Khong, A.; Cross Jr, R. J.; Grayson, M.; Gross, M. L.; Benedetto, A. F.; Weisman, R. B. *J. Am. Chem. Soc.* **1999**, *121*, 1591.

[104] Cross, R. J.; Khong, A.; Saunders, M. *J. Org. Chem.* **2003**, *68*, 8281.

[105] Saunders, M.; Jiménez-Vázquez, H. A.; Cross, R. J.; Poreda, R. J. *Science* **1993**, *259*, 1428.

[106] Saunders, M.; Jiménez-Vázquez, H. A.; Cross, R. J.; Mroczkowski, S.; Gross, M. L.; Giblin, D. E.; Poreda, R. J. *J. Am. Chem. Soc.* **1994**, *116*, 2193.

[107] Becker, L.; Poreda, R. J.; Bada, J. L. *Science* **1996**, *272*, 249.

[108] Shimshi, R.; Khong, A.; Jiménez-Vázquez, H. A.; Cross, R. J.; Saunders, M. *Tetrahedron* **1996**, *52*, 5143.

[109] Jiménez-Vázquez, H. A.; Cross, R. J. *J. Chem. Phys.* **1996**, *104*, 5589.

[110] Murry, R. L.; Scuseria, G. E. *Science* **1994**, *263*, 791.

[111] Rubin, Y. *Chem. Eur. J.* **1997**, *3*, 1009.

[112] Murata, M.; Murata, Y.; Komatsu, K. *Chem. Commun.* **2008**, 6083.

[113] Stanisky, C. M.; Cross, R. J.; Saunders, M.; Murata, M.; Murata, Y.; Komatsu, K. *J. Am. Chem. Soc.* **2005**, *127*, 299.

[114] Whitener, K. E.; Frunzi, M.; Iwamatsu, S.-i.; Murata, S.; Cross, R. J.; Saunders, M. *J. Am. Chem. Soc.* **2008**, *130*, 13996.

[115] Murata, M.; Murata, Y.; Komatsu, K. *J. Am. Chem. Soc.* **2006**, *128*, 8024.

[116] Iwamatsu, S.-i.; Uozaki, T.; Kobayashi, K.; Re, S.; Nagase, S.; Murata, S. *J. Am. Chem. Soc.* **2004**, *126*, 2668.

[117] Iwamatsu, S.-i.; Stanisky, C. M.; Cross, R. J.; Saunders, M.; Mizorogi, N.; Nagase, S.; Murata, S. *Angew. Chem. Int. Ed.* **2006**, *45*, 5337.

[118] Murata, M.; Maeda, S.; Morinaka, Y.; Murata, Y.; Komatsu, K. *J. Am. Chem. Soc.* **2008**, *130*, 15800.

[119] Son, M.-S.; Sung, Y. K. *Chem. Phys. Lett.* **1995**, *245*, 113.

[120] Albert, V. V.; Sabin, J. R.; Harris, F. E. *Int. J. Quantum Chem.* **2007**, *107*, 3061.

[121] Yan, H.; Yu, S.; Wang, X.; He, Y.; Huang, W.; Yang, M. *Chem. Phys. Lett.* **2008**, *456*, 223.

[122] Giblin, D. E.; Gross, M. L.; Saunders, M.; Jiménez-Vázquez, H.; Cross, R. J. *J. Am. Chem. Soc.* **1997**, *119*, 9883.

[123] Khong, A.; Jiménez-Vázquez, H. A.; Saunders, M.; Cross, R. J.; Laskin, J.; Peres, T.; Lifshitz, C.; Strongin, R.; Smith, A. B. *J. Am. Chem. Soc.* **1998**, *120*, 6380.

[124] Laskin, J.; Peres, T.; Lifshitz, C.; Saunders, M.; Cross, R. J.; Khong, A. *Chem. Phys. Lett.* **1998**, *285*, 7.

[125] Sternfeld, T.; Hoffman, R. E.; Saunders, M.; Cross, R. J.; Syamala, M. S.; Rabinovitz, M. *J. Am. Chem. Soc.* **2002**, *124*, 8786.

[126] Peres, T.; Cao, B.; Cui, W.; Khong, A.; Cross, R. J.; Saunders, M.; Lifshitz, C. *Int. J. Mass. Spectrom.* **2001**, *210*, 241.

[127] Darzynkiewicz, R. B.; Scuseria, G. E. *J. Phys. Chem. A* **1997**, *101*, 7141.

[128] Lee, T. B.; McKee, M. L. *J. Am. Chem. Soc.* **2008**, *130*, 17610.

[129] Peng, R. F.; Chu, S. J.; Huang, Y. M.; Yu, H. J.; Wang, T. S.; Jin, B.; Fu, Y. B.; Wang, C. R. *J. Mater. Chem.* **2009**, *19*, 3602.

[130] Krapp, A.; Frenking, G. *Chem. Eur. J.* **2007**, *13*, 8256.

[131] Giese, T. J.; York, D. M. *Int. J. Quantum Chem.* **2004**, *98*, 388.

[132] Slavicek, P.; Kalus, R.; Paska, P.; Odvarkova, I.; Hobza, P.; Malijevsky, A. *J. Chem. Phys.* **2003**, *119*, 2102.

[133] Ogilvie, J. F.; Wang, F. Y. *J. Mol. Struct. (Theochem)* **1992**, *273*, 277.

[134] Diederich, F.; Thilgen, C. *Science* **1996**, *271*, 317.

[135] Saunders, M.; Jimenez-Vazquez, H. A.; Bangerter, B. W.; Cross, R. J.; Mroczkowski, S.; Freedberg, D. I.; Anet, F. A. L. *J. Am. Chem. Soc.* **2002**, *116*, 3621.

[136] Becker, L.; Poreda, R. J.; Bunch, T. E. *Proc. Nat. Acad. Sci.* **2000**, *97*, 2979.

[137] Hirsch, A.; Brettreich, M. *Fullerenes: Chemistry and Reactions*; WILEY-VCH Verlag GmbH and Co. KGaA: Weinheim, 2004.

[138] Hirsch, A. *Synthesis* **1995**, 895.

[139] Diels, O.; Alder, K. *Ann.* **1928**, *460*, 98.

[140] Matito, E.; Poater, J.; Duran, M.; Solà, M. *J. Mol. Struct. (Theochem)* **2005**, *727*, 165.

[141] Smith, L. I. *Chem. Rev.* **1938**, *23*, 193.

[142] Huisgen, R. *Proc. Chem. Soc.* **1961**, 357.

[143] Huisgen, R. *Angew. Chem. Int. Ed. Engl.* **1963**, *2*, 633.

[144] Huisgen, R. *Angew. Chem. Int. Ed. Engl.* **1963**, *2*, 565.

[145] Woodward, R. B.; Hoffmann, R. *Angew. Chem. Int. Ed. Engl.* **1969**, *8*, 781.

[146] Carey, F.; Sundberg, R. J. *Advanced Organic Chemistry, Part B: Reactions and Synthesis*; Plenum Publishers: New York, 2001.

[147] Clayden, J.; Greeves, N.; Warren, S.; Wothers, P. *Organic chemistry*; Oxford University Press: New York, 2001.

[148] Firestone, R. A. *J. Org. Chem.* **1968**, *33*, 2285.

[149] Houk, K. N. *Acc. Chem. Res.* **1975**, *8*, 361.

[150] Houk, K. N.; Gonzalez, J.; Li, Y. *Acc. Chem. Res.* **1995**, *28*, 81.

[151] Houk, K. N.; Firestone, R. A.; Munchausen, L. L.; Mueller, P. H.; Arison, B. H.; Garcia, L. A. *J. Am. Chem. Soc.* **1985**, *107*, 7227.

[152] Houk, K. N.; Sims, J.; Duke, R. E.; Strozier, R. W.; George, J. K. *J. Am. Chem. Soc.* **1973**, *95*, 7287.

[153] Houk, K. N.; Sims, J.; Watts, C. R.; Luskus, L. J. *J. Am. Chem. Soc.* **1973**, *95*, 7301.

[154] Huisgen, R. *Angew. Chem. Int. Ed. Engl.* **1968**, *7*, 321.

[155] Huisgen, R. *J. Org. Chem.* **1968**, *33*, 2291.

[156] Huisgen, R.; Mloston, G.; Langhals, E. *J. Am. Chem. Soc.* **1986**, *108*, 6401.

[157] Huisgen, R.; Mloston, G.; Langhals, E. *J. Org. Chem.* **1986**, *51*, 4085.

[158] Pascal, Y. L.; Chanetray, J.; Vessiere, R.; Zeroual, A. *Tetrahedron* **1992**, *48*, 7197.

[159] Sustmann, R.; Trill, H. *Angew. Chem. Int. Ed. Engl.* **1972**, *11*, 838.

[160] Hiberty, P. C.; Ohanessian, G.; Schlegel, H. B. *J. Am. Chem. Soc.* **1983**, *105*, 719.

[161] McDouall, J. J. W.; Robb, M. A.; Niazi, U.; Bernardi, F.; Schlegel, H. B. *J. Am. Chem. Soc.* **1987**, *109*, 4642.

[162] Su, M. D.; Liao, H. L.; Chung, W. S.; Chu, S. Y. *J. Org. Chem.* **1999**, *64*, 6710.

[163] Nguyen, J. T.; Chandra, A. K.; Sakai, S.; Morokuma, K. *J. Org. Chem.* **1999**, *64*, 65.

[164] Fukui, K. *Acc. Chem. Res.* **1971**, *4*, 57.

[165] Fukui, K. *Angew. Chem. Int. Ed. Engl.* **1982**, *21*, 801.

[166] Salem, L. *J. Am. Chem. Soc.* **1968**, *90*, 543.

[167] Salem, L. *J. Am. Chem. Soc.* **1968**, *90*, 553.

[168] Sustmann, R. *Tetrahedron Lett.* **1971**, *29*, 2717.

[169] Biermann, D.; Schimdt, W. *J. Am. Chem. Soc.* **1980**, *102*, 3163.

[170] Evans, M. G.; Polanyi, M. *Trans. Faraday Soc.* **1938**, *34*, 0011.

[171] Koeppl, G. W.; Kresge, A. J. *J. Chem. Soc. Chem. Commun.* **1973**, 371.

[172] Marcus, R. A. *Pure Appl. Chem.* **1997**, *69*, 13.

[173] Ess, D. H.; Houk, K. N. *J. Am. Chem. Soc.* **2007**, *129*, 10646.

[174] Ess, D. H.; Houk, K. N. *J. Am. Chem. Soc.* **2008**, *130*, 10187.

[175] Dimroth, O. *Angew. Chem.* **1933**, *46*, 571.

[176] Guthrie, J. P. *Chem. Phys. Chem.* **2003**, *4*, 809.

[177] Strozier, R. W.; Caramella, P.; Houk, K. N. *J. Am. Chem. Soc.* **1979**, *101*, 1340.

[178] Ziegler, T.; Rauk, A. *Theor. Chim. Acta* **1977**, *46*, 1.

[179] Morokuma, K. *J. Chem. Phys.* **1971**, *55*, 1236.

[180] Diefenbach, A.; Bickelhaupt, F. M. *J. Phys. Chem. A* **2004**, *108*, 8460.

[181] Hayden, A.; Houk, K. N. *J. Am. Chem. Soc.* **2009**, *131*, 4084.

[182] Domingo, L. R.; Sáez, J. A. *Org. Biomol. Chem.* **2009**, *7*, 3576.

[183] Xu, L.; Doubleday, C. E.; Houk, K. N. *Angew. Chem. Int. Ed.* **2009**, *48*, 2746.

[184] Filippone, S.; Barroso, M. I.; Martín-Domenech, A.; Osuna, S.; Solà, M.; Martín, N. *Chem. Eur. J.* **2008**, *14*, 5198.

[185] Holzinger, M.; Vostrowsky, O.; Hirsch, A.; Hennrich, F.; Kappes, M.; Weiss, R.; Jellen, F. *Angew. Chem. Int. Ed.* **2001**, *40*, 4002.

[186] Maggini, M.; Scorrano, G.; Prato, M. *J. Am. Chem. Soc.* **1993**, *115*, 9798.

[187] Prato, M.; Maggini, M. *Acc. Chem. Res.* **1998**, *31*, 519.

[188] Tagmatarchis, N.; Prato, M. *J. Mater. Chem.* **2004**, *14*, 437.

[189] Collman, J. P.; Devaraj, N. K.; Chidsey, C. E. D. *Langmuir* **2004**, *20*, 1051.

[190] Speers, A. E.; Adam, G. C.; Cravatt, B. F. *J. Am. Chem. Soc.* **2003**, *125*, 4686.

[191] Seo, T. S.; Bai, X. P.; Ruparel, H.; Li, Z. M.; Turro, N. J.; Ju, J. Y. *Proc. Natl. Acad. Sci. USA* **2004**, *101*, 5488.

[192] Krasinski, A.; Radic, Z.; Manetsch, R.; Raushel, J.; Taylor, P.; Sharpless, K. B.; Kolb, H. C. *J. Am. Chem. Soc.* **2005**, *127*, 6686.

[193] Wu, W.; Wieckowski, S.; Pastorin, G.; Benincasa, M.; Klumpp, C.; Briand, J. P.; Gennaro, R.; Prato, M.; Bianco, A. *Angew. Chem. Int. Ed.* **2005**, *44*, 6358.

[194] Cases, M.; Duran, M.; Mestres, J.; Martín, N.; Solà, M. The reactivity of the [5,6]-bond in cycloadditions to fullerenes. In *Fullerenes for the New Millennium*; Kamat, P. V., Guldi, D. M., Kadish, K. M., Eds.; 2001; Vol. 2000, p 244.

[195] Prato, M.; Lucchini, V.; Maggini, M.; Stimpfl, E.; Scorrano, G.; Eiermann, M.; Suzuki, T.; Wudl, F. *J. Am. Chem. Soc.* **1993**, *115*, 8479.

[196] Giovane, L. M.; Barco, J. W.; Yadav, T.; Lafleur, A. L.; Marr, J. A.; Howard, J. B.; Rotello, V. M. *J. Phys. Chem.* **1993**, *97*, 8560.

[197] Rotello, V. M.; Howard, J. B.; Yadav, T.; Conn, M. M.; Viani, E.; Giovane, L. M.; Lafleur, A. L. *Tetrahedron Lett.* **1993**, *34*, 1561.

[198] Pang, L. S. K.; Wilson, M. A. *J. Phys. Chem.* **1993**, *97*, 6761.

[199] Sarova, G. H.; Berberan-Santos, M. N. *Chem. Phys. Lett.* **2004**, *397*, 402.

[200] Tsuda, T.; Ishida, T.; Nogami, T.; Kurono, S.; Ohashi, M. *J. Chem. Soc., Chem. Commun.* **1993**, 1296.

[201] Rubin, Y.; Khan, S.; Freedberg, D. I.; Yeretzian, C. *J. Am. Chem. Soc.* **1993**, *115*, 344.

[202] Kräutler, B.; Maynollo, J. *Angew. Chem. Int. Ed. Engl.* **1995**, *34*, 87.

[203] Kräutler, B.; Puchberger, M. *Helv. Chim. Acta* **1993**, *76*, 1626.

[204] Kräutler, B.; Maynollo, J. *Tetrahedron* **1996**, *52*, 5033.

[205] Meidine, M. F.; Roers, R.; Langley, G. J.; Avent, A. G.; Darwish, A. D.; Firth, S.; Kroto, H. W.; Taylor, R.; Walton, D. R. M. *J. Chem. Soc. Chem. Commun.* **1995**, 1342.

[206] Ohkita, M.; Ishigami, K.; Tsuji, T. *J. Chem. Soc., Chem. Commun.* **1995**, 1769.

[207] Ohno, M.; Kojima, S.; Eguchi, S. *J. Chem. Soc., Chem. Commun.* **1995**, 565.

[208] Meidine, M. F.; Roers, R.; Langley, G. J.; Avent, A. G.; Darwish, A. D.; Firth, S.; Kroto, H. W.; Taylor, R.; Walton, D. R. M. *J. Chem. Soc., Chem. Commun.* **1993**, 1342.

[209] Krautler, B.; Maynollo, J. *Angew. Chem. Int. Ed. Engl.* **1995**, *34*, 87.

[210] Krautler, B.; Muller, T.; Maynollo, J.; Gruber, K.; Kratky, C.; Ochsenbein, P.; Schwarzenbach, D.; Burgi, H. B. *Angew. Chem. Int. Ed. Engl.* **1996**, *35*, 1204.

[211] Hirsch, A.; Lamparth, I.; Grosser, T.; Karfunkel, H. R. *J. Am. Chem. Soc.* **1994**, *116*, 9385.

[212] Lamparth, I.; Maichlemossmer, C.; Hirsch, A. *Angew. Chem. Int. Ed. Engl.* **1995**, *34*, 1607.

[213] Hirsch, A.; Lamparth, I.; Karfunkel, H. R. *Angew. Chem. Int. Ed. Engl.* **1994**, *33*, 437.

[214] Belik, P.; Gügel, A.; Spickermann, J.; Müllen, K. *Angew. Chem. Int. Ed. Engl.* **1993**, *32*, 78.

[215] Gügel, A.; Kraus, A.; Spickermann, J.; Belik, P.; Müllen, K. *Angew. Chem. Int. Ed. Engl.* **1994**, *33*, 559.

[216] Filippone, S.; Barroso, M. I.; Martín-Domenech, A.; Osuna, S.; Solà, M.; Martín, N. *Chem. Eur. J.* **2008**, *14*, 5198.

[217] Lukoyanova, O.; Cardona, C. M.; Altable, M.; Filippone, S.; Domenech, A. M.; Martín, N.; Echegoyen, L. *Angew. Chem. Int. Ed.* **2006**, *45*, 7430.

[218] Martín, N.; Altable, M.; Filippone, S.; Martín-Domenech, A.; Echegoyen, L.; Cardona, C. M. *Angew. Chem. Int. Ed.* **2006**, *45*, 110.

[219] Martín, N.; Altable, M.; Filippone, S.; Martín-Domenech, A.; Martínez-Álvarez, R.; Suárez, M.; Plonska-Brzezinska, M. E.; Lukoyanova, O.; Echegoyen, L. *J. Org. Chem.* **2007**, *72*, 3840.

[220] Maggini, M.; Scorrano, G.; Prato, M. *J. Am. Chem. Soc.* **1993**, *115*, 9798.

[221] Yurovskaya, M. A.; Ovcharenko, A. A. *Chem. Heterocycl. Compd.* **1998**, 291.

[222] Illescas, B. M.; Martín, N. *J. Org. Chem.* **2000**, *65*, 5986.

[223] Illescas, B. M.; Rife, J.; Ortuño, R. M.; Martín, N. *J. Org. Chem.* **2000**, *65*, 6246.

[224] Meier, M. S.; Poplawska, M. *J. Org. Chem.* **1993**, *58*, 4524.

[225] Meier, M. S.; Poplawska, M. *Tetrahedron* **1996**, *52*, 5043.

[226] Brizzolara, D.; Ahlemann, J. T.; Roesky, H. W.; Keller, K. *Bull. Soc. Chim. Fr.* **1993**, *130*, 745.

[227] Ishida, H.; Ohno, M. *Tetrahedron Lett.* **1999**, *40*, 1543.

[228] Ishida, H.; Itoh, K.; Ohno, M. *Tetrahedron* **2001**, *57*, 1737.

[229] Jagerovic, N.; Elguero, J.; Aubagnac, J. L. *J. Chem. Soc., Perkin Trans. 1* **1996**, 499.

[230] Averdung, J.; Albrecht, E.; Lauterwein, J.; Luftmann, H.; Mattay, J.; Mohn, H.; Müller, W. H.; Termeer, H. U. *Chem. Ber.* **1994**, *127*, 787.

[231] Averdung, J.; Mattay, J. *Tetrahedron* **1996**, *52*, 5407.

[232] Tsunenishi, Y.; Ishida, H.; Itoh, K.; Ohno, M. *Synlett* **2000**, 1318.

[233] Kavitha, K.; Manoharan, M.; Venuvanalingam, P. *J. Org. Chem.* **2005**, *70*, 2528.

[234] Álvarez, A.; Ochoa, E.; Verdecia, Y.; Suárez, M.; Solà, M.; Martín, N. *J. Org. Chem.* **2005**, *70*, 3256.

[235] Cases, M.; Duran, M.; Mestres, J.; Martín, N.; Solà, M. *J. Org. Chem.* **2001**, *66*, 433.

[236] Zhuang, X. X.; Yang, Z. Y.; Zhang, J. C.; Cao, W. L. *J. Mol. Struct. (Theochem)* **2006**, *760*, 45.

[237] Iezzi, E. B.; Duchamp, J. C.; Harich, K.; Glass, T. E.; Lee, H. M.; Olmstead, M. M.; Bach, A. L.; Dorn, H. C. *J. Am. Chem. Soc.* **2002**, *124*, 524.

[238] Lee, H. M.; Olmstead, M. M.; Iezzi, E.; Duchamp, J. C.; Dorn, H. C.; Balch, A. L. *J. Am. Chem. Soc.* **2002**, *124*, 3494.

[239] Campanera, J. M.; Bo, C.; Poblet, J. M. *J. Org. Chem.* **2006**, *71*, 46.

[240] Mayer, I. *Chem. Phys. Lett.* **1983**, *97*, 270.

[241] Haddon, R. C.; Chow, S. Y. *J. Am. Chem. Soc.* **1998**, *120*, 10494.

[242] Haddon, R. C. *J. Phys. Chem. A* **2001**, *105*, 4164.

[243] Cardona, C. M.; Kitaygorodskiy, A.; Ortiz, A.; Herranz, M. A.; Echegoyen, L. *J. Org. Chem.* **2005**, *70*, 5092.

[244] Lu, X.; Nikawa, H.; Feng, L.; Tsuchiya, T.; Maeda, Y.; Akasaka, T.; Mizorogi, N.; Slanina, Z.; Nagase, S. *J. Am. Chem. Soc.* **2009**, *131*, 12066.

[245] Yamada, M.; Okamura, M.; Sato, S.; Someya, C. I.; Mizorogi, N.; Tsuchiya, T.; Akasaka, T.; Kato, T.; Nagase, S. *Chem. Eur. J.* **2009**, *15*, 10533.

[246] Cardona, C. M.; Elliott, B.; Echegoyen, L. *J. Am. Chem. Soc.* **2006**, *128*, 6480.

[247] Rodríguez-Fortea, A.; Campanera, J.; Cardona, C.; Echegoyen, L.; Poblet, J. *Angew. Chem. Int. Ed.* **2006**, *45*, 8176.

[248] Chen, N.; Fan, L. Z.; Tan, K.; Wu, Y. Q.; Shu, C. Y.; Lu, X.; Wang, C. R. *J. Phys. Chem. C* **2007**, *111*, 11823.

[249] Cai, T.; Xu, L. S.; Anderson, M. R.; Ge, Z. X.; Zuo, T. M.; Wang, X. L.; Olmstead, M. M.; Balch, A. L.; Gibson, H. W.; Dorn, H. C. *J. Am. Chem. Soc.* **2006**, *128*, 8581.

[250] Cai, T.; Slebodnick, C.; Xu, L.; Harich, K.; Glass, T. E.; Chancellor, C.; Fettinger, J. C.; Olmstead, M. M.; Balch, A. L.; Gibson, H. W.; Dorn, H. C. *J. Am. Chem. Soc.* **2006**, *128*, 6486.

[251] Stevenson, S.; Stephen, R. R.; Amos, T. M.; Cadorette, V. R.; Reid, J. E.; Phillips, J. P. *J. Am. Chem. Soc.* **2005**, *127*, 12776.

[252] Cai, T.; Ge, Z. X.; Iezzi, E. B.; Glass, T. E.; Harich, K.; Gibson, H. W.; Dorn, H. C. *Chem. Comunn.* **2005**, 3594.

[253] Chen, N.; Zhang, E. Y.; Tan, K.; Wang, C. R.; Lu, X. *Org. Lett.* **2007**, *9*, 2011.

[254] Chaur, M. N.; Melin, F.; Athans, A. J.; Elliott, B.; Walker, B. C., K. Holloway; Echegoyen, L. *Chem. Commun.* **2008**, 2665.

[255] Cai, T.; Xu, L.; Gibson, H.; Dorn, H.; Chancellor, C.; Olmstead, M.; Balch, A. *J. Am. Chem. Soc.* **2007**, *129*, 10795.

[256] Cai, T.; Xu, L.; Shu, C.; Champion, H. A.; Reid, J.; Anklin, C.; Anderson, M. R.; Gibson, H. W.; Dorn, H. C. *J. Am. Chem. Soc.* **2008**, *130*, 2136.

[257] Frunzi, M.; Cross, R. J.; Saunders, M. *J. Am. Chem. Soc.* **2007**, *129*, 13343.

[258] Frunzi, M.; Xu, H.; Cross, R. J.; Saunders, M. *J. Phys. Chem. A* **2009**, *113*, 4996.

[259] Georgakilas, V.; Bourlinos, A.; Gournis, D.; Tsoufis, T.; Trapalis, C.; Mateo-Alonso, A.; Prato, M. *J. Am. Chem. Soc.* **2008**, *130*, 8733.

[260] Georgakilas, V.; Kordatos, K.; Prato, M.; Guldi, D. M.; Holzinger, M.; Hirsch, A. *J. Am. Chem. Soc.* **2002**, *124*, 760.

[261] Li, J.; Grennberg, H. *Chem. Eur. J.* **2006**, *12*, 3869.

[262] Tasis, D.; Tagmatarchis, N.; Bianco, A.; Prato, M. *Chem. Rev.* **2006**, *106*, 1105.

[263] Tasis, D.; Tagmatarchis, N.; Georgakilas, V.; Prato, M. *Chem. Eur. J.* **2003**, *9*, 4001.

[264] Araujo, R.; Fernandes, F. M.; Proenca, M. F.; Silva, C. J. R.; Paiva, M. C. *J. Nanosci. Nanotech.* **2007**, *7*, 3441.

[265] Tagmatarchis, N.; Maigne, A.; Yudasaka, M.; Iijima, S. *Small* **2006**, *2*, 490.

[266] Georgakilas, V.; Guldi, D. M.; Signorini, R.; Bozio, R.; Prato, M. *J. Am. Chem. Soc.* **2003**, *125*, 14268.

[267] Rettenbacher, A. S.; Elliott, B.; Hudson, J. S.; Amirkhanian, A.; Echegoyen, L. *Chem. Eur. J.* **2006**, *12*, 376.

[268] Cassell, A. M.; Asplund, C. L.; Tour, J. M. *Angew. Chem. Int. Ed. Engl.* **1999**, *38*, 2403.

[269] Tagmatarchis, N.; Prato, M. *J. Mater. Chem.* **2004**, *14*, 437.

[270] Alvaro, M.; Atienzar, P.; de la Cruz, P.; Delgado, J. L.; Garcia, H.; Langa, F. *J. Phys. Chem. B* **2004**, *108*, 12691.

[271] Delgado, J. L.; de la Cruz, P.; Langa, F.; Urbina, A.; Casado, J.; Lopez Navarrete, J. T. *Chem. Commun.* **2004**, 1734.

[272] Lu, X.; Tian, F.; Xu, X.; Wang, N. Q.; Zhang, Q. *J. Am. Chem. Soc.* **2003**, *125*, 10459.

[273] Brunetti, F. G.; Herrero, M. A.; Munoz, J. M.; Giordani, S.; Diaz-Ortiz, A.; Filippone, S.; Ruaro, G.; Meneghetti, M.; Prato, M.; Vazquez, E. *J. Am. Chem. Soc.* **2007**, *129*, 14580.

[274] Sayre, L. M.; Perry, G.; Smith, M. A. *Chem. Res. Toxicol.* **2008**, *21*, 172.

[275] Dib, M.; Garrel, C.; Favier, A.; Robin, V.; Desnuelle, C. *J. Neurol.* **2002**, *249*, 367.

[276] Krusic, P. J.; Wasserman, E.; Keizer, P. N.; Morton, J. R.; Preston, K. F. *Science* **1991**, *254*, 1183.

[277] Morton, J. R.; Preston, K. F.; Krusic, P. J.; Hill, A. S.; Wasserman, E. *J. Phys. Chem.* **1992**, *96*, 3576.

[278] Morton, J. R.; Negri, F.; Preston, K. F. *Acc. Chem. Res.* **1998**, *31*, 63.

[279] Morton, J. R.; Preston, K. F.; Krusic, P. J.; Hill, A. S.; Wasserman, E. *J. Am. Chem. Soc.* **1992**, *114*, 5454.

[280] Morton, J. R.; Preston, K. F.; Krusic, P. J.; Hill, A. S.; Wasserman, E. *J. Chem. Soc., Perkin Trans. 2* **1992**, 1425.

[281] Krusic, P. J.; Roe, D. C.; Johnston, E.; Morton, J. R.; Preston, *J. Phys. Chem.* **1993**, *97*, 1736.

[282] Borghi, R.; Lunazzi, L.; Placucci, G.; Krusic, P. J.; Dixon, D. A.; Matsuzawa, N.; Ata, M. *J. Am. Chem. Soc.* **1996**, *118*, 7608.

[283] Ford, W. T.; Nishioka, T.; Qiu, F.; D'Souza, F.; Choi, J. P.; Kutner, W.; Noworyta, K. *J. Org. Chem.* **1999**, *64*, 6257.

[284] Ford, W. T.; Nishioka, T.; Qiu, F.; D'Souza, F.; Choi, *J. Org. Chem.* **2000**, *65*, 5780.

[285] Yoshida, M.; Suzuki, D.; Iyoda, M. *Chem. Lett.* **1996**, 1097.

[286] Yoshida, M. S. F.; Uchiyama, N.; Yamada, T.; Iyoda, M. *Tetrahedron Lett.* **1999**, *40*, 735.

[287] Cremonini, M. A.; Lunazzi, L.; Placucci, G.; Krusic, P. J. *J. Org. Chem.* **1993**, *58*, 4735.

[288] Borghi, R.; Guidi, B.; Lunazzi, L.; Placucci, G. *J. Org. Chem.* **1996**, *61*, 5667.

[289] Borghi, R.; Lunazzi, L.; Placucci, G.; Cerioni, G.; Plumitalio, A. *J. Org. Chem.* **1996**, *61*, 3327.

[290] Krusic, P. J.; Wasserman, E.; Parkinson, B. A.; Malone, B.; Holler, E. R.; Keizer, P. N.; Morton, J. R.; Preston, K. F. *J. Am. Chem. Soc.* **1991**, *113*, 6274.

[291] Hirsch, A.; Lamparth, I.; Karfunkel, H. R. *Angew. Chem. Int. Ed. Engl.* **1994**, *33*, 437.

[292] Dugan, L. L.; Lovett, E. G.; Quick, K. L.; Lotharius, J.; Lin, T. T.; O'Malley, K. L. *Parkinsonism Relat. Disord.* **2001**, *7*, 243.

[293] Ali, S. S.; Hardt, J. I.; Quick, K. L.; Kim-Han, J. S.; Erlanger, B. F.; Huang, T. T.; Epstein, C. J.; Dugan, L. L. *Free Radical Biol. Med.* **2004**, *37*, 1191.

[294] Liu, G. F.; Filipovic, M.; Ivanovic-Burmazovic, I.; Beuerle, F.; Witte, P.; Hirsch, A. *Angew. Chem. Int. Ed.* **2008**, *47*, 3991.

[295] Witte, P.; Beuerle, F.; Hartnagel, U.; Lebovitz, R.; Savouchkina, A.; Sali, S.; Guldi, D.; Chronakis, N.; Hirsch, A. *Org. Biomol. Chem.* **2007**, *5*, 3599.

[296] Yin, J.; Lao, F.; Fu, P. P.; Wamer, W. G.; Zhao, Y.; Wang, P. C.; Qiu, Y.; Sun, B.; Xing, G.; Dong, J.; Liang, X. J.; Chen, C. *Biomaterials* **2009**, *30*, 611.

[297] Beuerle, F.; Witte, P.; Hartnagel, U.; Lebovitz, R.; Parng, C.; Hirsch, A. *J. Exp. Nanosci.* **2007**, *2*, 147.

[298] Quick, K. L.; Ali, S. S.; Arch, R.; Xiong, C.; Wozniak, D.; Dugan, L. L. *Neurobiol. Aging* **2008**, *29*, 117.

[299] Lin, A. M.; Chyi, B. Y.; Wang, S. D.; Yu, H. H.; Kanakamma, P. P.; Luh, T. Y.; Chou, C. K.; Ho, L. T. *J. Neurochem.* **1999**, *72*, 1634.

[300] Dexter, D. T.; Holley, A. E.; Flitter, W. D.; Slater, T. F.; Wells, F. R.; Daniel, S. E.; Lees, A. J.; Jenner, P.; Marsden, D. C. *Mov. Disord.* **1994**, *9*, 92.

[301] Hirsch, E. C. *Eur. Neurol.* **1993**, *33*, 52.

[302] Sofic, E.; Paulus, W.; Jellinger, K.; Riederer, P.; Youdim, M. B. H. *J. Neurochem.* **1991**, *56*, 978.

[303] Wang, J. et al. *Biochem. Pharmacol.* **2006**, *71*, 872.

[304] Bisaglia, M.; Natalini, B.; Pellicciari, R.; Straface, E.; Malorni, W.; Monti, C.; Franceschi, D.; Schettini, G. *J. Neurochem.* **2000**, *74*, 1197.

[305] Monti, D.; Moretti, L.; Salvioli, S.; Straface, E.; Malorni, W.; Pellicciari, R.; Schettini, G.; Bisaglia, M.; Pincelli, C.; Fumelli, C.; Bonafè, M.; Franceschi, C. *Biochem. Biophys. Res. Commun.* **2000**, *277*, 711.

[306] Szabo, A.; Ostlund, N. S. *Modern Quantum Chemistry: Introduction to Advanced Electronic Structure Theory*; Dover Publications: Mineola NY, 1996.

[307] Nebot, I.; Ugalde, J. M.; Caballol, R.; Solà, M.; Novoa, J.; Largo, A.; Illas, F.; Ricart, J. M.; Alvariño, J. M.; Borondo, F.; Merchán, M.; Frau, J.; Sánchez, E.; Andrés, J. *Química Teórica y Computacional*; Universitat Jaume I: Castelló de la Plana, 2000.

[308] Jensen, F. *Introduction to Computational Chemistry*; John wiley and Sons Ltd: New York, 1999.

[309] Hohenberg, P.; Kohn, W. *Phys. Rev.* **1964**, *136*, B864.

[310] Kohn, W.; Sham, L. *Phys. Rev.* **1965**, *140*, A1133.

[311] Block, F. *Z. Physik.* **1929**, *57*, 545.

[312] Slater, J. C. *Phys. Rev.* **1951**, *81*, 385.

[313] Vosko, S. H.; Wilk, L.; Nusair, M. *Can. J. Phys.* **1980**, *58*, 1200.

[314] Becke, A. *Int. J. Quantum Chem.* **1983**, *23*, 1915.

[315] Perdew, J. P.; Wang, Y. *Phys. Rev. B* **1986**, *33*, 8800.

[316] Becke, A. D. *Phys. Rev. A* **1988**, *38*, 3098.

[317] Lee, C.; Yang, W.; Parr, R. *Phys. Rev. B* **1988**, *37*, 785.

[318] Perdew, J. P. *Phys. Rev. B* **1986**, *33*, 8800.

[319] Perdew, J. P.; Wang, Y. *Phys. Rev. B* **1992**, *45*, 13244.

[320] Perdew, J. P.; Chevary, J. A.; Vosko, S. H.; Jackson, K. A.; Pederson, M. R.; Singh, D. J.; Fiolhais, C. *Phys. Rev. B* **1992**, *46*, 6671.

[321] Fernández-Rico, J.; López, R.; Ema, I.; Ramírez, G. *J. Comput. Chem.* **2004**, *25*, 1987.

[322] te Velde, G.; Bickelhaupt, F. M.; Baerends, E. J.; Fonseca Guerra, C.; van Gisbergen, S. J. A.; Snijders, J. G.; Ziegler, T. *J. Comput. Chem.* **2001**, *22*, 931.

[323] Bofill, J. *J. Comput. Chem.* **1994**, *15*, 1.

[324] Swart, M.; Bickelhaupt, F. M. *Int. J. Quant. Chem.* **2006**, *106*, 2536.

[325] Atkins, P. W. *Physical Chemistry*; Oxford University Press: New York, 1982.

[326] van Bochove, M. A.; Swart, M.; Bickelhaupt, F. M. *J. Am. Chem. Soc.* **2006**, *128*, 10738.

[327] Roux, B.; Simonson, T. *Biophys. Chem.* **1999**, *78*, 1.

[328] Tomasi, J.; Persico, M. *Chem. Rev.* **1994**, *94*, 2027.

[329] Foresman, J.; Keith, T.; Wiberg, K.; Snoonian, J.; Frisch, M. *J. Phys. Chem.* **1996**, *100*, 16098.

[330] Cossi, M.; Barone, V.; Cammi, R.; Tomasi, J. *Chem. Phys. Lett.* **1996**, *255*, 327.

[331] Truong, T.; Stefanovich, E. V. *Chem. Phys. Lett.* **1995**, *240*, 253.

[332] Klamt, A. *J. Phys. Chem.* **1995**, *99*, 2224.

[333] Dapprich, S.; Komaromi, I.; Byun, K. S.; Morokuma, K.; Frisch, M. J. *J. Mol. Struct. (Theochem)* **1999**, *462*, 1.

[334] Svensson, M.; Humbel, S.; Froese, R. D. J.; Matsubara, T.; Sieber, S.; Morokuma, K. *J. Phys. Chem.* **1996**, *100*, 19357.

[335] Swart, M. *Int. J. Quant. Chem.* **2003**, *91*, 177.

[336] Haddon, R. C. *QCPE 508/QCMP 044, QCPE Bull.* **1988**, *8*, 48.

[337] Campanera, J. M.; Bo, C.; Olmstead, M. M.; Balch, A. L.; Poblet, J. M. *J. Phys. Chem. A* **2002**, *106*, 12356.

[338] Mestres, J.; Solà, M. *J. Org. Chem.* **1998**, *63*, 7556.

[339] Mayr, H.; Ofial, A. R. *Angew. Chem. Int. Ed.* **2006**, *45*, 1844.

[340] Klamt, A.; Schüürmann, G. J. *Chem. Soc. Perkin Trans.* **1993**, *2*, 799.

[341] Pye, C. C.; Ziegler, T. *Theor. Chem. Acc.* **1999**, *101*, 396.